NAVAL POSTGRADUATE SCHOOL
Monterey, California

THESIS

HIGH-ACCURACY DISTRIBUTED SENSOR
TIME-SPACE-POSITION INFORMATION SYSTEM FOR
CAPTIVE-CARRY FIELD EXPERIMENTS

by

Andrew W. Rowe

December 1996

Thesis Advisor   Phillip E. Pace

Approved for public release; distribution is unlimited.

DTIC QUALITY INSPECTED 1

19970509 053

REPORT DOCUMENTATION PAGE

Form Approved OMB No. 0704-0188

1. AGENCY USE ONLY *(Leave blank)*	2. REPORT DATE December 1996	3. REPORT TYPE AND DATES COVERED Master's Thesis

4. TITLE AND SUBTITLE TITLE OF THESIS: HIGH-ACCURACY DISTRIBUTED SENSOR TIME-SPACE-POSITION INFORMATION SYSTEM FOR CAPTIVE-CARRY FIELD EXPERIMENTS	5. FUNDING NUMBERS
6. AUTHOR(S) Rowe, Andrew W.	
7. PERFORMING ORGANIZATION NAME(S) AND ADDRESS(ES) Center for Joint Services Electronic Warfare Naval Postgraduate School Monterey CA 93943-5000	8. PERFORMING ORGANIZATION REPORT NUMBER
9. SPONSORING/MONITORING AGENCY NAME(S) AND ADDRESS(ES) Integrated Electronic Warfare Simulations Branch, Code 5760, Naval Research Laboratory, Washington, D.C. 20375-5339	10. SPONSORING/MONITORING AGENCY REPORT NUMBER

11. SUPPLEMENTARY NOTES The views expressed in this thesis are those of the author and do not reflect the official policy or position of the Department of Defense or the U.S. Government.

12a. DISTRIBUTION/AVAILABILITY STATEMENT Approved for public release; distribution is unlimited.	12b. DISTRIBUTION CODE

13. ABSTRACT *(maximum 200 words)*

Operational EW test and evaluation experiments require that the position of the aircraft and other moving objects on the range be known precisely as a function of time. Terminal Time-Space-Position Information (TSPI) systems involve the range platforms interacting at close distances and therefore require precise trajectory information over a restricted volume of space. Terminal TPSI systems are used for tactics evaluation and the evaluation of simulated weapons firings (e.g., captive-carry hardware-in-the-loop missile simulators). Distributed sensor TSPI systems consist of two or more measurement sensors located some distance from each other. Each sensor makes a measurement of target angle and range. Distributed sensor systems are more complex than single-point systems involving multiple hardware installations, complex mathematical computations to extract coordinate information, synchronization of multiple measurements and calibration of a number of different stations.

This paper presents a novel distributed sensor TSPI architecture that provides precise positioning information of the target relative to a fixed inertial coordinate system. The architecture efficiently integrates the information from an inertial navigation system (INS), a global positioning system (GPS) and any number of distributed RF sensors which may be located onboard a captive-carry aircraft. The significance of this work is that by knowing the target's position in a fixed inertial frame of reference (derived from the integration process) an evaluation can be made as to the effectiveness of any electronic attack or off-board decoys that might have been launched during the field test scenario. The induced INS, GPS and sensor noise and the corresponding errors due to the integration process are evaluated numerically as a function of the weapon system being used. The accuracy in the targeting information is also quantified and compared with the true expected values.

14. SUBJECT TERMS. Distributed Sensor Time-Space-Position Information System, Differential Global Position System, Inertial Navigation System, Modeling, Hardware-in-the-Loop, Anti-Ship Cruise Missile Simulation, Electronic Countermeasures	15. NUMBER OF PAGES: 166
	16. PRICE CODE

17. SECURITY CLASSIFICATION OF REPORT Unclassified	18. SECURITY CLASSIFICATION OF THIS PAGE Unclassified	19. SECURITY CLASSIFICATION OF ABSTRACT Unclassified	20. LIMITATION OF ABSTRACT UL

NSN 7540-01-280-5500

Standard Form 298 (Rev. 2-89)

HIGH-ACCURACY DISTRIBUTED SENSOR TIME-SPACE-POSITION INFORMATION SYSTEM FOR CAPTIVE-CARRY FIELD EXPERIMENTS

Andrew W. Rowe
Lieutenant, United States Navy
B.S., USNA, Annapolis MD, 1987

Submitted in partial fulfillment of the
requirements for the degree of

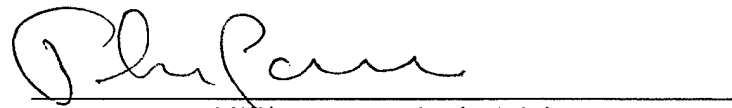**MASTER OF SCIENCE IN APPLIED PHYSICS**
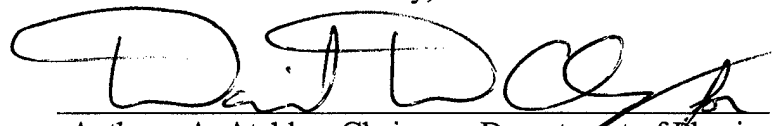
from the

NAVAL POSTGRADUATE SCHOOL

December 1996

Author: _____
Andrew W. Rowe

Approved by: _____
Phillip E. Pace, Thesis Advisor

_____
Robert C. Harney, Second Reader

_____
Anthony A. Atchley, Chairman, Department of Physics

iii

iv

ABSTRACT

Operational EW test and evaluation experiments require that the position of the aircraft and other moving objects on the range be known precisely as a function of time. Terminal Time-Space-Position Information (TSPI) systems involve the range platforms interacting at close distances and therefore require precise trajectory information over a restricted volume of space. Terminal TPSI systems are used for tactics evaluation and the evaluation of simulated weapons firings (e.g., captive-carry hardware-in-the-loop missile simulators). Distributed sensor TSPI systems consist of two or more measurement sensors located some distance from each other. Each sensor makes a measurement of target angle and range. Distributed sensor systems are more complex than single-point systems involving multiple hardware installations, complex mathematical computations to extract coordinate information, synchronization of multiple measurements and calibration of a number of different stations.

This paper presents a novel distributed sensor TSPI architecture that provides precise positioning information of the target relative to a fixed inertial coordinate system. The architecture efficiently integrates the information from an inertial navigation system (INS), a global positioning system (GPS) and any number of distributed RF sensors which may be located onboard a captive-carry aircraft. The significance of this work is that by knowing the target's position in a fixed inertial frame of reference (derived from the integration process) an evaluation can be made as to the effectiveness of any electronic attack or off-board decoys that might have been launched during the field test scenario. The induced INS, GPS and sensor noise and the corresponding errors due to the integration process are evaluated numerically as a function of the weapon system being used. The accuracy in the targeting information is also quantified and compared with the true expected values.

TABLE OF CONTENTS

LIST OF FIGURES

LIST OF TABLES

ACKNOWLEDGEMENT

I. INTRODUCTION

A. CAPTIVE CARRY ASM EXPERIMENTS

Currently, the Naval Research Laboratory, Washington, DC conducts captive-carry anti-ship missile (ASM) experiments onboard a modified P-3 aircraft. The purpose of the experiments is to evaluate the effectiveness of ship defensive systems against various types of anti-ship missiles. Currently, the evaluation process involves collecting information pertaining to the time and location of certain events which occur during a particular test scenario for post-test analysis. One of the goals of the post-test analysis is to accurately locate the P-3, the unit(s) involved in the exercise, and any offboard countermeasure devices (i.e., CHAFF, RUBBER DUCKS, etc.). By accurately locating the players in the scenario, the effectiveness of the countermeasures can be accurately determined.

NRL's P-3 research aircraft is shown in Figure 1.1. It has the capability of carrying eight ASM Simulators beneath its main wings. Each ASM Simulator has an active seeker installed. Each ASM Simulator has the capability of providing the following information:

- Target tracking accuracy
- Seeker guidance type
- Transmit frequency
- Pulse width
- Pulse repetition interval
- Scan rate
- Search sector

1

- Beamwidth

- Transmit Power

- Antenna Gain

- Azimuth, Elevation and Range to target
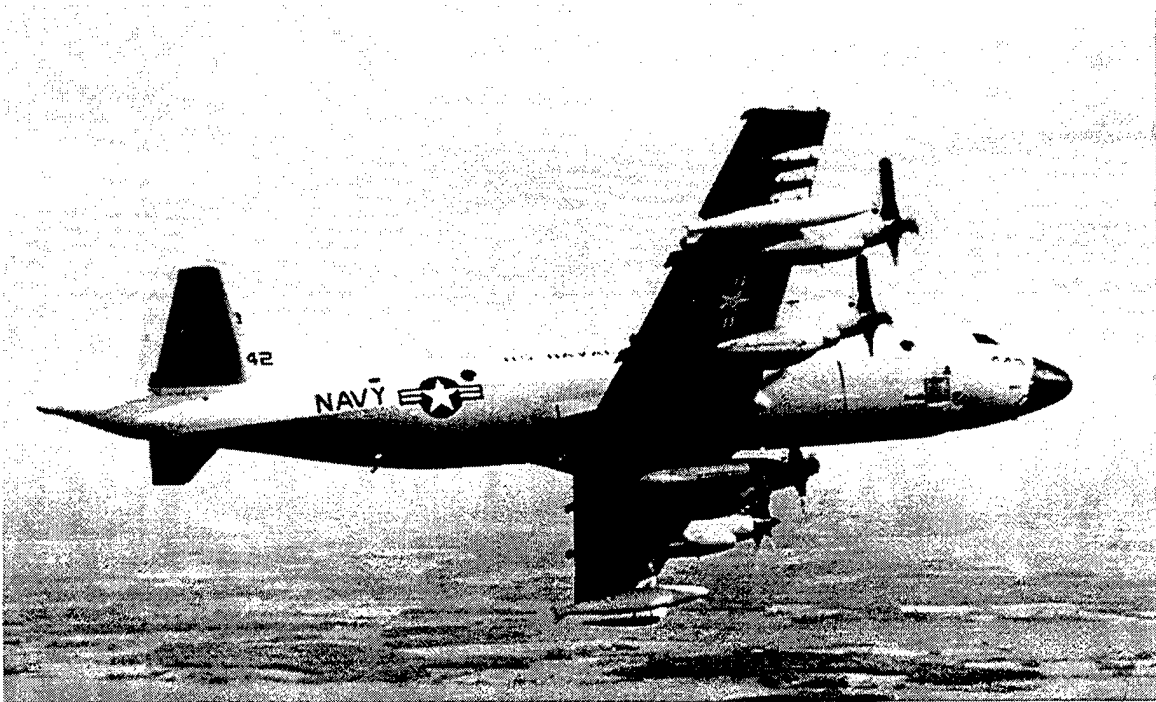
Figure 1.1: NRL's P-3 RESEARCH AIRCRAFT

A typical scenario involves the P-3 aircraft equipped with the ASM Simulators and the appropriate data recording equipment flying towards a Naval Surface combatant with a self protection suite onboard (e.g., AN/SLQ-32(V)4). The P-3 makes several passes at the participating unit from several different aspect angles. Usually, the P-3 begins each run at a range of twelve nautical miles from the unit. At this range the seekers are turned on to begin the search for the target. As the aircraft approaches the ship, eventually, the seeker switches from search to track mode. In track mode the seeker locks on to the target in

range and azimuth until the P-3 flies past the target or a countermeasure is employed. When a countermeasure is employed, the seeker may or may not break lock on the target.

B.   PRINCIPAL CONTRIBUTIONS

The algorithms presented in this thesis provide a precise time-space-position information system (TSPI) based on the inputs from a number of distributed RF sensors, a GPS and an INS. The target's position in a fixed inertial frame of reference is derived from the integration of the INS/GPS/Radar systems that are located onboard NRL's P-3 research aircraft. The significance of this thesis is that it provides the necessary tools to help NRL perform an evaluation of the shipboard self protection system effectiveness. By knowing the target's position as derived from the integration process an evaluation is also made as to the effectiveness of any launched decoys during the test scenario. These algorithms help the test engineers determine if the seeker broke lock on the target to track an offboard decoy (e.g. chaff).

Also, the relevance of this thesis applies to other applications as well. By knowing a target's position relative to a fixed inertial reference frame, the targeting information can be sent to any platform and be understood immediately. This type of targeting information is ideal for remote firing of weapons that use GPS as an input.

This thesis develops new algorithms to integrate the INS and GPS along with the distributed onboard seekers for determining the target position relative to a fixed inertial frame of reference. Mathematical models of the P-3, INS, GPS, and the ASM seekers are developed using SIMULINK. These models are used to provide the necessary inputs for the distributed sensor TSPI (DSTSPI) algorithms. Evaluation of the algorithms indicates a

significant increase in the accuracy of the target position. The results make evident the importance of the INS/GPS integration process in knowing the ASM seeker's position in a fixed inertial frame of reference. The induced INS, GPS and RF sensor noise and the corresponding errors due to the integration process are evaluated numerically as a function of the weapon system being used. The accuracy in the targeting information is also quantified and compared with the true expected values.

C. THESIS ORGANIZATION

Parts of this thesis assume the reader has a background in the areas of radar and aeronautics. Thorough discussions are provided in the areas specifically relevant to the algorithms presented in this thesis.

In Chapter II, the background information needed to gain a full appreciation of this thesis is discussed. First, the errors associated with the Global Positioning System (GPS) and Inertial Navigation System (INS) are discussed along with basic system descriptions. Because both GPS and INS reside within fixed inertial frames of reference, a thorough discussion of the fixed inertial coordinate systems that are used in this thesis are provided. Also, because of the dynamics of the P-3 during the test scenario, a general methodology on how to use lever arm corrections is discussed. Finally, this chapter discusses the equations used in the modeling of the monopulse and conical scan seekers that are used in the simulation.

In Chapter III, the DSTSPI algorithms are thoroughly developed. Here, a general description of the process is given along with an explanation of the SIMULINK block diagrams that are used.

In Chapter IV, a discussion is provided on the results of the DSTSPI algorithms. Several plots are used to aid in the validation and analysis of the results. In addition, a further examination is made as to the utility of the algorithm and whether or not it can live up to the user's expectations based on the relevance to the ASM/EW test scenario.

Chapter V discusses some important considerations involving the hardware and software integration process onboard the P-3. Finally, Chapter VI discusses conclusions that are made in the process of this analysis.

II. BACKROUND INFORMATION

A. GLOBAL POSITIONING SYSTEM

The Global Positioning System (GPS) consists of 24 satellites that orbit the earth. Of the 24 satellites three are ready service spares. GPS provides locating information to an unlimited number of users. Today, GPS is widely used by both the military and the civilian sector. More and more civilians are purchasing inexpensive GPS receivers for recreational use. The applications of GPS seem limitless. [Ref. 1, p. 121]

GPS is no doubt the most powerful navigational aid available today. There are, however, a few drawbacks to the system. First, the positioning information available from GPS is updated at a **10 Hz** rate for high-end systems and at a **1 Hz** rate for most other systems. The update rate becomes important when the application involves real time processing. In the case where an update rate greater than 10 Hz is required, the positioning information from the GPS receiver must be smoothed by employing a Kalman filter or some other predictive algorithm. Some higher-end GPS receivers do provide a smoothed output that the user is able to sample at higher frequencies.

There are several factors that determine the GPS accuracy of each position fix. The accuracy can vary based on the time of day, the location of the GPS antenna relative to the GPS satellites and the type of GPS receiver used.

The major sources of error for GPS are summarized as follows: [Ref. 1,p 125]

- Selective availability
- Clock differences
- Receiver noise
- Multipath
- Atmospheric delays
- Ephemeris error

The sources of error are detailed below.

1. Atmospheric Delay

Atmospheric delays occur mainly in the ionosphere and the troposphere. In the ionosphere, time delays occur because the charged particles interact with the transmitted GPS signals. As a result of this interaction, the GPS signal arrives at the receiver with some inherent time delay. Since the rate of propagation is nearly the speed of light, any delay in the receipt of the signal translates to an increase in the calculated range.

The equation for the ionospheric delay is given by

$$\Delta t = \frac{40.3}{cf^2} TEC \tag{2-1}$$

where Δt is the delay in seconds, **f** is the frequency in Hz, **c** is the speed of light in **m/s**, **TEC** is the total electron content (**electrons/m²**) along the signal path and 40.3 is an empirically derived constant with units (**m³/s²/electrons**). Since, in the ionosphere, the charged particles are typically between **100** to **1000** kilometers above the earth, the path length for interaction can be very large. The pseudorange error can be as great as 40 meters depending upon the time of day, time of year, the solar cycle and the geographic location. [Ref. 1,p 126]

The lower part of the atmosphere can also cause significant delays in the GPS signal. This portion of the atmosphere is called the troposphere. These delays are caused by the interaction of the GPS signal with water molecules entrained in the atmosphere. Here, a 2 meter error can occur in the pseudorange calculation when a satellite is directly overhead and a 28 meter error when a satellite is just above the horizon. There are models available that can predict the errors from both the ionospheric and tropospheric delays. These models improve the performance of the GPS receiver.

2. Selective Availability

Selective availability is the status of GPS when the Department of Defense degrades the position accuracy to 100 meters. This is accomplished by dithering the individual satellite's clock signal. Dithering is a process by which the clock signals of the satellites are encoded such that only military users are able to take advantage of the highest accuracy.

3. Clock Errors

No matter how precise and accurate a clock is said to be, all clocks are plagued by bias and drift errors. Bias is a fixed error associated with the offset of the clock from the correct time. Drift is defined as the rate of change of the accuracy of a clock with time. Typical clock errors are on the order of a few nanoseconds. A one nanosecond error equates to roughly three tenths of a meter error in the pseudorange calculation.

4. Ephemeris Error

Ephemeris errors occur when a satellite's position is different from the position contained within the navigation message that is sent by each satellite. The Ephemeris errors are typically on the order of a half meter in the radial direction and three and a half meters in the planar direction.

5. Multipath

Multipath errors result when the signal does not take a direct path from the satellite to the receiver. A signal may bounce off a particular object before reaching the GPS antenna. This causes delays in the reception of the signal which can directly translate into errors in the pseudorange calculation. Because of the design of current GPS receivers, this effect is usually insignificant and is ignored.

6. Receiver Noise

All receivers inherently add noise to the signal they receive. A typical receiver has a noise value which contributes around 7.5 meters to the error in the pseudorange calculation. The overall error associated with receiver noise is wholly dependent upon the quality of the receiver being used.

One method in eliminating most of the errors inherent with GPS is to use Differential GPS. Differential GPS (DGPS) involves having another GPS receiver fixed to a known location within close proximity of the user's GPS receiver. This is called a differential GPS station. This differential station becomes susceptible to the same errors as the user's GPS receiver. Because the exact location of the differential station is known, the differential station can transmit its location along with the corrections for the errors

discussed above. This process greatly improves the accuracy of the positioning system. An advertised value for position accuracy for a DGPS receiver is around one meter. [Ref. 3]

The DSTSPI algorithms use a DGPS model for the input of the GPS positioning information. This model assumes a position accuracy of one meter with an update rate of 10 Hz. The development of this model is not discussed in this work. Details are found in Reference 1, pages 141-152.

B.   INERTIAL NAVIGATION SYSTEM

The inertial navigation system (INS) detects changes in the total acceleration of a body relative to an inertial frame of reference. The primary component of the INS is the inertial measuring unit (IMU). The IMU consists of three accelerometers, three rate gyros, and two inclinometers. The accelerometers measure the linear, centripetal and gravitational acceleration effects on the body. The INS removes the gravitation component of the acceleration from the total acceleration. This resultant acceleration is integrated once over time to find the velocity of the body and twice to find the position of the body. The rate gyros of the IMU measure the angular velocities of the body. The inclinometers measure the orientation of the body relative to the inertial frame of reference. This orientation is typically denoted as the pitch, roll and yaw. [Ref. 1, p. 136-139]

There are two types of inertial navigation systems. The first type is the gimbaled system. Here, the gimbaled IMU is allowed to rotate about four gimbals while a controller maintains the IMU platform in a local level orientation towards true North. The relative

11

differences between the gimbals and the platform provide the inertial quantities. The problem with the gimbaled systems is that they are usually very heavy and bulky. Because of this, the gimbaled system is not very well suited for an aircraft implementation.

The second type of inertial navigation is the strapdown system. Here, the IMU is literally strapped down to the aircraft. In this manner the IMU maintains a constant orientation to the local coordinate system of the aircraft. Because of this configuration, the output of the IMU is given relative to the aircraft's coordinates. The INS transforms the output of the strapdown IMU to accelerations and angular velocities relative to the inertial frame. These transformations require substantially more computing power than what is needed for the gimbaled system. Because computers are relatively fast and inexpensive, the strapdown system is the one generally found on most aircraft.

The error sources for the INS are mainly due to errors pertaining to the IMU. These errors are categorized as follows: bias, cross-axis sensitivity and noise floor. The bias error results when the output has a constant offset from the correct value. If there are no accelerations on the body, the total acceleration should be zero. Any other value would indicate a bias error. A cross-axis sensitivity error occurs when the IMU is not properly aligned with the aircraft's coordinate system. Because it is virtually impossible to achieve a perfect alignment of two mechanical systems, a cross-sensitivity error is always present. The noise floor for INS prevents measurements below a specified value. It acts as a threshold for the output of the INS. The noise floor is caused by the mechanical and electrical components of the INS.

The DSTSPI algorithms use a strapdown INS model for the input of the pitch, roll and yaw of the P-3. This model assumes an accuracy of 0.5 degrees in the determination of the pitch, roll and yaw. The development of the INS model is not discussed in this work. Details are found in Reference 1, pages 152-157.

C.   COORDINATE SYSTEMS

Several coordinate systems are used in the development of the DSTSPI algorithms. For this reason, a brief discussion is provided on the basic characteristics of these coordinate systems.

1. Earth-Centered-Earth-Fixed

The Earth-Centered-Earth-Fixed (ECEF) coordinate system is a right-hand orthogonal coordinate system that is fixed at the Earth's origin [0, 0, 0]. Figure 2.1 shows the ECEF coordinate system in relation to the Earth.
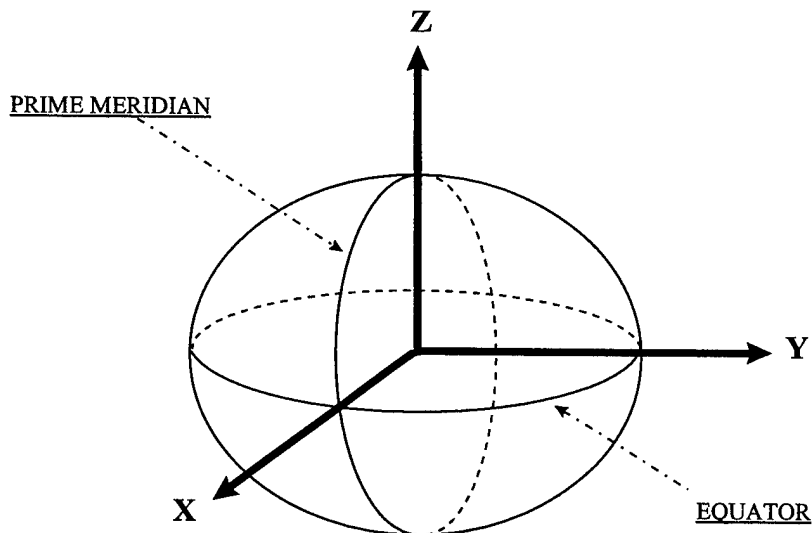
Figure 2.1: Earth-Centered-Earth Fixed Coordinates

13

The x-axis is defined as the direction from the origin through the intersection of 0° longitude and the equator. The y-axis is defined as the direction from the origin through the intersection of 90° east longitude and the equator. The z-axis is defined as the direction from the origin through the point defined as true north, or 90° latitude. The ECEF coordinate system rotates with the earth. One important advantage of the ECEF coordinate system is that all positions that are referenced to ECEF are independent of the model used for the irregularities of the Earth's surface. [Ref. 2, p. 4]

2. Geodetic Coordinate System

The geodetic coordinate system is the coordinate system that is most commonly used for navigation. Generally, objects which are fixed to the Earth's surface are located in the geodetic coordinate system by designating their latitude, ϕ, and longitude, λ. The latitude and longitude are defined by their relation to the prime meridian and the equator. The geodetic latitude, ϕ, is defined as the angle from the equatorial plane to the vertical direction of a line normal to the reference ellipsoid passing through a location on the reference ellipsoid. The geodetic longitude, λ, is defined as the angle between the reference plane and a plane passing though a location on the reference ellipsoid defined by N, where both planes are perpendicular to equatorial plane. The geodetic height, **h**, is defined as the distance from the reference ellipsoid to the location in a direction normal to the reference ellipsoid. The reference ellipsoid is a model that defines the shape of the Earth. Most modern navigation systems use the World Geodetic System -- 84 model (WGS-84). The WGS-84 model gives the model parameters for the shape of the Earth along with the local height correction for a particular latitude and longitude. [Ref. 2, p. 5]

14

Figure 2.2 shows a general depiction of the geodetic coordinate system. Here, **N** is the distance from the polar axis to the surface of the reference ellipsoid, **h** is the height correction for the terrain on the Earth's surface and **P** defines a position in geodetic coordinates.
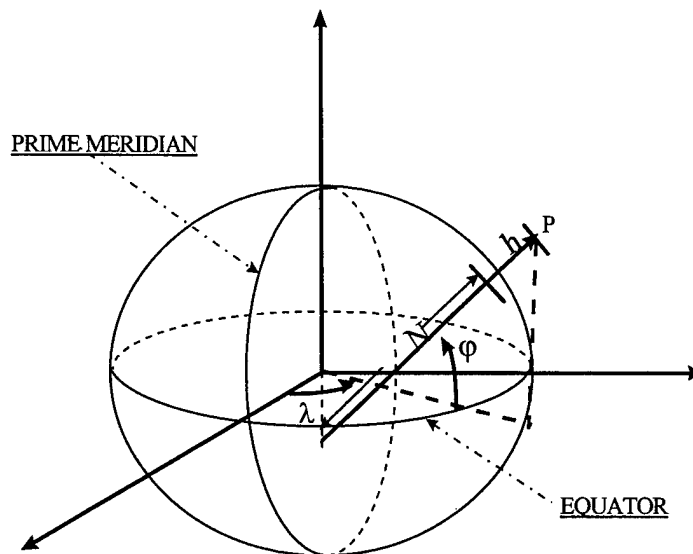
Figure 2.2: Geodetic Coordinate System

3. Tangent Plane Coordinate System

The tangent plane coordinate system is a right-hand orthogonal system. The origin of the tangent plane coordinate system is defined by passing a plane through a point on the earth's surface which is defined by a particular latitude and longitude. The axes, (X,Y,Z), of the tangent plane coordinate system are defined as: [Ref. 2, p. 5]

- X-axis points toward true North
- Y-axis points toward true East
- Z-axis points in the downward direction from the point where the tangent plane intersects the reference ellipsoid to a point on the polar axis on the earth

Figure 2.3 shows a general depiction of the tangent plane coordinate system.
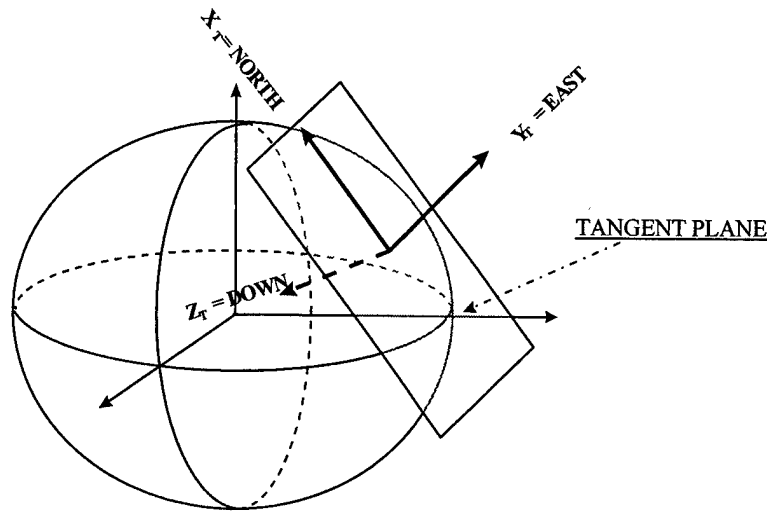
Figure 2.3: Tangent Plane Coordinate System

4. Navigation Coordinate System

The navigation coordinate system is a right-hand orthogonal coordinate system whose origin is collocated with the aircraft's center of gravity. It maintains a local level orientation to the reference ellipsoid in the same manner as the tangent plane. If the origin of the aircraft is collocated at the origin of the tangent plane, then the navigation coordinate system and tangent plane coordinate system are the same (assuming the orientations of the axes are the same.) The origin of the navigation coordinate system is defined to be the center of the aircraft's inertial navigation system. The orientation can be chosen to be East North Up (ENU), NED, etc.. [Ref. 2, p. 6]

Figure 2.4 shows the navigation coordinate system with a North East Down (NED) orientation. This is the orientation used in the DSTSPI algorithms developed in this thesis. It is convenient to choose NED for the orientation of the axes because the

16

coordinate system naturally aligns itself with true North. The difficulty in dealing with NED orientation is that altitude is a negative quantity.
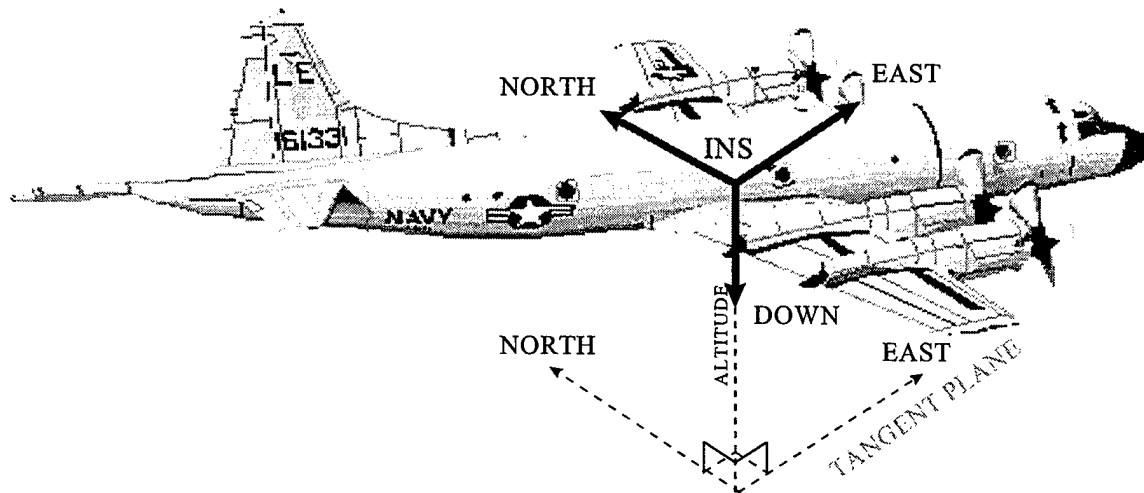
Figure 2.4: Navigation Coordinate System

5. Body Fixed Coordinates

The body fixed coordinate system is the right-hand orthogonal coordinate system that is attached to the aircraft and the axes of which are defined by the input axes of the inertial navigation system. The body fixed coordinate system rotates with the aircraft which implies that the body accelerations of the aircraft are the same as the body fixed accelerations if the inertial navigation system is a strapdown system. Figure 2.5 shows a depiction of the body fixed coordinate system on the P-3. The orientation of the axes are forward, right wing and down. The orientation is defined as a matter of convention. Notice that this orientation is the same orientation used for the navigation and tangent plane coordinate systems (e.g., forward in the body fixed coordinates is North in the tangent plane coordinates.) Keeping the axes orientations the same for these coordinate systems results in simpler coordinate transformations. [Ref. 2, p. 8]

17
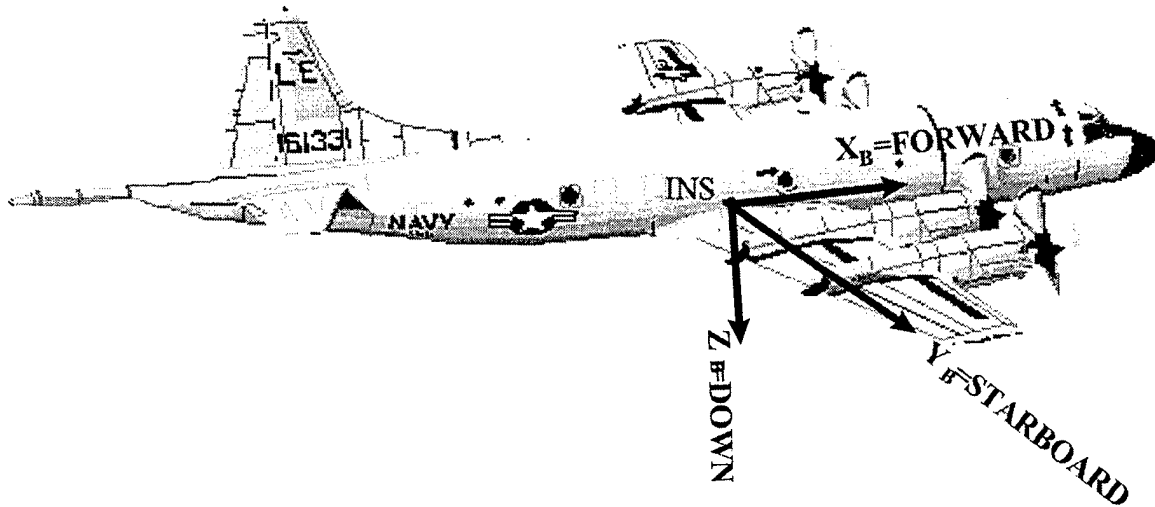
Figure 2.5: Body Fixed Coordinate System

D. LEVER ARM CORRECTION

To accurately locate the seekers for each ASM Simulator relative to a fixed coordinate system such as ECEF, the first problem that must be solved is the fact that each seeker is not collocated with the GPS antenna. If they were, the seeker's location would simply be the output of the GPS receiver. Since positioning information from the GPS receiver is given relative to the GPS antenna in ECEF or geodetic coordinates, natural position errors are inherent based upon the displacement between seeker and GPS antenna. In addition, because the P-3 is not, in general, locally level with the earth's surface (the reference ellipsoid), additional errors are inherent because of the pitch, roll and yaw of the aircraft. To correct for the position errors that result from GPS antenna displacement from each seeker and from the pitch, roll and yaw of the aircraft, a lever arm correction m is used. [Ref. 3, discussion]

18

The general algorithm for performing a lever arm correction is shown in Figure 2.6. Three things must be known before a lever arm correction is made. The first is some known fixed inertial position that is located somewhere on the P-3. This is usually the position of the GPS antenna given in ECEF coordinates, or the position of the INS given in navigation coordinates. The fixed inertial coordinates that are chosen are those in which the intended local body position is to be referenced (e.g., if the user wants to reference all positions to the tangent plane coordinate system, then this is the coordinate system that should be chosen). This position is denoted $^{FI}P_{PT}$, where the subscript, **PT**, is defined as the local position (local positions refer to those positions located in the body fixed coordinate system which are to lever arm corrected to a fixed inertial coordinate system.) An example of a local position is the seeker location. The superscript, **FI**, is defined as the fixed inertial coordinate system in which the local position is to be resolved.
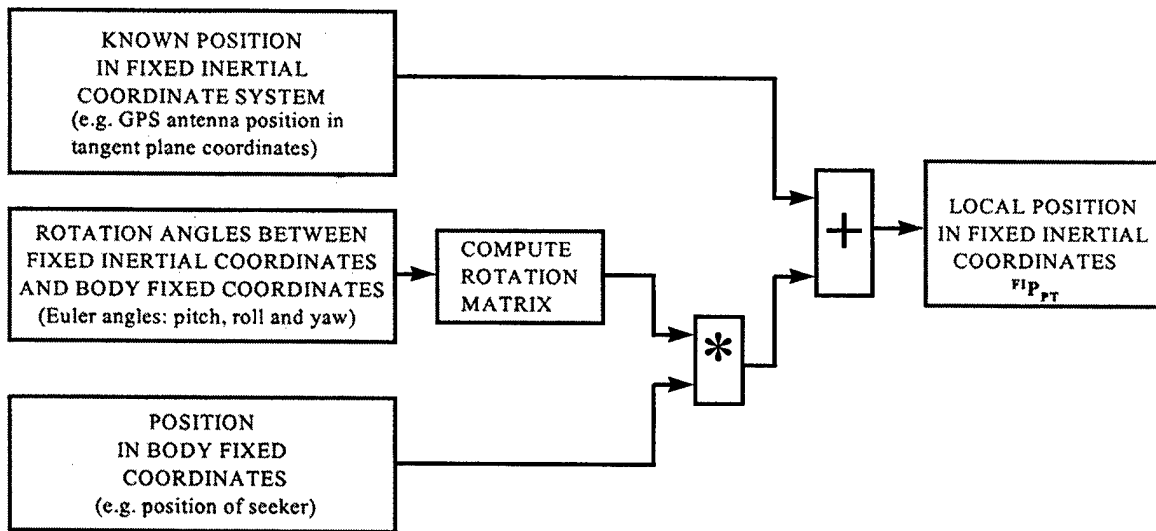
Figure 2.6: Lever Arm Correction Algorithm

To accurately perform a lever arm correction, the positions of the GPS antenna and the individual seekers for each ASM Simulator must be known relative to the center of the

aircraft in the body fixed coordinate system. These measurements are extracted from the existing drawings of the P-3 or taken manually. The overall accuracy of the lever arm correction depends upon the accuracy and precision of the measurements of the relative positions of the distributed sensors. Each simulator has two position vectors that must be determined in body fixed coordinates. One position vector describes the location of the associated distributed seeker and the other describes the after position of the ASM simulator. These two position vectors are used later in the analysis to determine the attitude of the Simulator. Notice that the forward location of the ASM simulator is essentially the location of the seeker. These position vectors are notionally depicted in Figure 2.7.
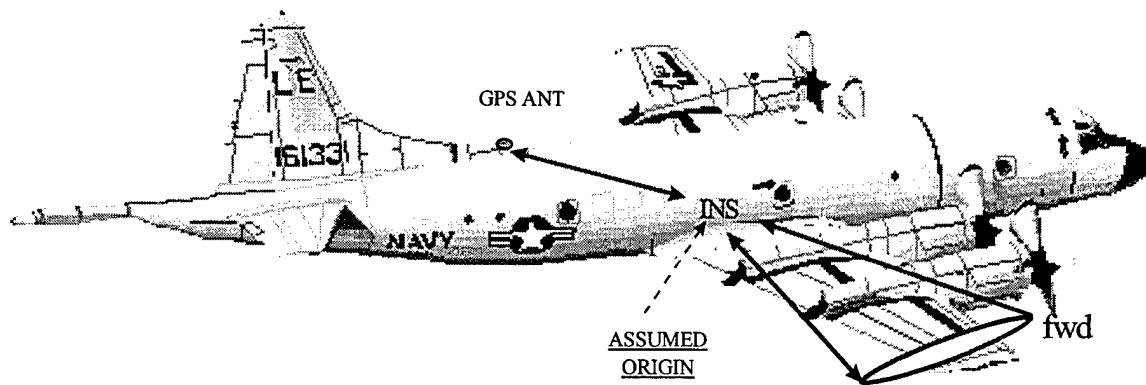
Figure 2.7: General layout of systems requiring lever arm corrections

Once the position vectors for the GPS antenna and the ASM Simulators are known in the body fixed coordinate system relative to the origin of the P-3 (which is the location of the INS), the next step is to compute the rotation matrix between the body fixed coordinate system and the tangent plane coordinate system[1]. This is done by first knowing the pitch, roll and yaw of the aircraft. The pitch, roll and yaw of the aircraft are taken

from the inertial navigation system (INS). The pitch, roll and yaw are defined as the Euler angles between the body fixed coordinate system and the tangent plane coordinate system when the origins of the two coordinate systems are collocated. We define pitch as Θ, yaw as Ψ, and roll as Φ. [Ref. 1, p. 17]

In order to derive the rotation matrix between the body fixed coordinate system and the tangent plane coordinate system the following notation and assumptions are used:

- {T} represents the inertial tangent plane coordinate system.
- {B} represents the body fixed coordinate system.
- The INS is located at the center of gravity of the P-3 aircraft or the origin of {B}. Any displacement errors of INS from the true center gravity of the P-3 are assumed to be negligible.
- The {B} coordinate system is defined with X_B as the direction forward of motion with Y_B pointing in the starboard direction (right wing) and Z_B pointing in the downward direction.
- The {T} coordinate system is defined with X_T in the direction of true north, Y_T in the direction of east and Z_T pointing down towards the center of the earth
- Roll, Φ, is positive when the rotation about X_B is clockwise when looking in the positive X_B direction.
- Pitch, Θ, is positive when the rotation about Y_B is clockwise when looking in the positive Y_B direction.
- Yaw, Ψ, is positive when the rotation about Z_B is clockwise when looking in the positive Z_B direction.

The Euler angles are depicted in Figure 2.8. Using the right-hand rule defines the direction for rotation for roll, pitch and yaw.

---

[1] Note that the tangent plane and navigation coordinates systems differ only by the altitude of the aircraft.
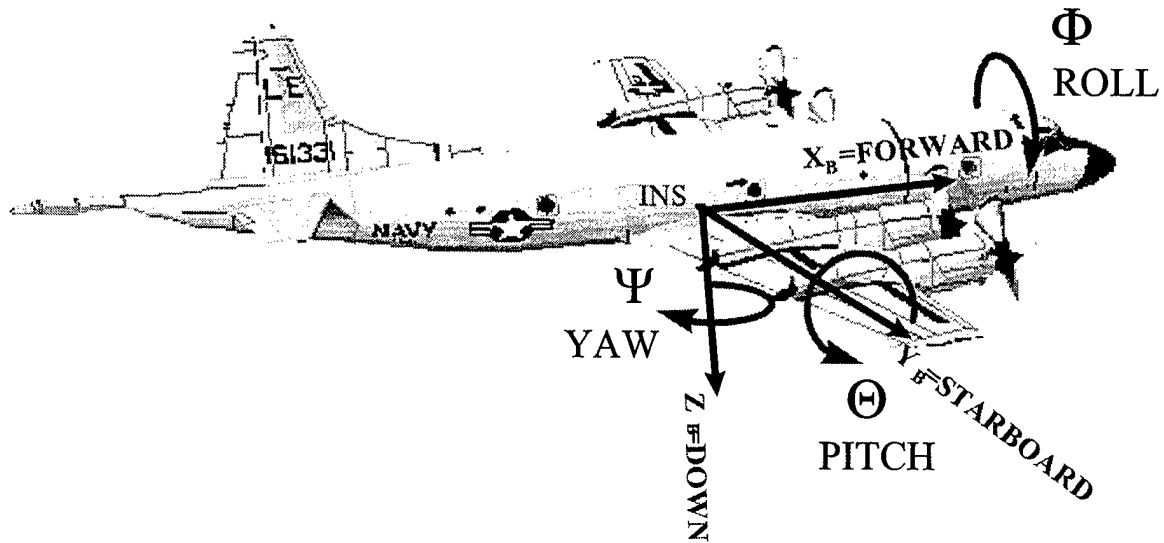
Figure 2.8: Directions Euler angles relative to body fixed coordinates

When finding the rotation matrix, the order in which the rotation is taken is important because Euler angles are not vectors. The sum of $\Phi+\Theta$ is not generally equal to $\Theta+\Phi$. For purposes of this derivation the order is taken to be **Z-Y-X**, or rotate about **Z** first, then **Y** and **X** last. [Ref. 1, p. 18] [Ref. 2, p.13]

It is convenient to collocate the origins of the body fixed and tangent plane coordinate systems as seen in Figure 2.9. By collocating these coordinate systems, the trigonometric relationships between them are easily found.

22
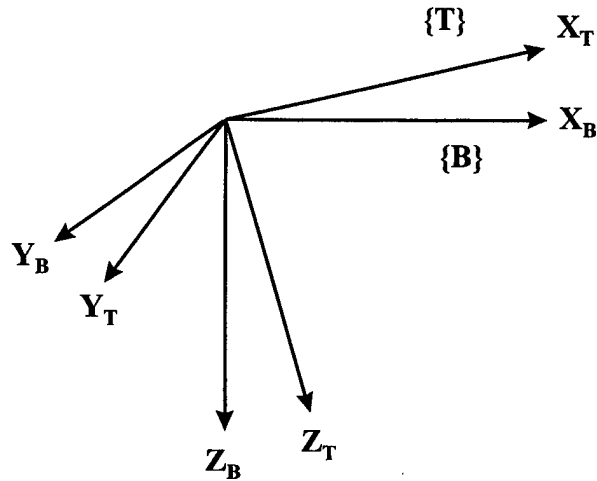
Figure 2.9: Collocated body fixed and tangent plane coordinate systems

Given a position vector, $^B\mathbf{P}$, which is resolved in {**B**}, the goal is to find the components of $^B\mathbf{P}$ that are resolved in {**T**}. To do this, first rotate the {**B**} coordinates about $\mathbf{Z_B}$. The angle by which {**B**} must be rotated is defined by Ψ. Therefore, the first rotation matrix is a function of Ψ. Figure 2.10 shows the rotation about the $\mathbf{Z_B}$ axis.
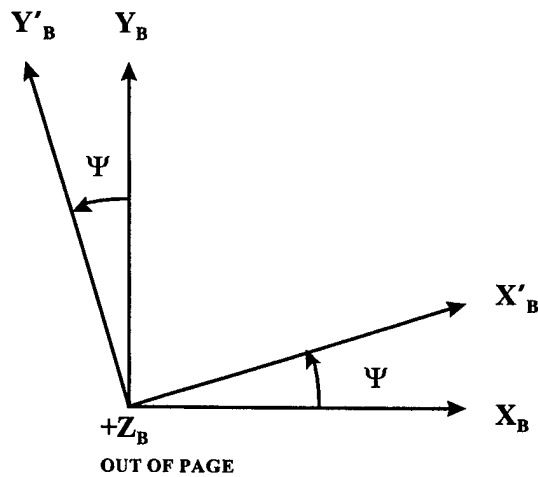
Figure 2.10: {B} rotated about Z_B

23

After the rotation through the yaw angle the new axes are defined as $\left(X_B', Y_B', Z_B'\right)$.

The trigonometric relationships between the unprimed and primed frames are used to derive the transformation matrix between the two frames. These trigonometric relationships are depicted in Figure 2.11.
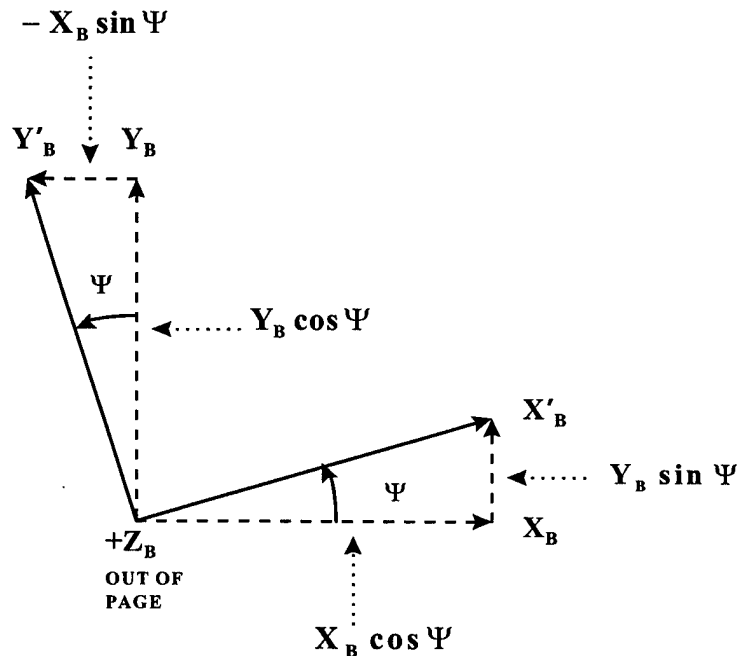
Figure 2.11: Trigonometric relationships when rotated about Z_B

From Figure 2.11, we see that the components of the new primed system are a function of the unprimed system and Ψ. X_B' is simply the result of the projection of X_B onto X_B' and the $Y_B\sin\Psi$ term. This results in Equation (2-2). Equation (2-3) is derived in a similar fashion. Also, since the rotation occurred about the Z_B axis the z components do not change during the rotation. This is summarized by the following relationships:

$$X_B' = X_B \cos\Psi + Y_B \sin\Psi \tag{2-2}$$

$$Y_B' = -X_B \sin\Psi + Y_B \cos\Psi \tag{2-3}$$

$$Z'_B = Z_B \qquad (2\text{-}4)$$

In matrix form equations (2-2), (2-3) and (2-4) simplify to

$$\begin{bmatrix} X'_B \\ Y'_B \\ Z'_B \end{bmatrix} = \begin{bmatrix} \cos\Psi & \sin\Psi & 0 \\ -\sin\Psi & \cos\Psi & 0 \\ 0 & 0 & 1 \end{bmatrix} \begin{bmatrix} X_B \\ Y_B \\ Z_B \end{bmatrix}. \qquad (2\text{-}5)$$

Now define the rotation matrix for Ψ as

$$T(\Psi) = \begin{bmatrix} \cos\Psi & \sin\Psi & 0 \\ -\sin\Psi & \cos\Psi & 0 \\ 0 & 0 & 1 \end{bmatrix}. \qquad (2\text{-}6)$$

Next, rotate the primed coordinates about Y'_B through the angle Θ, which is the pitch angle of the aircraft. This rotation is seen in Figure 2.12.
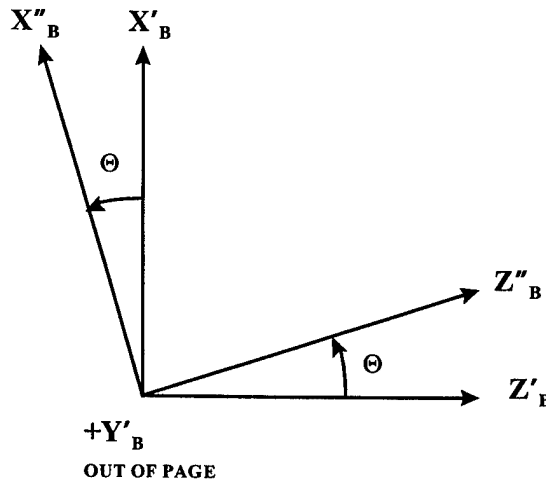
Figure 2.12: {B} rotated about Y'_B

The trigonometric relationships for this rotation are defined in Figure 2.13.
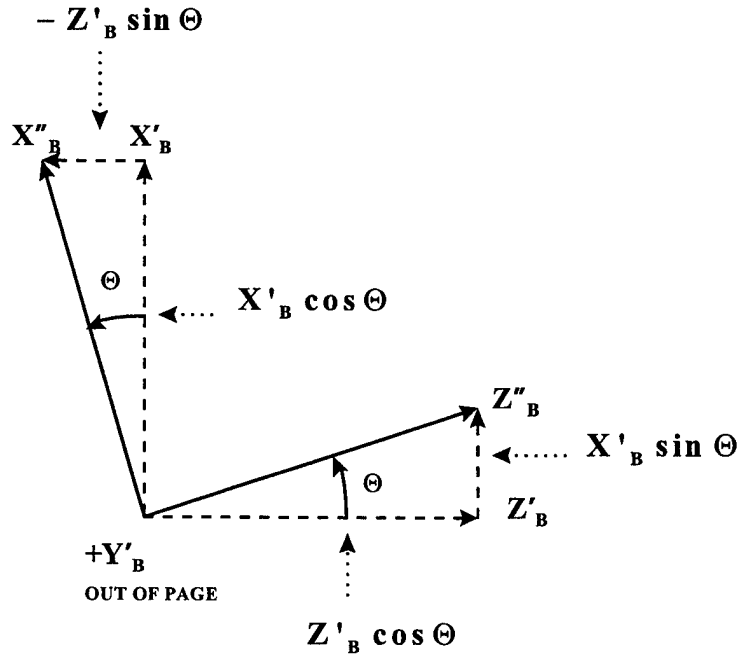
Figure 2.13: Trigonometric relationships when rotated about Y'$_B$

From Figure 2.13, the double primed coordinates is defined by the following relationships:

$$X_B^{"} = X_B^{'} \cos\Theta - Z_B^{'} \sin\Theta \qquad (2\text{-}7)$$

$$Y_B^{"} = Y_B^{'} \qquad (2\text{-}8)$$

$$Z_B^{"} = X_B^{'} \sin\Theta + Z_B^{'} \cos\Theta \qquad (2\text{-}9)$$

In matrix form these equations become

$$\begin{bmatrix} X_B^{"} \\ Y_B^{"} \\ Z_B^{"} \end{bmatrix} = \begin{bmatrix} \cos\Theta & 0 & -\sin\Theta \\ 0 & 1 & 0 \\ \sin\Theta & 0 & \cos\Theta \end{bmatrix} \begin{bmatrix} X_B^{'} \\ Y_B^{'} \\ Z_B^{'} \end{bmatrix}, \qquad (2\text{-}10)$$

with the rotation matrix for Θ as

$$T(\Theta) = \begin{bmatrix} \cos\Theta & 0 & -\sin\Theta \\ 0 & 1 & 0 \\ \sin\Theta & 0 & \cos\Theta \end{bmatrix}.$$

(2-11)

Next, rotate the double primed coordinates through the angle Φ, which is the roll of the aircraft. The result is depicted in Figure 2.14.
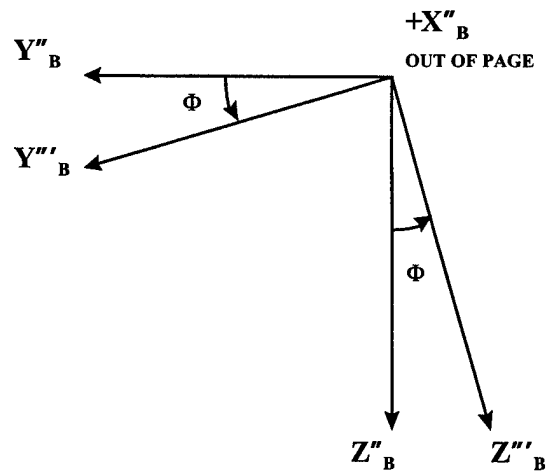
Figure 2.14: {B} rotated about X"$_B$

The trigonometric relationships between the double primed and triple primed coordinates are depicted in Figure 2.15.
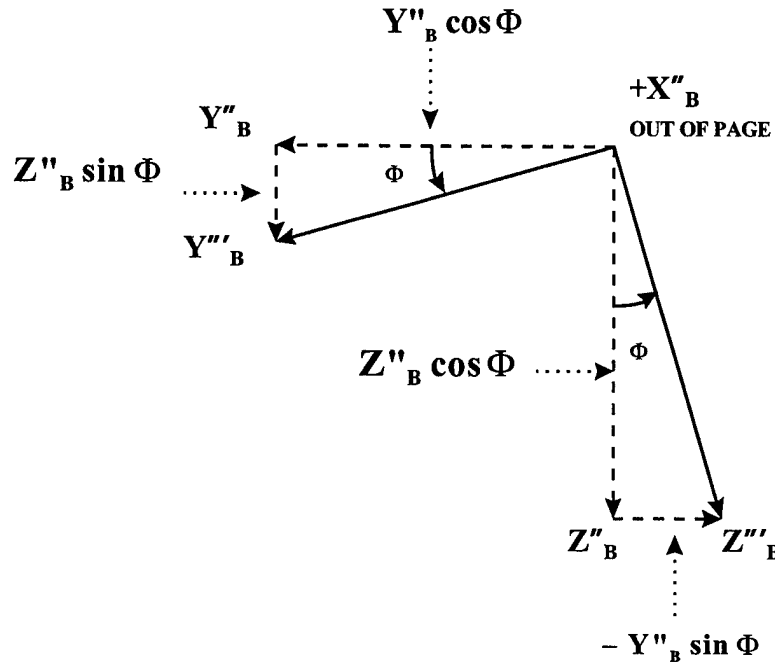
Figure 2.15: Trigonometric relationships when rotated about X"ᴮ

From Figure 2.15, the triple primed coordinates are defined in terms of the double primed coordinate and the angle Φ. The result is the following equations:

$$X_B''' = X_B''$$
(2-12)

$$Y_B''' = Y_B'' \cos \Phi + Z_B'' \sin \Phi$$
(2-13)

$$Z_B''' = -Y_B'' \sin \Phi + Z_B'' \cos \Phi$$
(2-14)

In matrix form, these equations become

$$\begin{bmatrix} X_B''' \\ Y_B''' \\ Z_B''' \end{bmatrix} = \begin{bmatrix} 1 & 0 & 0 \\ 0 & \cos\Phi & \sin\Phi \\ 0 & -\sin\Phi & \cos\Phi \end{bmatrix} \begin{bmatrix} X_B'' \\ Y_B'' \\ Z_B'' \end{bmatrix},$$
(2-15)

with the corresponding rotation matrix for Φ defined as

$$T(\Phi) = \begin{bmatrix} 1 & 0 & 0 \\ 0 & \cos\Phi & \sin\Phi \\ 0 & -\sin\Phi & \sin\Phi \end{bmatrix}. \tag{2-16}$$

Combining Equations (2-5), (2-10) and (2-15) and adhering to a [Z-Y-X] rotation sequence results in the following equation:

$$\begin{bmatrix} X \\ Y \\ Z \end{bmatrix}_{\{B\}} = \begin{bmatrix} 1 & 0 & 0 \\ 0 & \cos\Phi & \sin\Phi \\ 0 & -\sin\Phi & \cos\Phi \end{bmatrix} \begin{bmatrix} \cos\Theta & 0 & -\sin\Theta \\ 0 & 1 & 0 \\ \sin\Theta & 0 & \cos\Theta \end{bmatrix} \begin{bmatrix} \cos\Psi & \sin\Psi & 0 \\ -\sin\Psi & \cos\Psi & 0 \\ 0 & 0 & 1 \end{bmatrix} \begin{bmatrix} X \\ Y \\ Z \end{bmatrix}_{\{T\}} \tag{2-17}$$

For a lever arm correction, the lever arm coordinates are known in the body fixed coordinates. Equation (2-17) applies to knowing a position vector in tangent plane coordinates and then finding the position in the body fixed coordinates based on the Euler angles. To find the lever arm position vector resolved in the tangent plane coordinates, find the inverse of Equation (2-17). The matrix form that results is conveniently written as

$$\begin{bmatrix} X \\ Y \\ Z \end{bmatrix}_{\{T\}} = INV \left\{ \begin{bmatrix} 1 & 0 & 0 \\ 0 & \cos\Phi & \sin\Phi \\ 0 & -\sin\Phi & \cos\Phi \end{bmatrix} \begin{bmatrix} \cos\Theta & 0 & -\sin\Theta \\ 0 & 1 & 0 \\ \sin\Theta & 0 & \cos\Theta \end{bmatrix} \begin{bmatrix} \cos\Psi & \sin\Psi & 0 \\ -\sin\Psi & \cos\Psi & 0 \\ 1 & 0 & 1 \end{bmatrix} \right\} \begin{bmatrix} X \\ Y \\ Z \end{bmatrix}_{\{B\}}. \tag{2-18}$$

Now, define the rotation matrix, $_B^T R$ as

$$_B^T R = INV \left\{ \begin{bmatrix} 1 & 0 & 0 \\ 0 & \cos\Phi & \sin\Phi \\ 0 & -\sin\Phi & \cos\Phi \end{bmatrix} \begin{bmatrix} \cos\Theta & 0 & -\sin\Theta \\ 0 & 1 & 0 \\ \sin\Theta & 0 & \cos\Theta \end{bmatrix} \begin{bmatrix} \cos\Psi & \sin\Psi & 0 \\ -\sin\Psi & \cos\Psi & 0 \\ 1 & 0 & 1 \end{bmatrix} \right\}. \tag{2-19}$$

which is the rotation from the body fixed coordinates to the tangent plane coordinates. This is more compactly written as

$$_B^T R = INV\{T(\Phi)T(\Theta)T(\Psi)\}. \tag{2-20}$$

29

Now, by taking a known position that is resolved in tangent plane coordinates, say the GPS antenna position, and adding this position to a position vector that is rotated from the body coordinates to the tangent plane coordinate, the result is a position in the body fixed coordinate system that is resolved in a fixed inertial frame of reference. To find a position resolved in tangent plane coordinates given a position resolved in body fixed coordinates with the origins collocated the following equation is applied

$$^{T}P_{1}={}_{B}^{T}R\times{}^{B}P_{1} \qquad (2\text{-}21)$$

where the subscript 1 means a point somewhere in the body fixed coordinate system. Now, by adding this position to the GPS position in the tangent plane coordinate system (fixed in the body frame), results in

$$^{T}P_{1}={}^{T}P_{GPS}+{}_{B}^{T}R\times{}^{B}P_{1}. \qquad (2\text{-}22)$$

which is the addition of two position vectors resolved in the same coordinate system. Equation (2-22) is a simple recipe for performing a lever arm correction.

E.   SEEKER MODELS

This thesis uses both a conical scan on receive only seeker (COSRO) model and a monopulse seeker model to help in the validation process of the DSTSPI algorithms. These models are used because they reflect the most common types of seekers found in a typical missile inventory throughout the world. The parameters chosen for these models are based on typical performance parameters associated with each seeker type. These parameters are summarized in Table 2.1:

Estimated Parameter	COSRO	MONOPULSE
Peak Power, P_T (kilowatts)	250	30
First side lobe Ratio (dB)		24
Frequency, f (GHz)	9	17
Antenna Gain, G (dB)	33	23.4
Half Power Beam Width, θ_{3dB} (degrees)	4.5	8
Noise Bandwidth, B (MHz)	10	10
Noise Figure, F (dB)	11	9.5
Range resolution (meters)	100	20
Number of Pulses Integrated, n	100	100

Table 2.1: Estimated seeker parameters

1. Single Pulse Signal to Noise Ratio

The first step in modeling a seeker is to estimate the signal to noise ratio (**S/N**) as a function of the range between the seeker and the target. First, an assumption must be made about the radar cross section of the target, σ. In general, the radar cross section of a typical naval surface combatant is of the order of **3000 m²**. [Ref. 5, p. 129]

The peak power radiated by any radar transmitter is defined as P_T in watts. The power density at a given range, **R**, from an omnidirectional antenna is given by [Ref. 7] and [Ref. 4, p. 10] as

$$\frac{P_T e^{-\alpha R}}{4\pi R^2} \tag{2-23}$$

where α is the attenuation coefficient given in nepers/km. The attenuation coefficient is estimated to be 0.055 dB/km at both 9 and 17 GHz. [Ref. 4, p. 278]

The power density from a directional antenna with an antenna gain of G_T is given by

$$\frac{P_T G_T e^{-\alpha R}}{4\pi R^2} . \qquad (2\text{-}24)$$

The power that is intercepted by the target and re-radiated back to the radar antenna is given by

$$\frac{P_T G_T \sigma e^{-\alpha R}}{4\pi R^2} \qquad (2\text{-}25)$$

where σ is the radar cross section of the target in square meters. [Ref. 4, p. 11]

The power density received from the re-radiated power is given by

$$\frac{P_T G_T \sigma e^{-2\alpha R}}{\left(4\pi R^2\right)^2} \qquad (2\text{-}26)$$

since the attenuation and spreading are over twice the distance.

The signal collected by the antenna is given by

$$\frac{P_T G_T A_R \sigma e^{-2\alpha R}}{\left(4\pi\right)^2 R^4} \qquad (2\text{-}27)$$

where A_R is the effective area of the receiving antenna which is equivalent to

$$A_r = \frac{G_R \lambda^2}{4\pi} . \qquad (2\text{-}28)$$

Now, by assuming the transmitted gain of the antenna, G_T, is equivalent to the received gain of the antenna, G_R, the received signal power is approximated by the following:

$$\frac{P_T G_T^2 \sigma e^{-2\alpha R} \lambda^2}{\left(4\pi\right)^3 R^4} , \text{(watts)}. \qquad (2\text{-}29)$$

Now, define the noise power in the receiver as

32

$$NOISE = kTBF \text{ , (watts),} \tag{2-30}$$

where **k** is Boltzman's constant, **T** is the temperature in degrees Kelvin, **B** is the receiver noise bandwidth and **F** is the receiver noise figure. The temperature is assumed to be 300 degrees Kelvin. Therefore, **kT** is **4.14 x 10^{-21}** watts/Hz at **300 K**. The single pulse signal to noise ratio is defined as the signal power collected by the antenna divided by the noise in the receiver or

$$(S/N)_m = \frac{P_T G_T^2 \sigma e^{-2\alpha R} \lambda^2}{(4\pi)^3 R^4 (kTBF)}. \tag{2-31}$$

Given the single pulse signal to noise ratio as a function of range, the precision in the angular measurement for a COSRO and monopulse seeker can be evaluated.

2. COSRO Seeker

For a COSRO type seeker, the error caused by thermal noise over the **n** pulses integrated by the servo loop in each coordinate (azimuth and elevation) is [Ref. 4, p. 383]

$$\sigma_\theta = \frac{\theta_{3dB} \sqrt{L_k}}{k_s \sqrt{(S/N)_m \, n}} \tag{2-32}$$

where **k$_s$** is the conical-scan error slope, **(S/N)$_m$** is the single pulse signal to noise ratio, **n** is the number of pulses being integrated and **L$_k$** is the crossover loss due to beam squint.

33
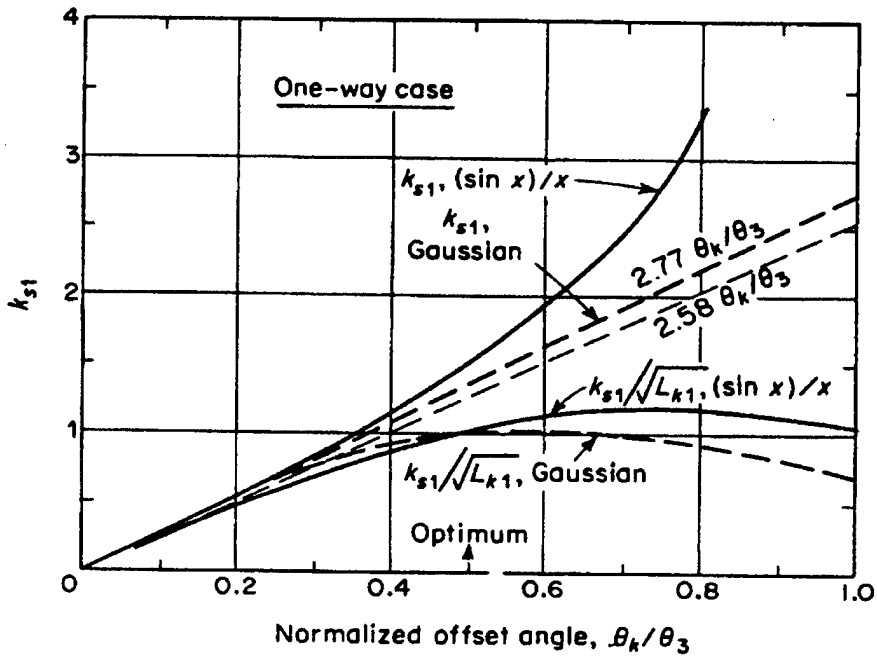
Figure 2.16: One-way error slope [Ref. 4, p.389]

The conical scan error slope, k_s, and the crossover loss, L_k, are shown in Figure 2.16 as a function of the normalized squint (offset) angle, θ_k/θ_{3dB}. It is assumed that the beam has a Gaussian shape which results in an optimum error slope of **1.0** at a normalized offset angle of **0.5**.

With $k_s/\sqrt{L_k} = 1$, the error due to thermal noise becomes

$$\sigma_\theta = \frac{\theta_{3dB}}{\sqrt{(S/N)_m n}} . \qquad (2\text{-}33)$$

The scintillation error associated with a conical scan seeker is given by

$$\sigma_s = 0.225 \left(\frac{\theta_{3dB}}{f_s k_s} \right) \sqrt{\frac{\beta_n}{t_c'}} \qquad (2\text{-}34)$$

34

where t_c' is the envelope correlation time, f_s is the nutation frequency, and β_n is the servo bandwidth. Assuming a target with an envelope correlation time $t_c' = 0.06$ s, a scan frequency of $f_s = 60$ Hz and a servo bandwidth $\beta_n = 2$ Hz, for an optimized squint angle $\theta_k = 0.5\theta_{3dB}$ results in a scintillation error of

$$\sigma_s = 0.0125\theta_{3dB} . \tag{2-35}$$

The total error in the precision of the angular measurement for a conical scan seeker is found by adding Equations (2-33) and (2-35). The error in the angular measurement, $\delta\theta$, or $\delta\phi$ is assumed to be Gaussian distributed and is given by

$$\delta\theta = \delta\phi = \frac{1}{\sqrt{2\pi\left(\sigma_s^2 + \sigma_\theta^2\right)}} e^{-\frac{1}{2}\left(\frac{\theta-\theta_{true}}{\sigma_s+\sigma_\theta}\right)^2} , \tag{2-36}$$

where σ_s is a function of the single pulse signal to noise ratio. These equations and the parameter estimations found in Table 2.1 are used to develop a model for a COSRO seeker type.

3. Monopulse Seeker

The next step is to find the precision of the angular measurement for a monopulse seeker. The precision of the angular measurement in a thermal noise environment is

$$\sigma_{\theta MP} = \frac{\theta_{3dB}}{k_m \sqrt{2(S/N)n}} . \tag{2-37}$$

Here, k_m is the difference slope and n is the number of pulses being integrated. The value for the monopulse error slope is determined from Figure 2.17. It is assumed that the shape

35

of the pulse is Gaussian. From Figure 2.17 with a first sidelobe of 24 dB, the value of k_m

is approximately 1.9.
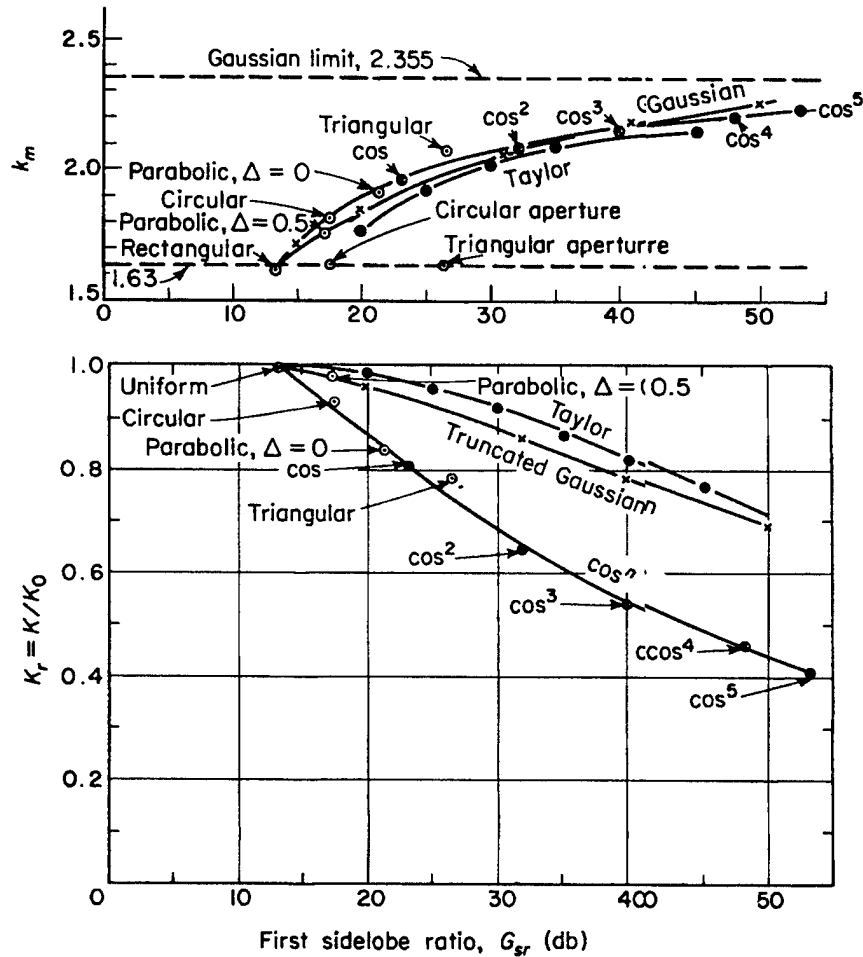
Figure 2.17: Difference slope versus sidelobe level [Ref. 4,p. 403]

The error in the angular measurement, $\delta\theta$, or $\delta\phi$ is assumed to be Gaussian

distributed and is given by

$$\delta\theta = \delta\phi = \frac{1}{\sqrt{2\pi\left(\sigma_{\theta MP}\right)^2}} e^{-\frac{1}{2}\left(\frac{\theta - \theta_{true}}{\sigma_{\theta MP}}\right)^2} \quad ,$$

(2-38)

36

where σ_s is a function of the single pulse signal to noise ratio. These equations and the parameter estimations found in Table 2.1 are used to develop a model for a monopulse seeker type.

III. ALGORITHM DEVELOPMENT

A. GENERAL DESCIPTION OF ALGORITHM

This section provides a general description of the DSTSPI algorithms. One of the goals of the DSTSPI algorithms is to minimize the errors in the derived target position due to the displacement of the GPS antenna from the positions of the distributed ASM seekers and the pitch, roll and yaw of the P-3. As mentioned in Chapter II, this is accomplished by using lever arm corrections. Another goal of the DSTSPI algorithms is to provide the necessary coordinate transformations and corrections to the seeker-to-target information resulting in a derived target position in a fixed inertial coordinate system.

Figure 3.1 depicts the overall functionality for the algorithm. The integration algorithms perform the necessary lever arm corrections and compute the pitch and yaw of each Simulator. The output from the integration algorithms in conjunction with the target data received from the ASM seekers is used to derive the target position in a fixed inertial frame of reference.

DISTRIBUTED SENSOR TSPI

P-3 POSITION @ CG
AND PITCH, ROLL,
AND YAW

P-3 POSITION @
GPS ANTENNA

SENSOR POSITIONS
ON P-3

INTEGRATION ALGORITHMS

SEEKER#1 AND SEEKER#2
POSITIONS, SIMULATOR#1
AND SIMULATOR#2
YAW AND PITCH

DERIVE TGT POSITION

RANGE
AZIMUTH
ELEVATION
TO TGT

DERIVED TGT POSITION
FROM INS/GPS/RADAR

SENSORS

SEEKER #1

SEEKER #2
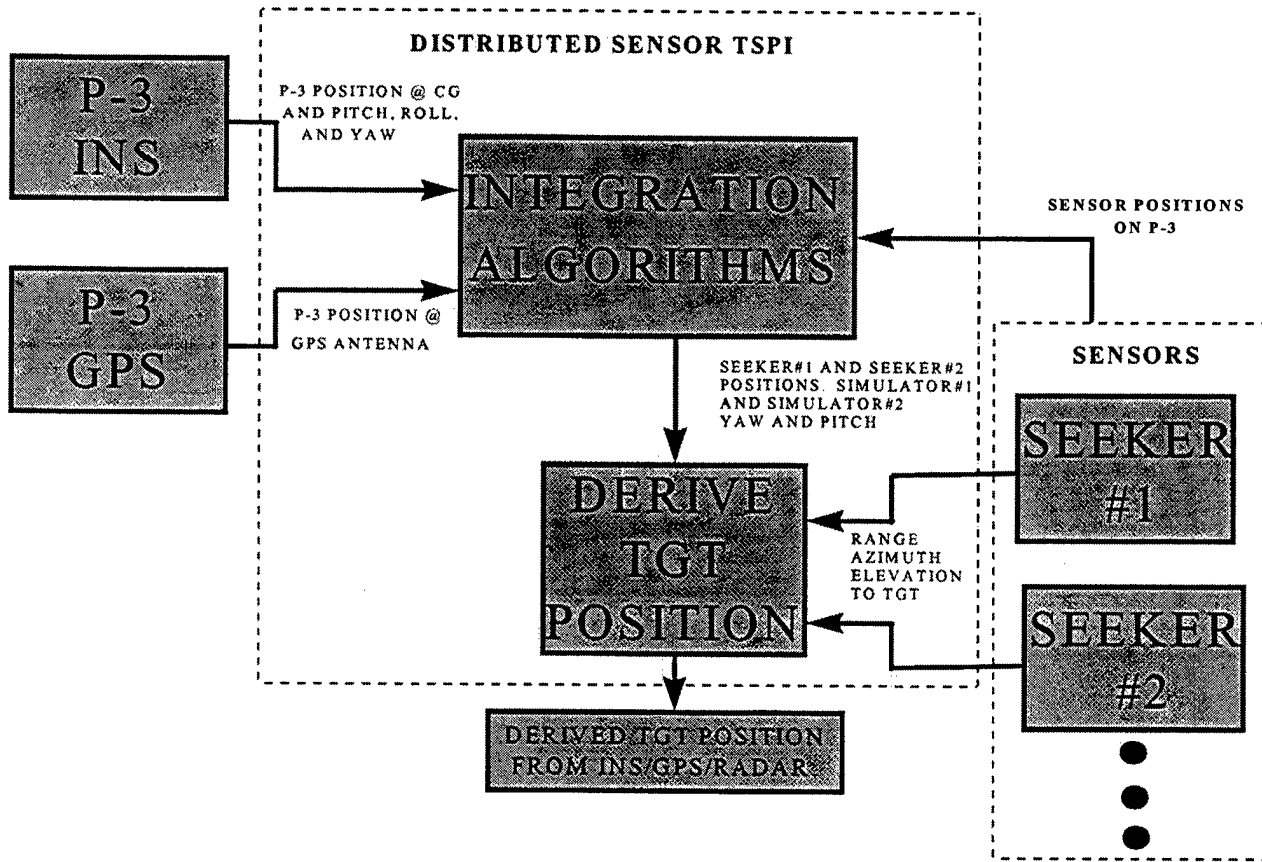
Figure 3.1: General DSTSPI functionality

B.   EXPLANATION OF SIMULINK BLOCK DIAGRAMS

In the development of the DSTSPI algorithm, SIMULINK® is used as the primary

tool for the analysis. SIMULINK is a non-linear simulation package developed by The

MathWorks Inc. for use with MATLAB®. One distinct advantage in using SIMULINK is

that the results can be viewed in real time or sent to a file for post simulation analysis.

Another distinct advantage of SIMULINK is that, like functional block diagrams, it is easy

to see the logical progression of the algorithm. For this reason several SIMULINK block

diagrams are included in this section.

The underlying assumptions for the algorithm are as follows:

- GPS antenna is located at the **[-5m, 0m, 0m]** position in the body fixed coordinates and its position is denoted by P_{ANT}.

- INS is located at the center of gravity of the P-3 which is the origin of the body fixed coordinate system and its position is denoted by P_{CEN}.

- Each Simulator is assumed to be 4 meters in length, which is strictly arbitrary.

- Simulator #1 is located between the body fixed coordinates **[2m, 5m, 0m]** and **[-2m, 5m, 0m]**. The aft position of the Simulator #1 is denoted by P_{A1}. The forward position of the Simulator or the seeker is denoted by P_{F1}.

- Simulator #2 is located between the body fixed coordinates **[2m, -5m, 0m]** and **[-2m, -5m, 0m]**. The aft position of the Simulator #2 is denoted by P_{A2}. The forward position of the Simulator or the seeker is denoted by P_{F2}.

- The target position is denoted by P_{TAR}.

- The derived target position is denoted by P_{Tder}.

- DGPS is used with an update frequency of 10 Hz.

Figure 3.2 shows the relationships of the ASM Simulators and the GPS antenna in the body fixed coordinate system. Here, the values for the positions are given in meters.
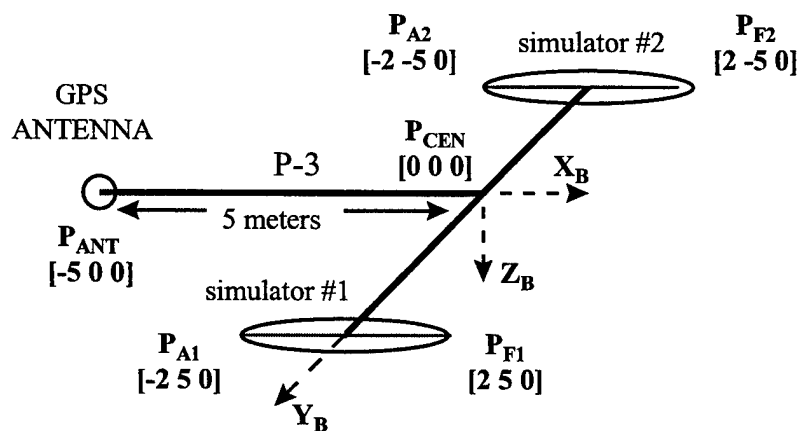
Figure 3.2: Sensors in the body fixed coordinates (positions given in meters)

The notation used in the development of the DSTSPI algorithms is unique and needs to be well defined. The following is a list of notational definitions:

- A superscript in front of the position signifies the coordinate system the position is resolved in. For example, $^B P_{ANT}$ is the GPS antenna resolved in the body fixed coordinates and $^T P_{ANT}$ is the GPS antenna position resolved in the tangent plane coordinate system.

- The rotation matrix is denoted as $^Y_X R$ where X is the coordinate system from which the rotation is occurring and Y is the coordinate system to which the rotation is to occur.

- A primed variable indicates a value with no associated noise added to it. These are the actual or true values associated with the flight of the P-3 (e.g., position, Euler angles, etc.).

- An unprimed variable indicates a value with noise added to it. These are the derived values (e.g. GPS, INS, etc.).
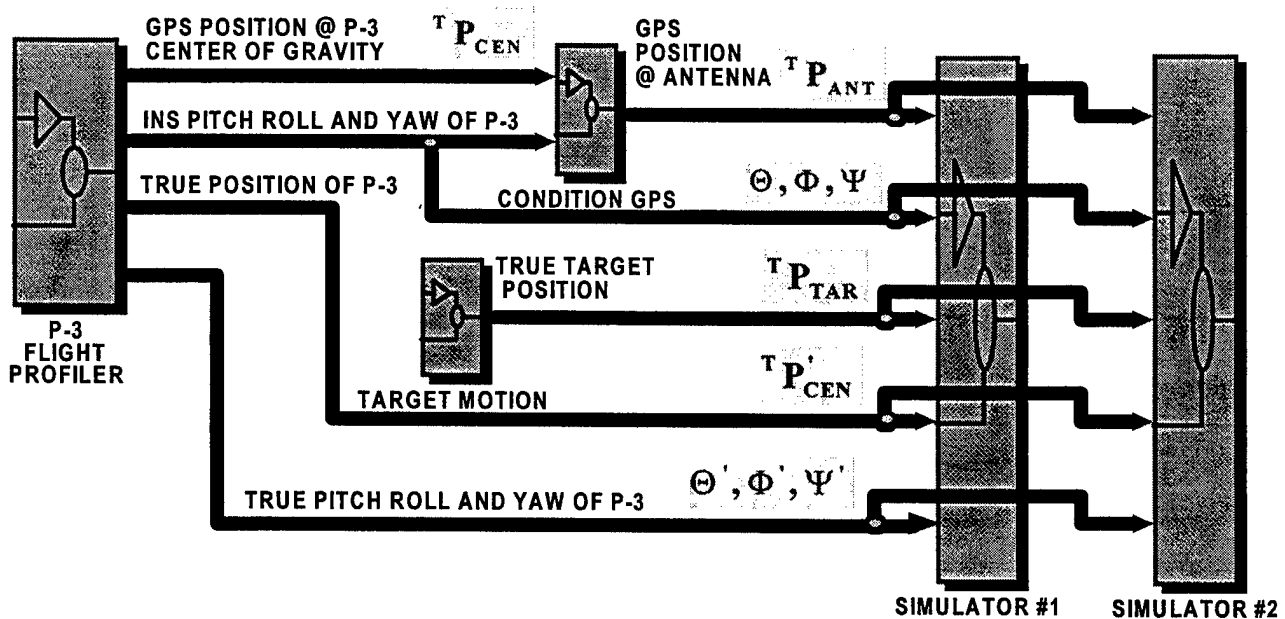
Figure 3.3: DISTRIBUTED SENSOR TSPI Block Diagram

Figure 3.3 is the top-level block diagram for the DSTSPI algorithms. Here, the **"P-3 FLIGHT PROFILER"** provides the GPS position at the aircraft's center of gravity ($^T P_{CEN}$), the INS pitch, roll and yaw(Θ, Φ, Ψ), the true position of the aircraft ($^T P'_{CEN}$) and the true pitch roll and yaw of the aircraft (Θ', Φ', Ψ'). Because the GPS position is the location of the GPS antenna in tangent plane coordinates, the block **"CONDITION GPS"** converts the center of gravity position ($^T P_{CEN}$) to a position located at the GPS antenna ($^T P_{ANT}$). The **"TARGET MOTION"** block generates a target in tangent plane coordinates ($^T P'_{TAR}$) for use in the algorithm and the validation process. The **"SIMULATOR #1"** block is identical to the **"SIMULATOR #2"** block except for the specific values used in the lever arm corrections and the seeker models employed. For this reason, the discussion of the DSTSPI algorithms only includes Simulator #1. The components of the **"SIMULATOR #1"** block are discussed in more detail later in this chapter.
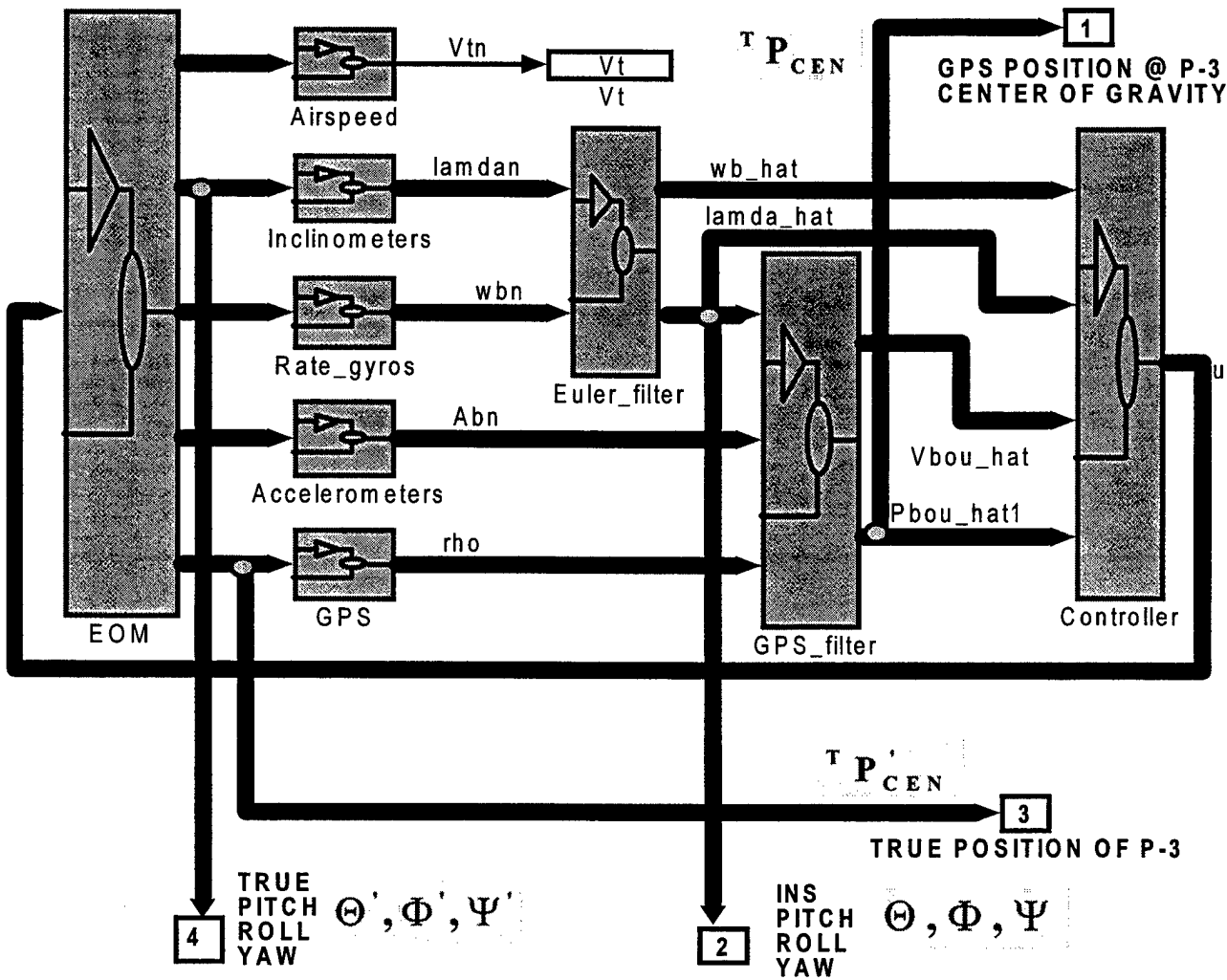
Figure 3.4: P-3 FLIGHT PROFILER Block Diagram

The "P-3 FLIGHT PROFILER" is depicted in Figure 3.4. The development of this part of the model was performed by LT Chuck Gill, et al, as part of a class project in the Aeronautical Engineering Department at the Naval Postgraduate School. A thorough discussion of this part of the algorithm is found in Reference 6. Although this block is an integral part of the analysis, its only function is to provide the outputs required for this algorithm which are assumed to be available on the P-3 test flight vehicle.
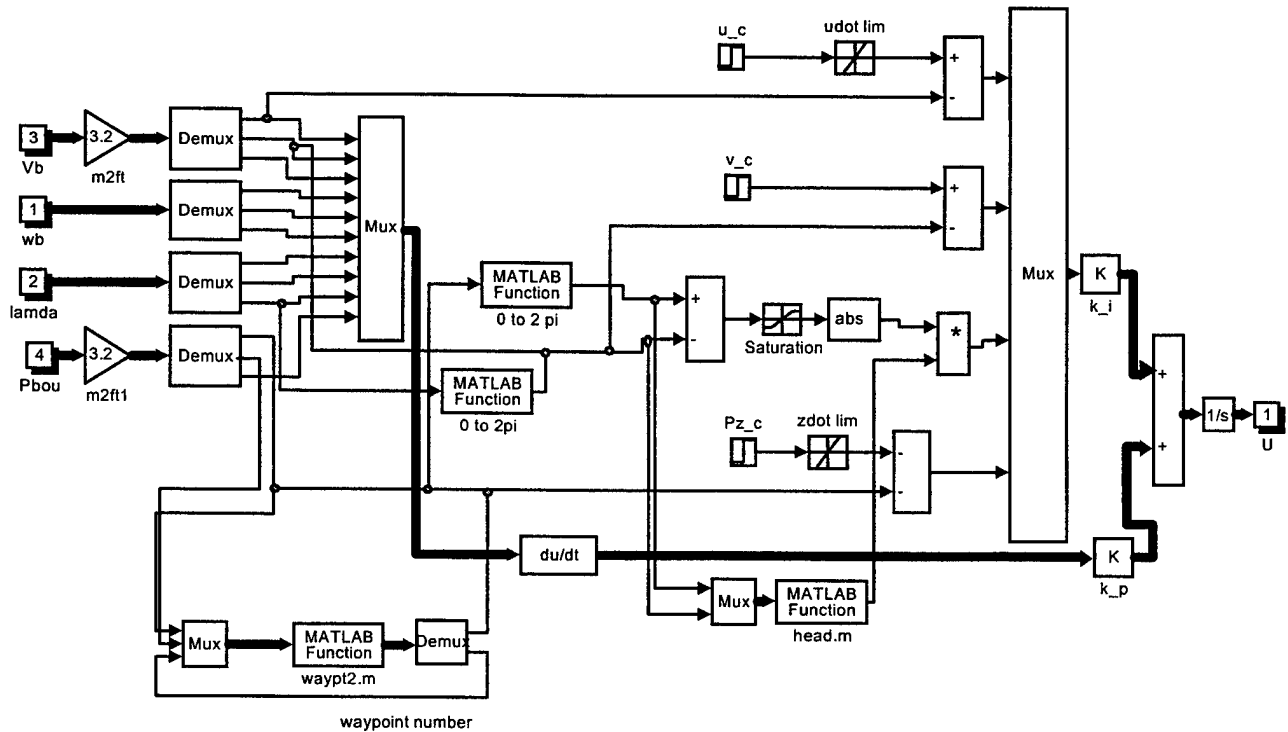
Figure 3.5: P-3 FLIGHT PROFILER CONTROLLER Block Diagram

The controller used with the P-3 flight profiler required a few modifications to make it fully compatible with the DSTSPI algorithm. First, the controller, which is shown in Figure 3.5, is modified to allow the aircraft to steer courses in both the starboard and port directions. Prior to this modification, the aircraft would only turn in the port direction regardless of the ordered course. This correction is made by writing two MATLAB programs which corrects the inconsistencies in the flight controller. These programs are listed in Appendix A as "HEAD.M" and "OVER2PI.M." Another problem corrected is the instabilities in the controller for steer commands greater than, say, 30 degrees. This correction is made by limiting the difference between the ordered steer course and the

45

actual steer course. This gave the controller time to adjust its output to match to required response.
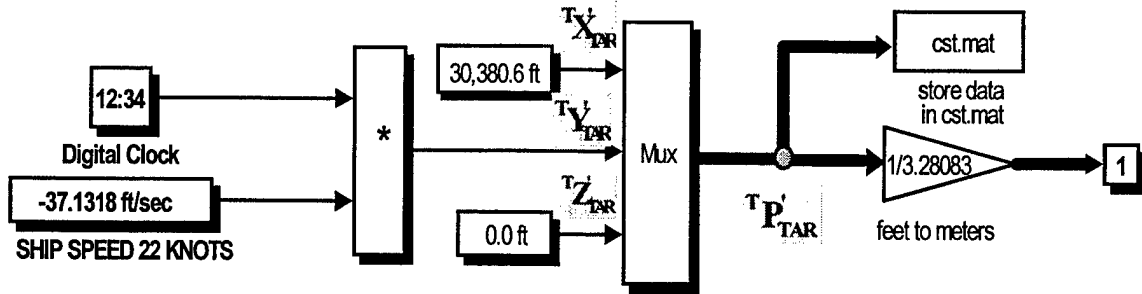
Figure 3.6: TARGET MOTION Block Diagram

The **"TARGET MOTION"** block diagram is shown in Figure 3.6. The target motion is simulated by assuming an initial displacement from the location of the origin of the model's tangent plane coordinate system (which can be any fixed inertial coordinate system). The initial displacement of the target is **[5, 0, 0]** in nautical miles, with the **x** axis pointing toward true North, the **y** axis pointing towards true East and the **z** axis pointing downward. The velocity of the target is fixed at **22 knots** in a westerly direction which translates to **-37.131 feet/second** in the **y** direction. By simply multiplying this fixed rate by the elapsed time a new target position is calculated for each time step. The true position of the target ($^T\mathbf{P}'_{TAR}$) is then stored in the file "CST.MAT" for post simulation analysis. The block is changed to simulate different types of target motion. This is done to obtain the results in Chapter IV.
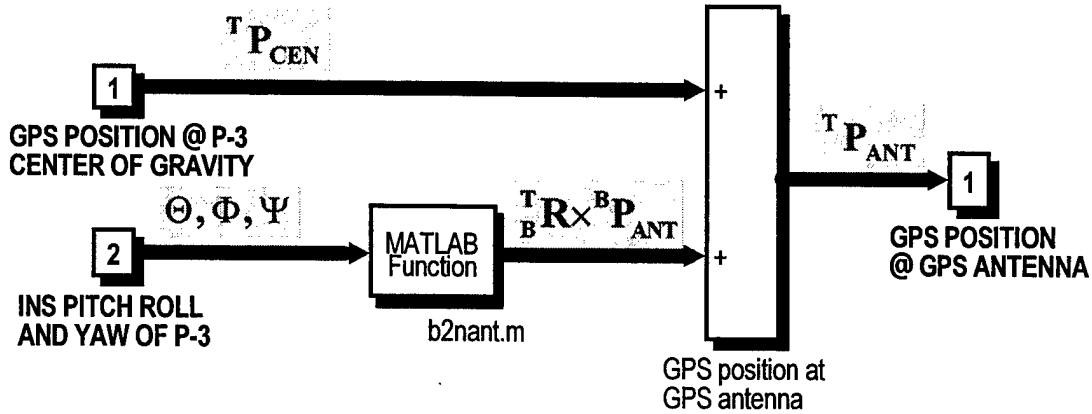
Figure 3.7: CONDITION GPS Block Diagram

The **"CONDITION GPS"** block diagram shown in Figure 3.7 performs a lever

arm correction to translate the GPS position at the center of gravity of the aircraft ($^T\mathbf{P}_{CEN}$)

to the GPS position at the GPS antenna location ($^T\mathbf{P}_{ANT}$). As mentioned earlier, the GPS

antenna is assumed to be at the **[-5, 0, 0]** location in body fixed coordinates. This is done

to invoke realism into the algorithm. In a hardware implementation of this algorithm, the

GPS input would be initially referenced to the antenna location. To perform the lever arm

correction the INS generated values for the pitch, roll and yaw (Θ, Φ, Ψ) are used by the

function "B2NANT.M" to compute the rotation matrix $^T_B\mathbf{R}$. By multiplying the rotation

matrix and the position $^B\mathbf{P}_{ANT}$ and, then, adding the result to the GPS position located at

the center of gravity of the P-3, results in the following:

$$^T\mathbf{P}_{ANT} = {}^T\mathbf{P}_{CEN} + {}^T_B\mathbf{R} \times {}^B\mathbf{P}_{ANT} \qquad (3\text{-}1)$$

$^T P_{ANT}$

1

GPS POSITION
@ ANTENNA

Θ, Φ, Ψ

2

INS PITCH, ROLL
AND YAW OF P-3

P-3
INTEGRATION

$^T P_{FI}$ INS/GPS DERIVED POSITION OF SEEKER #1

Ψ_{SIM} INS/GPS DERIVED SIMULATOR YAW

Θ_{SIM} INS/GPS DERIVED SIMULATOR PITCH

SIMULATOR AZIMUTH,
ELEVATION AND RANGE
BETWEEN SEEKER #1
AND TARGET

INS/GPS/RADAR
DERIVED TARGET
POSITION

$^T P'_{TAR}$

3

TRUE TARGET
POSITION $^T P'_{CEN}$

4

TRUE POSITION
OF P-3 Θ', Φ', Ψ'

5

TRUE PITCH,
ROLL AND YAW
OF P-3

TRUTH MODEL

TRUE AZIMUTH
ELEVATION AND RANGE
BETWEEN SEEKER #1
AND TARGET

R'

$AZ' - \Psi'_{SIM}$

$EL' - \Theta'_{SIM}$

$^T P'_{FI}$ TRUE POSITION OF SEEKER #1

Ψ'_{SIM} TRUE SIMULATOR YAW

Θ'_{SIM} TRUE SIMULATOR PITCH

TRUE TARGET POSITION

R_{DER}

$AZ - \Psi'_{SIM}$

$EL - \Theta'_{SIM}$

SEEKER MODEL
FOR CONICAL
SCAN RADAR

TRUE DERIVED
TARGET POSITION

Figure 3.8: SIMULATOR #1 Block Diagram

The **"SIMULATOR #1"** block diagram is shown in Figure 3.8. This block

diagram performs several functions. First, it performs the integration of INS, GPS and the

ASM Simulator to derive a target position in the tangent plane coordinate system. Second,

it performs the same integration again but with true values for the relevant positions and

Euler angles of the P-3. In this way, the algorithm is validated. Third, this block diagram

stores the DSTSPI derived target positioning data and the true derived target positioning data for post simulation analysis.

To derive the target position from DSTSPI, the GPS antenna position ($^T\mathbf{P}_{ANT}$) and the Euler angles from INS (Θ, Φ, Ψ) are used to find the INS/GPS derived position of seeker #1 ($^T\mathbf{P}_{F1}$) in tangent plane coordinates and the INS/GPS derived yaw (Ψ_{SIM}) and pitch (Θ_{SIM}) of the Simulator. This is accomplished by the **"P-3 INTEGRATION"** block as shown in Figure 3.9. Second, this information derived from INS/GPS is then used in conjunction with the seeker-to-target information (from the seeker model) to derive the target position. The seeker-to-target parameters consist of the range, ($\mathbf{R}_{DER}$), azimuth ($\mathbf{AZ} - \Psi'_{SIM}$) and elevation ($\mathbf{EL} - \Theta'_{SIM}$) between seeker #1 and the target while accounting for the attitude of the Simulator. This information is consistent with the typical output of a seeker and is discussed in more detail later in this chapter.

The true target position ($^T\mathbf{P}'_{TAR}$), the true P-3 position ($^T\mathbf{P}'_{CEN}$) and the true Euler angles (Θ', Φ', Ψ'), are used to derive the true seeker position ($^T\mathbf{P}'_{F1}$), the true Simulator yaw (Ψ'_{SIM}) and pitch (Θ'_{SIM}) in the **"TRUTH MODEL"** block. The true position of seeker #1, the true yaw and pitch of the Simulator, and the true position of the target are used to derive the true seeker-to-target parameters, namely the true range ($\mathbf{R}'$), azimuth ($\mathbf{AZ}' - \Psi'_{SIM}$) and elevation ($\mathbf{EL}' - \Theta'_{SIM}$) between seeker #1 and the target. This information is used to validate the algorithm in the **"TRUE DERIVED TARGET POSITION"** block.
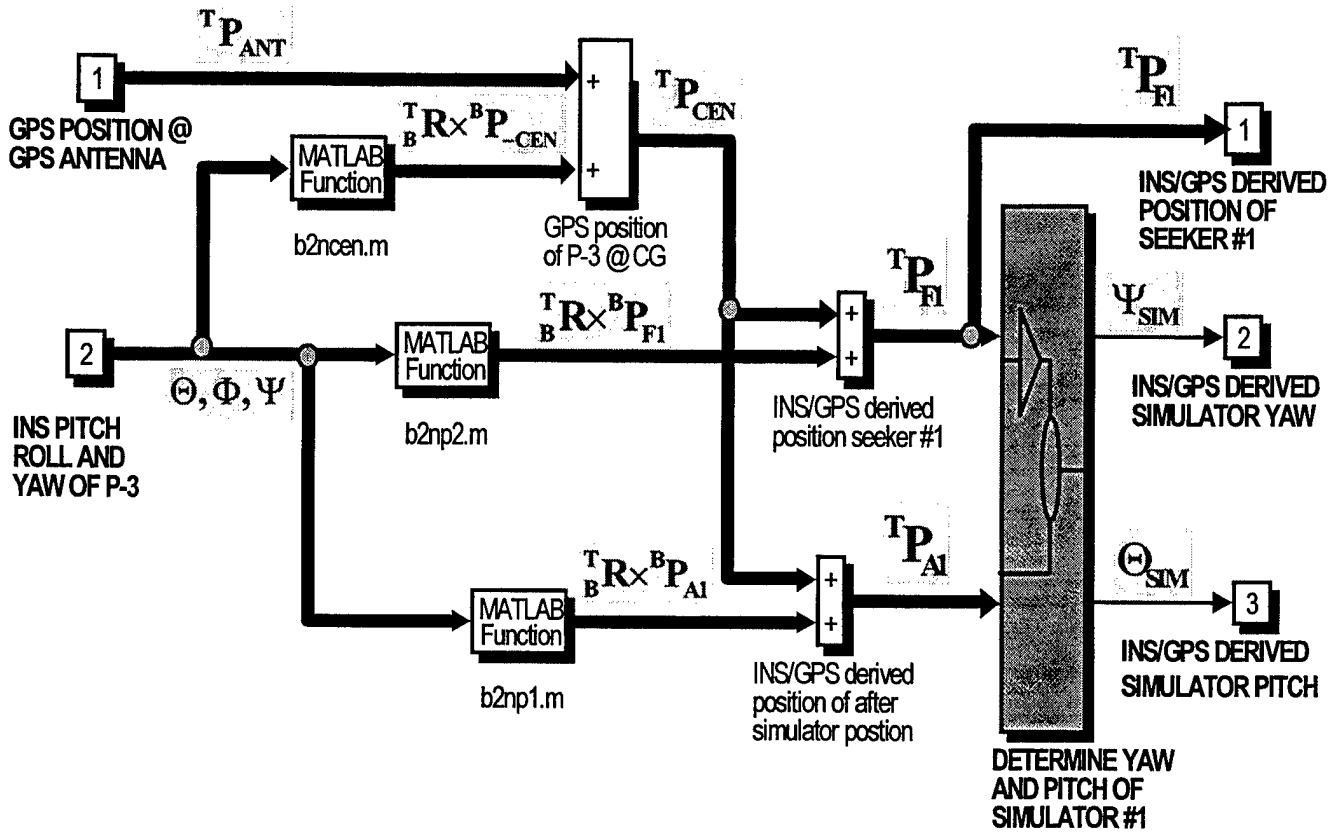
Figure 3.9: P-3 INTEGRATION Block Diagram

The **"P-3 INTERGRATION"** block diagram is shown in Figure 3.9. This block performs several functions. First, it takes the GPS position referenced to the GPS antenna ($^T P_{ANT}$) and lever arm corrects it to the center of gravity of the P-3 ($^T P_{CEN}$). Next, it takes the GPS position referenced to the center of gravity of the P-3 ($^T P_{CEN}$) and lever arm corrects this position to the forward and after positions of the ASM Simulator #1. These positions are denoted as $^T P_{F1}$ and $^T P_{A1}$ respectively. After these lever arm corrections are made, the forward and after positions of Simulator #1 are known in the tangent plane coordinate system. Next, the forward and after positions of Simulator #1 are used to

50

compute the yaw (Ψ_{SIM}) and pitch (Θ_{SIM}) of the Simulator in the tangent plane coordinate system.

Taking the GPS position at the GPS antenna and lever arm correcting it to the GPS position at the center of gravity of the P-3, results in the following:

$$^T\mathbf{P_{CEN}} = {}^T\mathbf{P_{ANT}} + {}^T_B\mathbf{R} \times {}^B\mathbf{P_{-CEN}} \tag{3-2}$$

Where, the value ${}^T_B\mathbf{R} \times {}^B\mathbf{P_{-CEN}}$ is computed by the function "B2NCEN.M" using the instantaneous values for Θ, Φ, Ψ. The negative sign indicates that the lever arm correction is taken from the antenna to the center of the aircraft.

Now, by using the GPS position at the center of gravity of the P-3 resolved in tangent plane coordinates and lever arm correcting it to the position at seeker #1, the following result is obtained:

$$^T\mathbf{P_{F1}} = {}^T\mathbf{P_{CEN}} + {}^T_B\mathbf{R} \times {}^B\mathbf{P_{F1}} \tag{3-3}$$

Where the value ${}^T_B\mathbf{R} \times {}^B\mathbf{P_{F1}}$ is computed by the function "B2NP2.M" using the instantaneous values for Θ, Φ, Ψ.

Likewise, taking the GPS position at the center of gravity of the P-3 and lever arm correcting it to the after part of Simulator #1, results in the following:

$$^T\mathbf{P_{A1}} = {}^T\mathbf{P_{CEN}} + {}^T_B\mathbf{R} \times {}^B\mathbf{P_{A1}} \tag{3-4}$$

Where the value ${}^T_B\mathbf{R} \times {}^B\mathbf{P_{A1}}$ is computed by the function "B2NP1.M" using the instantaneous values for Θ, Φ, Ψ. The functions "B2NP2.M" and "B2NP1.M" are found in Appendix A.

Given the forward and after positions of the Simulator #1 resolved in tangent plane coordinates, the yaw and pitch of Simulator #1 is determined. This is accomplished by using the "DETERMINE YAW AND PITCH OF SIMULATOR #1" block which is depicted in Figure 3.10.
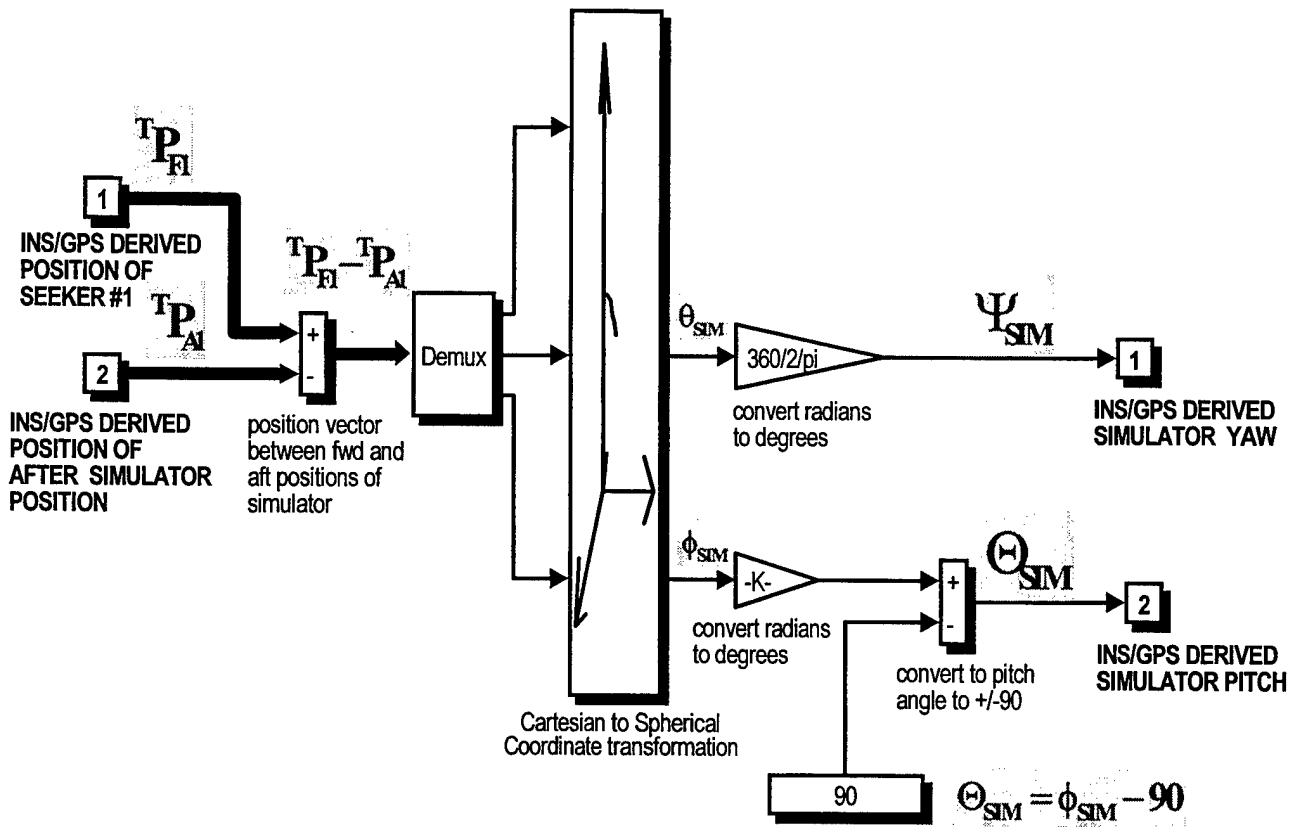

Figure 3.10: DETERMINE YAW AND PITCH OF SIMULATOR #1 Block Diagram

To determine the yaw and pitch of Simulator #1, first, the difference is taken between the forward and after positions of the Simulator. This is given by $^T P_{F1} - ^T P_{A1}$. This result is a position vector resolved in the tangent plane coordinate system. The length of this vector is equivalent to the absolute length of the Simulator. The angles this

52

position vector make with the tangent plane are defined in terms of spherical coordinates as shown in Figure 3.11.
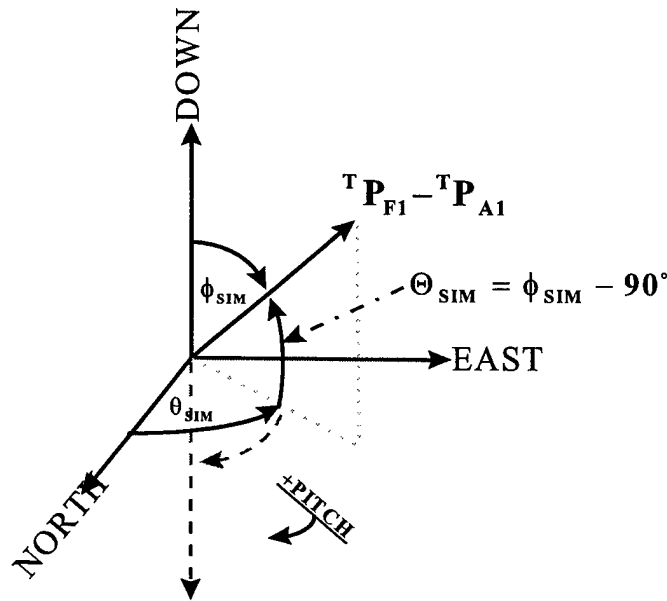

Figure 3.11: Difference between forward and aft Simulator positions resolved in spherical coordinates

From Figure 3.11 we see that the yaw angle is equivalent to the angle θ_{SIM} and the pitch angle is equivalent to Θ_{SIM}. The pitch angle is defined to be positive from true horizontal to a vertical elevation and negative from true horizontal to straight downward. Because the tangent plane coordinate system is defined in a **NED** orientation, the Cartesian to spherical coordinate transformation results in the wrong polarity for the pitch. This is why the pitch angle is equal to $\phi_{SIM} - 90°$ vice $90° - \phi_{SIM}$. The Simulator yaw angle, θ_{SIM} is defined in terms of the Eulerian notation, Ψ_{SIM} or $\Psi_{SIM} = \theta_{SIM}$.
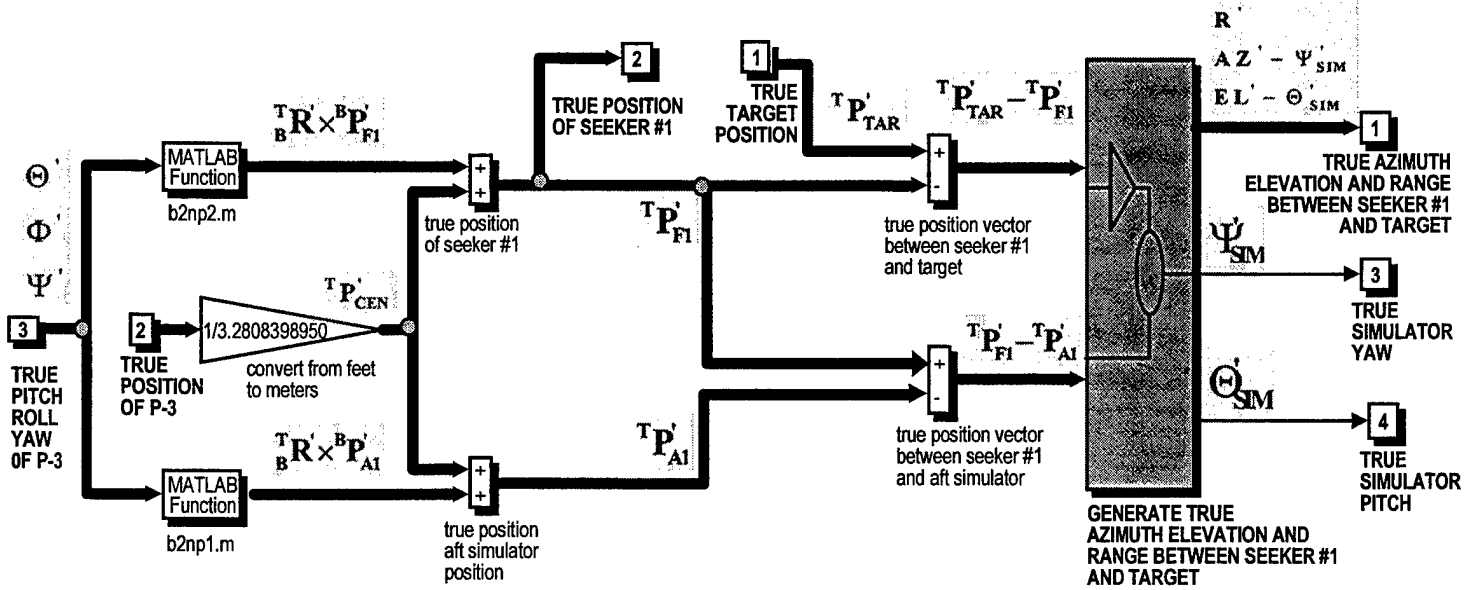
Figure 3.12: TRUTH MODEL Block Diagram

The block entitled **"TRUTH MODEL"** is shown in Figure 3.12. This block performs the some of the same basic functions as the **"P-3 INTEGRATION"** block as explained earlier in this chapter. First, it takes the true position of the P-3 referenced to the center of gravity of the aircraft ($^T P'_{CEN}$) and lever arm corrects this position to the forward and after positions of the ASM Simulator #1. These true positions are denoted as $^T P'_{F1}$ and $^T P'_{A1}$ respectively. Next, it takes forward and aft positions of Simulator #1 and computes the yaw (Ψ_{SIM}) and pitch (Θ_{SIM}) of the Simulator in the tangent plane coordinates by way of the **"GENERATE TRUE AZIMUTH ELEVATION RANGE BETWEEN SEEKER AND TARGET"** block as shown in Figure 3.13. Also, the difference is taken between the true seeker position and the true target position which results in the value $^T P'_{TAR} - ^T P'_F$. This value is used in Figure 3.13 to compute the true

54

seeker-to-target parameters namely the range (R'), the azimuth ($AZ' - \Psi'_{SIM}$) and the elevation ($EL' - \Theta'_{SIM}$).
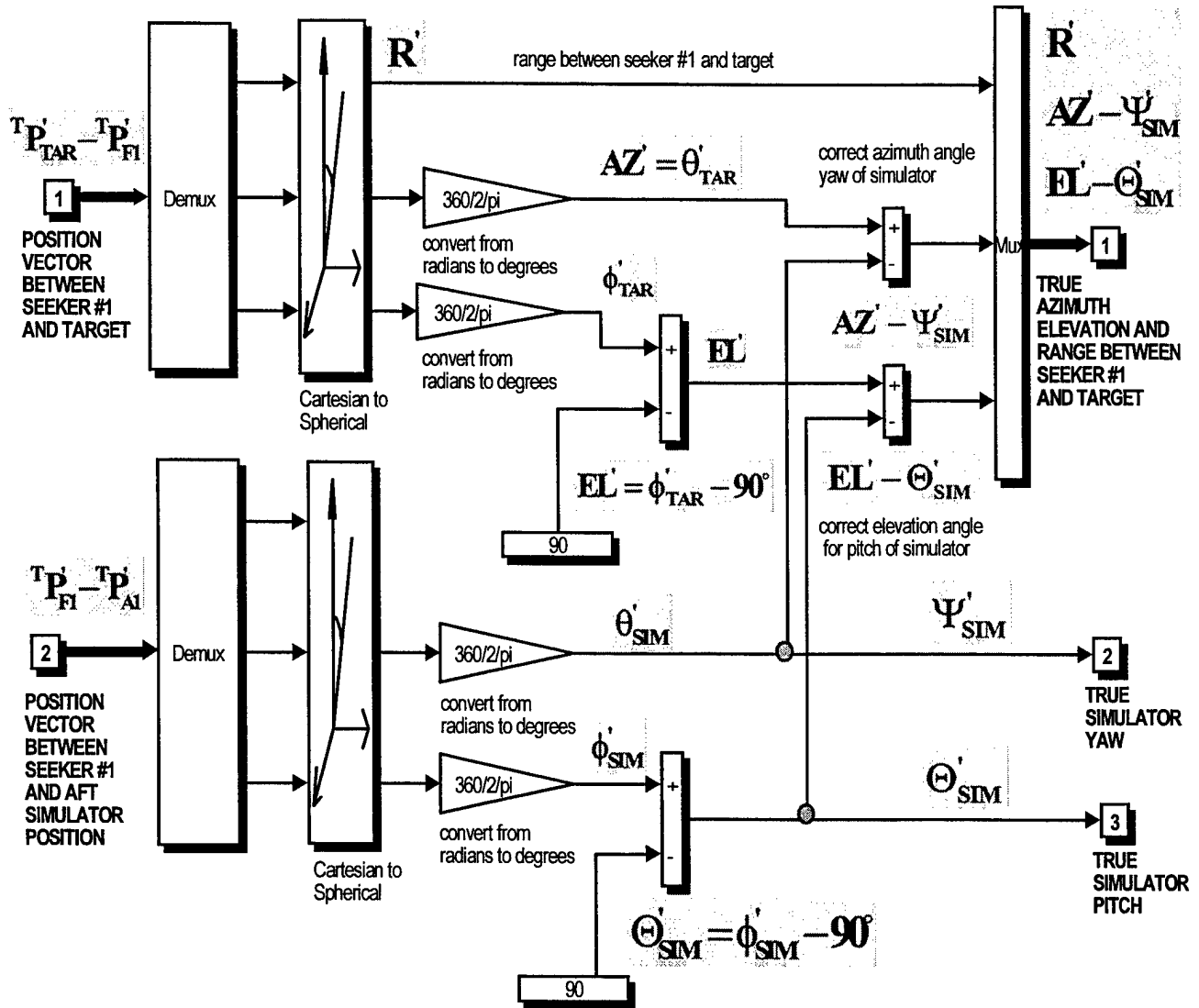

Figure 3.13: GENERATE TRUE AZIMUTH ELEVATION AND RANGE BETWEEN SEEKER #1 AND TARGET Block Diagram

Now, by using the true position at the center of gravity of the P-3 resolved in tangent plane coordinates and lever arm correcting it to the position at seeker #1, the following result is obtained:

55

$$^T\mathbf{P}'_{F1} = {^T}\mathbf{P}'_{CEN} + {^T_B}\mathbf{R}' \times {^B}\mathbf{P}'_{F1} \tag{3-5}$$

Where the value ${^T_B}\mathbf{R}' \times {^B}\mathbf{P}'_{F1}$ is computed by the function "B2NP2.M" using the instantaneous values for $\Theta', \Phi'.\Psi'$. Likewise, taking the true position at the center of gravity of the P-3 and lever arm correcting it to the after part of Simulator #1, results in the following :

$$^T\mathbf{P}'_{A1} = {^T}\mathbf{P}'_{CEN} + {^T_B}\mathbf{R}' \times {^B}\mathbf{P}'_{A1} \tag{3-6}$$

Where the value ${^T_B}\mathbf{R}' \times {^B}\mathbf{P}'_{A1}$ is computed by the function "B2NP1.M" using the instantaneous values for $\Theta', \Phi'.\Psi'$. Next, the true values of the forward and after positions of the Simulator #1 and the position vector between seeker #1 and the target are used in the SIMULINK block diagram pictured in Figure 3.13 to find the true yaw and pitch of the Simulator. To determine the true yaw and pitch of Simulator #1, the difference between the forward and after positions of the Simulator, $^T\mathbf{P}'_{F1} - {^T}\mathbf{P}'_{A1}$, is used. This is a position vector resolved in the tangent plane coordinates. Again, the angles this position vector make with the tangent plane are defined in terms of spherical coordinates. (Refer to Figure 3.11.) Using the same argument that was used in the derivation of the INS/GPS derived yaw and pitch, the true yaw angle of Simulator #1 is equivalent to the angle Ψ'_{SIM} and the true pitch angle of Simulator #1 is equivalent to Θ'_{SIM}. These values are obtained form the following equations:

$$\Psi'_{SIM} = \theta'_{SIM} \tag{3-7}$$

$$\Theta'_{SIM} = \phi'_{SIM} - 90° \tag{3-8}$$

Next, calculate the seeker-to-target parameters by using the value for the difference between the true seeker position and the true target position, $^{T}P'_{TAR} - {}^{T}P'_{F1}$, and the true yaw and pitch of Simulator #1. The value for $^{T}P'_{TAR} - {}^{T}P'_{F1}$ is a position vector resolved in tangent plane coordinates. The angles this vector makes with the tangent plane are defined by a Cartesian to spherical coordinate transformation. This is seen in Figure 3.14.
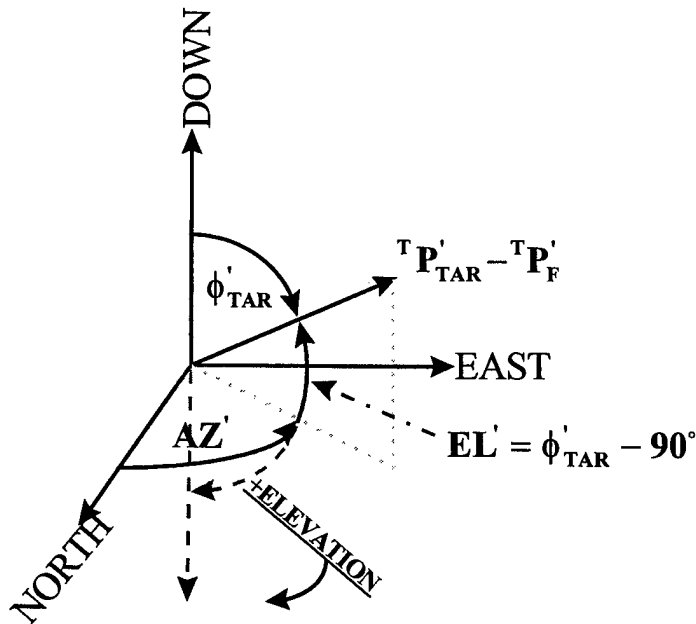

Figure 3.14: Difference between true seeker and target positions resolved in spherical coordinates

Here, the angle AZ' is the true azimuth angle between seeker #1 and the target without consideration for the yaw angle of the Simulator. The angle EL' is the elevation angle between seeker #1 and the target without consideration for the pitch angle of the Simulator and is defined with respect to horizontal. The values for AZ' and EL' are given by the following equations:

$$AZ' = \theta'_{TAR} \qquad\qquad (3\text{-}9)$$

$$EL' = \phi'_{TAR} - 90° \qquad\qquad (3\text{-}10)$$

To find the true azimuth angle between the seeker and the target, the azimuth must be compensated by an amount equal to the yaw angle of the Simulator. The goal is to get a value for the azimuth angle that is an expected output of the Simulator. A typical radar would not account for its orientation with its surroundings when giving its output. The result after compensation is $AZ' - \Psi'_{SIM}$. The true yaw angle of the Simulator is subtracted from the true azimuth angle to maintain consistency with true North. If, for example, the Simulator is pointing due East or 90° and the azimuth angle between the seeker and the target is also taken to be due East or 90°, then we would expect the Simulator to return an angle of zero for the azimuth.

Now, using the same reasoning, calculate a compensated elevation angle between the seeker and the target. This is given as $EL' - \Theta'_{SIM}$.

The true range between the seeker and the target is a easily obtained from the Cartesian to spherical coordinate transformation on the position vector $^T P'_{TAR} - {}^T P'_{F1}$ since the range does not care about what the Simulator is doing. This is given as R'.

To validate the algorithm, the **"TRUE DERIVED TARGET POSITION"** block diagram as pictured in Figure 3.15 is used. The goal of this block diagram is to find the target position in tangent plane coordinates using true values for inputs. This is accomplished be first taking the true seeker #1 to target parameters and correcting these

58

values for the true yaw and pitch of the Simulator. This allows for the extraction of the true position vector between the seeker and the target via a coordinate transformation.
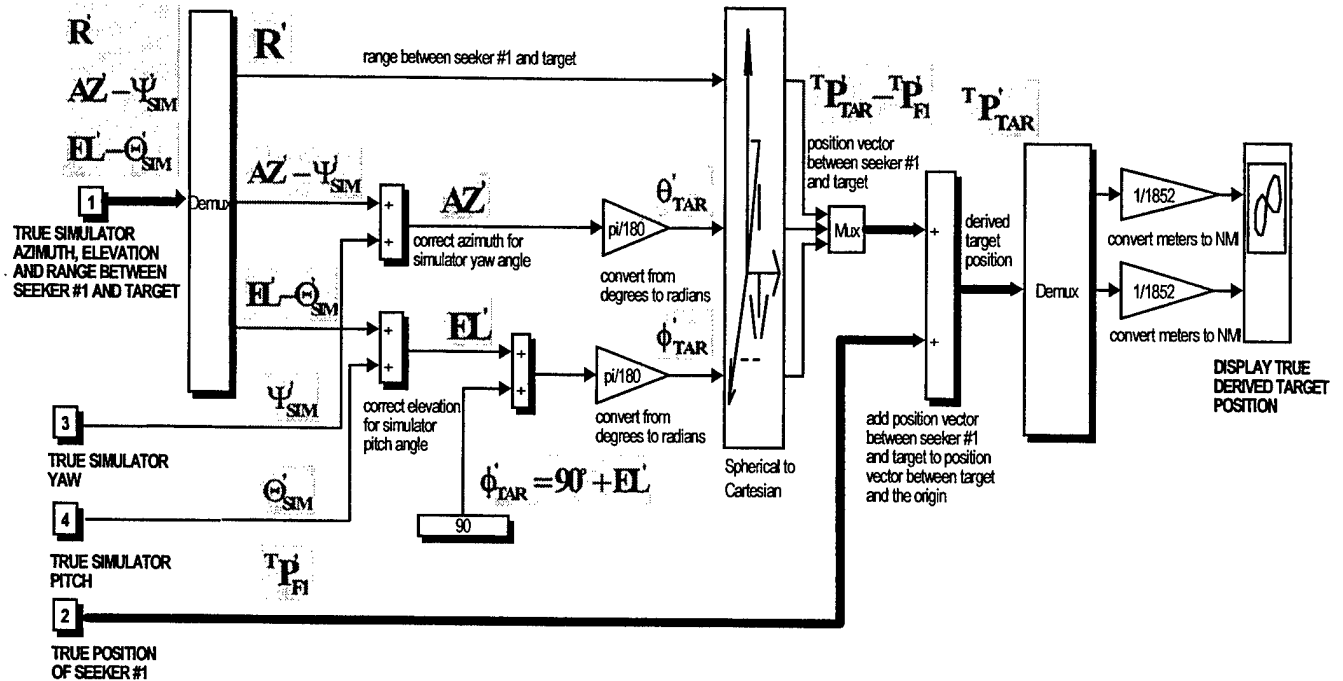

Figure 3.15: TRUE DERIVED TARGET POSITION Block Diagram

Given the true seeker to target parameters, $\mathbf{R}'$, $\mathbf{AZ}' - \Psi'_{SIM}$ and $\mathbf{EL}' - \Theta'_{SIM}$, first these values must be corrected for the true yaw and pitch of the Simulator. This is done by adding the respective values in the following manner:

$$\mathbf{AZ}' = \mathbf{AZ}' - \Psi'_{SIM} + \Psi'_{SIM} \tag{3-11}$$

$$\mathbf{EL}' = \mathbf{EL}' - \Theta'_{SIM} + \Theta'_{SIM} \tag{3-12}$$

If this correction were not made, the spherical to Cartesian coordinate transformation would result in severe displacement errors from the yaw and pitch of the Simulator. The elevation angle, as mentioned earlier, is defined with respect to horizontal. To put the elevation term in spherical coordinates simply add 90 degrees, or $\phi'_{TAR} = 90° + \mathbf{EL}'$.

59

Next, perform a spherical to Cartesian coordinate transformation. The result in tangent plane coordinates is the position vector $^T\mathbf{P}'_{TAR} - {}^T\mathbf{P}'_{F1}$. By adding the true position of seeker #1 to this quantity, the result is the true target position in tangent plane coordinates. This is seen in the following equation:

$$^T\mathbf{P}'_{TAR} = {}^T\mathbf{P}'_{TAR} - {}^T\mathbf{P}'_{F1} + {}^T\mathbf{P}'_{F1} \qquad (3\text{-}13)$$

The next step in the algorithm development is to talk about the seeker model for the conical scan radar. The block diagram entitled **"SEEKER MODEL FOR CONICAL SCAN RADAR"** is shown in Figure 3.16. The three parameters that are relevant to this algorithm are the range, elevation and azimuth angle between the modeled seeker and the target while accounting for the ASM Simulator's attitude. The output of a real seeker, as mentioned earlier, does not account for its surroundings. It only knows the target in a relative sense.
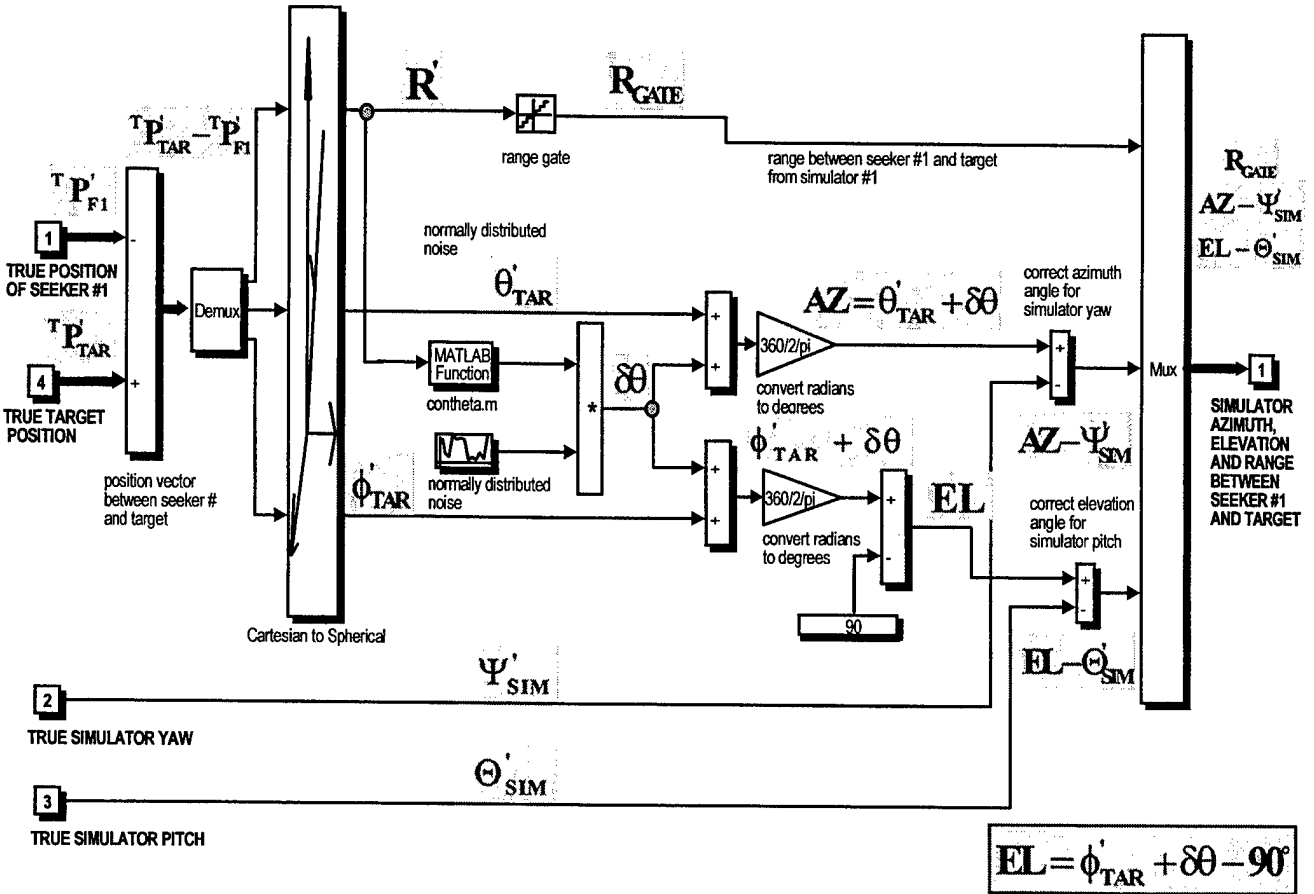
Figure 3.16: SEEKER MODEL FOR CONICAL SCAN RADAR Block Diagram

Because the information received from the seeker is not referenced to a particular coordinate system, true values for the position of the seeker are used to derive the seeker to target parameters. Also, because the attitude of the seeker is not accounted for in its output, true values for the yaw and pitch of the seeker are used.

Referring to Figure 3.16, first the difference is taken between the true seeker position and the true target position which results in the value $^{T}P'_{TAR} - {}^{T}P'_{F1}$. This value is used to help compute the modeled seeker to target parameters. The value for $^{T}P'_{TAR} - {}^{T}P'_{F1}$ is a position vector resolved in tangent plane coordinates. By performing a Cartesian to

spherical coordinate transformation on this position vector, the values R', ϕ'_{TAR}, and θ'_{TAR} are obtained. Note, that these values are based on the true positions of the seeker and the target as denoted by the prime.

Next, the value for R' is quantized in **100 meter** segments to simulate the range resolution of the modeled seeker. The output of the quantizer is R_{GATE}, which is the range between the seeker and the target that has an error component based on the range resolution of the seeker. This quantity is defined as

$$R_{DER} = R_{GATE} \tag{3-14}$$

where "DER" is defined as a derived value.

The MATLAB function "CONTHETA.M" adjusts the precision in the angular resolution of the seeker based on the signal to noise ratio and the scintillation as discussed in Chapter II. A similar MATLAB function, "THETAD.M," performs the same function as "CONTHEATA.M" but for the monopulse seeker model found in the block diagram entitled **"SIMULATOR #2"** The signal to noise ratio changes as a function of the range between the seeker and the target. The angular resolution is normally distributed resulting in the value $\delta\theta$. The value for $\delta\theta$ contributes errors in both directions of the solid angle subtended by the radar beam and, therefore, must be added to both θ'_{TAR} and ϕ'_{TAR}.

The angle **AZ** is the azimuth angle between seeker #1 and the target without considering the yaw angle of the Simulator. Likewise, the angle **EL** is the elevation angle between seeker #1 and the target without considering the pitch angle of the Simulator and is defined with respect to horizontal. The values for **AZ** and **EL** are given by the following equations:

$$AZ = \theta'_{TAR} + \delta\theta \qquad\qquad (3\text{-}15)$$

$$EL = \phi'_{TAR} + \delta\theta - 90° \qquad\qquad (3\text{-}16)$$

The azimuth angle between the seeker and the target after compensating for the true yaw of the Simulator is $AZ - \Psi'_{SIM}$. Again, the true yaw angle of the Simulator is subtracted from the azimuth angle to maintain consistency with true North. The elevation angle between the seeker and the target after compensating for the pitch angle of the seeker is given by $EL - \Theta'_{SIM}$.

The final step in the algorithm is derive the target position from the INS/GPS derived parameters and the seeker to target parameters. Shown in Figure 3.17 is the block diagram entitled "INS/GPS/RADAR DERIVED TARGET POSITION". This block performs the same basic functions as Figure 3.15 with a few minor modifications.

Given the derived seeker-to-target parameters, R_{DER}, $AZ - \Psi'_{SIM}$ and $EL - \Theta'_{SIM}$, these values must be corrected for the INS/GPS derived yaw and pitch of the Simulator. This is done by adding the respective values in the following manner:

$$AZ_{DER} = AZ - \Psi'_{SIM} + \Psi_{SIM} = \theta_{DER} \qquad\qquad (3\text{-}17)$$

$$EL_{DER} = EL - \Theta'_{SIM} + \Theta_{SIM} \qquad\qquad (3\text{-}18)$$

Notice that yaw and pitch terms of the Simulator do not fully cancel. The residual values are due to the errors involved with INS, GPS and the seeker. These errors translate directly into displacement errors in fixing the target's position in tangent plane coordinates. These errors are discussed in more detail in the following chapter entitled "VALIDATION AND ANALYSIS."
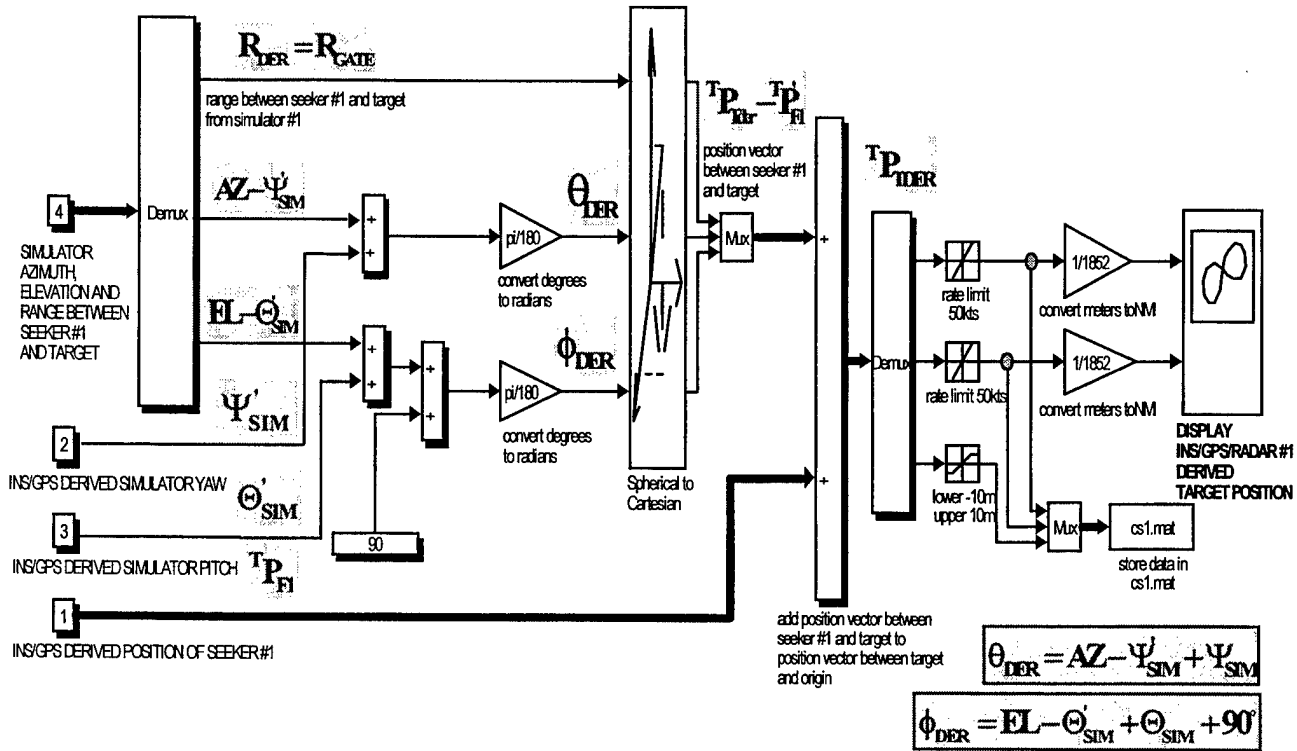
Figure 3.17: INS/GPS/RADAR #1 DERIVED TARGET POSITION Block Diagram

The elevation term, EL_{DER}, is not in the proper form. To put the elevation term in the form of spherical coordinates simply add 90 degrees, or $\phi_{DER} = 90° + EL_{DER}$. This results in all values in terms of spherical coordinates.

Next, perform a spherical to Cartesian coordinate transformation. The result in tangent plane coordinates is the position vector $^T P_{Tder} - ^T P'_{F1}$. To derive the target position in tangent plane coordinates, add the INS/GPS derived position of seeker #1 to this quantity. This is seen in the following equation:

$$^T P_{TDER} = {}^T P_{Tder} - {}^T P'_{F1} + {}^T P_{F1} \qquad (3\text{-}19)$$

Note, the true and derived position vectors of seeker #1 do not cancel. This is due to the fact that the derived seeker-to-target parameters are based on the true seeker position.

Next, assume the target has an upper limit on its speed. This means the **x, y** and **z** components of the DSTSPI derived target position can be rate limited to a specified value. In other words, the target position is not allowed to change by more than a specified amount. This rate of change is limited to a value of **50 KTS**. The **z** component of the target position could have been limited to values close to the surface, but, this would have possibly resulted in the miss detection of any airborne decoys such as a chaff cloud.

IV. VALIDATION AND ANALYSIS

All the figures in this chapter were generated using MATLAB. Also, all the figures were generated under the following conditions:

- The P-3's initial course is 000° true
- The P-3's initial altitude is 2000 feet
- The P-3's initial speed is 500 ft/sec or 296.242 kts
- The P-3's initial position in the tangent plane coordinate system is [0, 0,-2000] in feet
- The Target's initial course in Chapter IV, Section's A through C is 270° true
- The Target's speed is 22 kts throughout the simulation
- The Target's initial location in the tangent plane coordinate system is [5, 0, 0] in nautical miles
- All data collection periods were 60 seconds

A.   INS AND GPS ERRORS

This section looks at the modeled errors from both INS and GPS. Plots of these errors were generated using MATLAB. As discussed in Chapter II, there are several factors which contribute to the errors seen from INS and GPS. One of the limiting factors in the algorithm is the fact that these errors are always present. The biggest contributors to the displacement error in the derived target position are due to the errors from INS and the seekers. Although GPS errors are important, an error in the seeker's position only results in the same order magnitude error in the derived target's position. Simply stated, because the arc length is equal to the angle in radians multiplied by the radius (or the distance

67

between target and the seeker), any angular errors prove to be detrimental to the algorithm. These angular errors result from both the seeker's ability to measure the azimuth and elevation between the Simulator and the target and the INS's ability to measure the Euler angles. As a hypothetical case, assume that a particular seeker's position is known to within one meter and the pitch, roll and yaw of the Simulator are known to within **0.5°**, or **0.009** radians. If the seeker were **5** NMI from the target, this would translate to a cross range displacement error in the derived target position of roughly 83 meters assuming the seeker measured the azimuth and elevation precisely.

As mentioned in Chapter II, DGPS, theoretically, should provide positions to within a one meter accuracy. Figures 4.1 through 4.3 show the GPS position errors relative to a NED orientation. From these Figures one can conclude the maximum amplitude for the displacement error occurs at roughly 12 seconds into the simulation over the sample period. At this point the value for this amplitude is about 2.5 meters. These errors are roughly consistent with actual DGPS performance specifications.
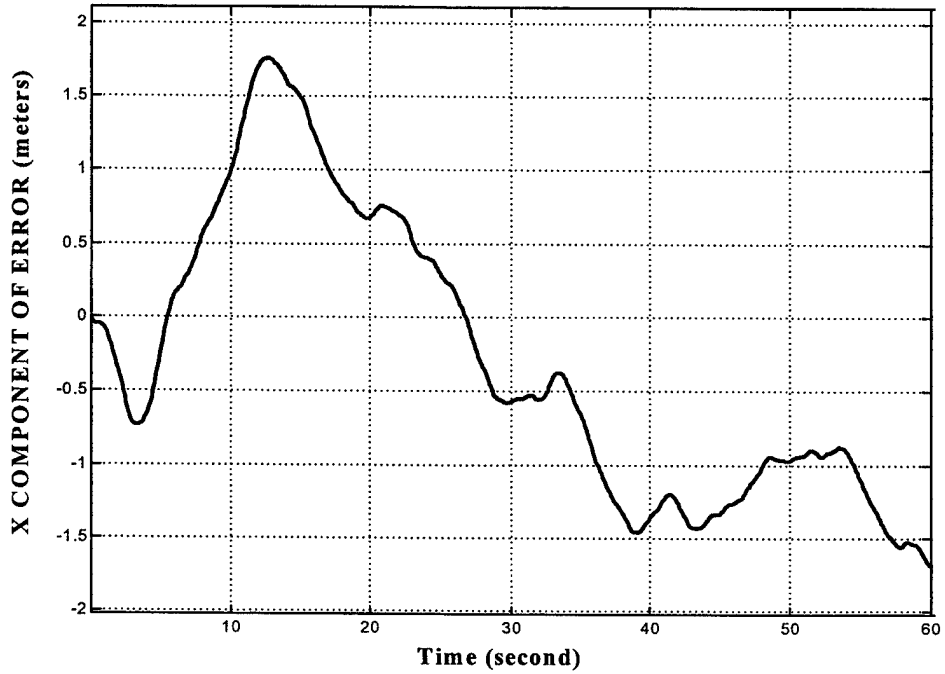
Figure 4.1: X-component of the GPS displacement error
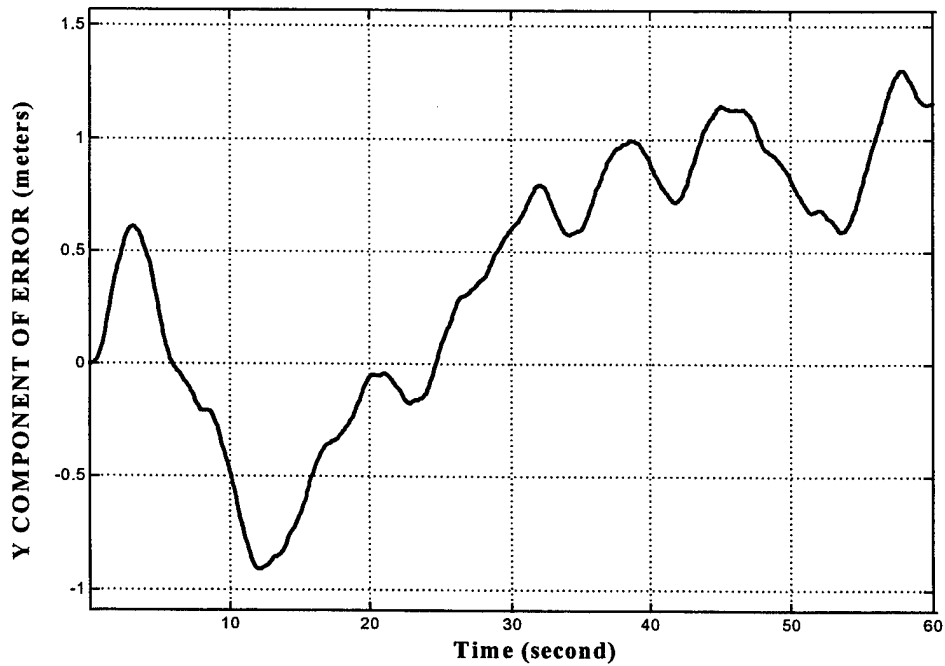
Figure 4.2: Y-component of the GPS displacement error
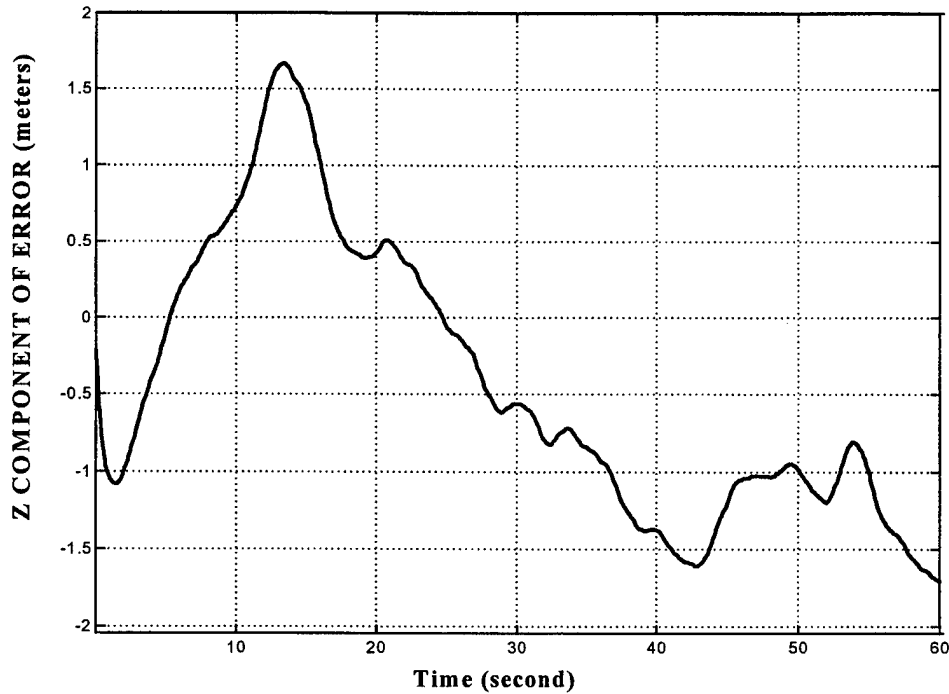
Figure 4.3: Z-component of the GPS displacement error

The errors in the INS values for pitch roll and yaw are depicted in Figures 4.4 through 4.6. From Figures 4.4 through 4.6, the maximum error in the INS's computation of the Euler angles is approximately +/- **0.4** degrees. This equates to a cross range displacement error in the derived target position of approximately 65 meters at a 5 NMI range. The errors in the Euler angle computation for this model are comparable to the errors found from an actual INS system. Specifically, NRL's P-3 uses the LTN-72 which is an INS with an advertised maximum amplitude for the Euler angle measurement error of less than **0.5** degrees. [Ref. 8, p. 35]
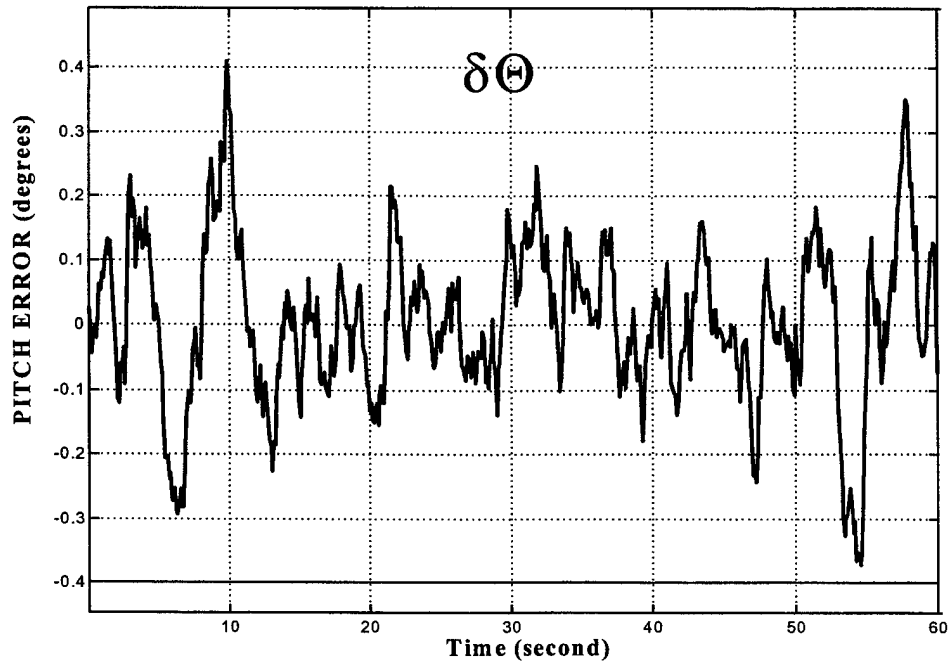
Figure 4.4: INS pitch error of the P-3
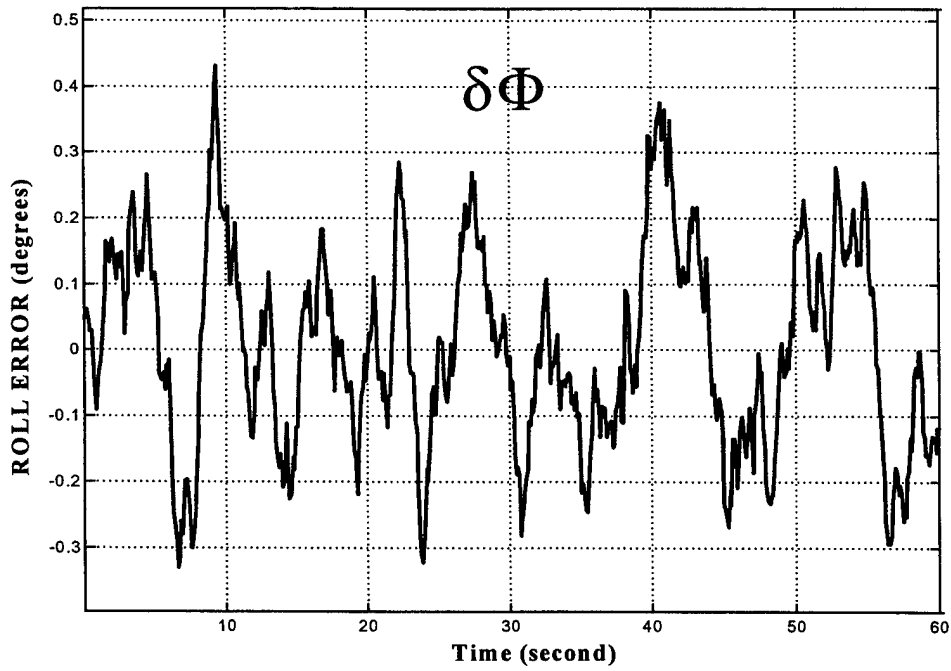
Figure 4.5: INS roll error of the P-3

71
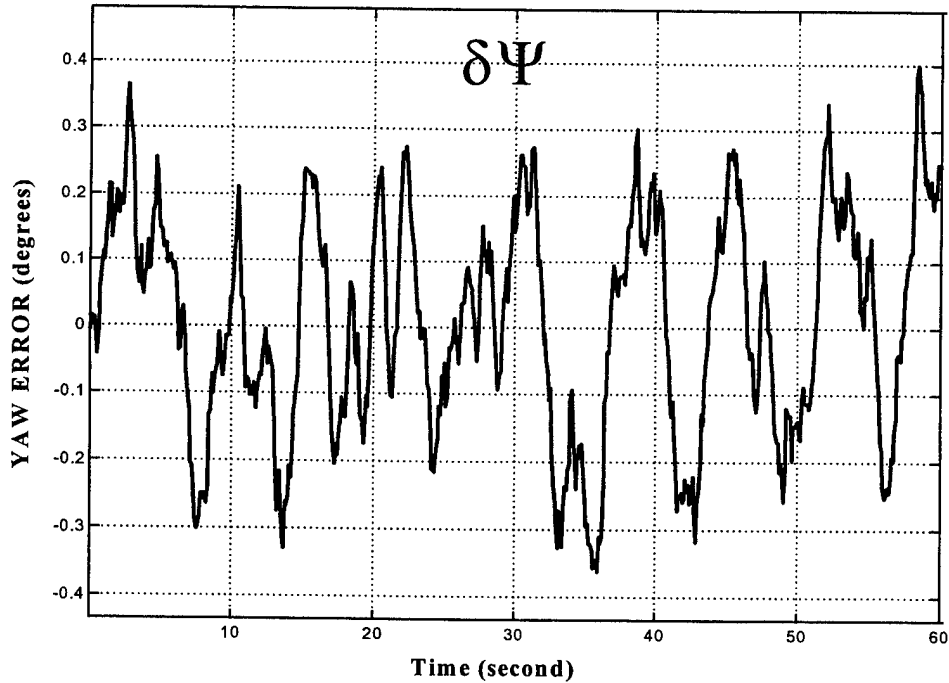
Figure 4.6: INS yaw error of the P-3

B. SEEKER POSITION ERRORS

Figures 4.7 through 4.12 show the position errors of seeker #1 and seeker #2. Notice, that these curves follow the errors associated with GPS very closely with slight variations due to the INS errors. As mentioned earlier, these errors translate to the same order magnitude errors in the derived target positions. There are two contributions to the overall error in deriving the position of each seeker. The first is the contribution from DGPS. The uncertainty in the DGPS position at the GPS antenna is lever arm corrected to the seeker position. In other words, the position errors of DGPS translate directly into position errors of the seekers.

Additionally, any angular errors from INS contribute to the overall position error of each seeker. A 0.5 degree error in any one of the Euler angle computations results in a 5 centimeter error in the position of each seeker for a lever arm of 5 meters. This means that the errors from INS are insignificant in deriving each seeker's position. This does not mean that the Euler angles are themselves are insignificant. Without the lever arm correction, the errors in deriving the seeker's position in a fixed inertial coordinate system would be substantially greater.
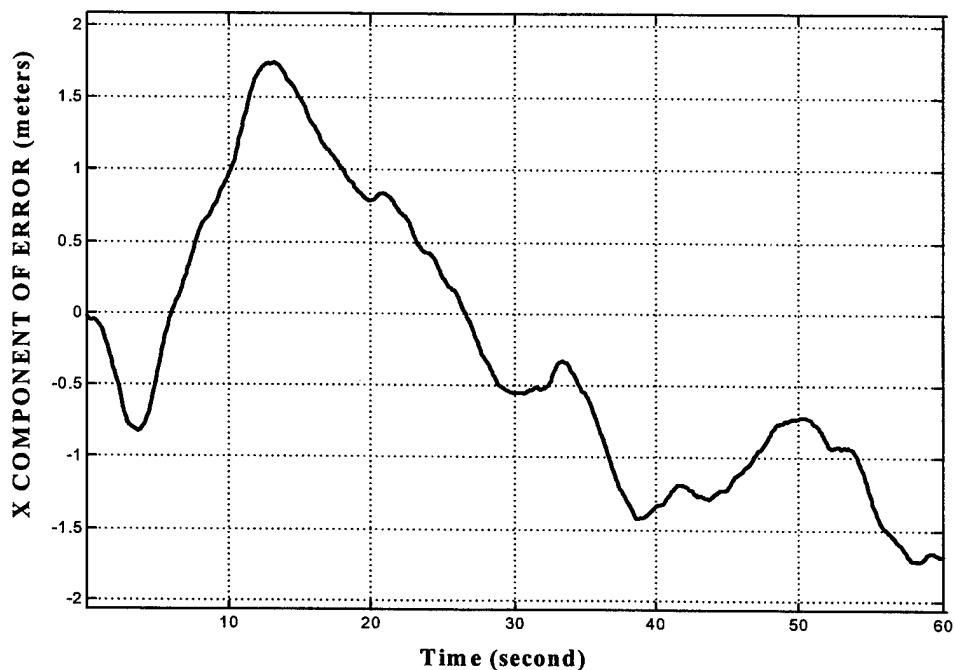
Figure 4.7: Seeker #1 position error in North/South direction

73
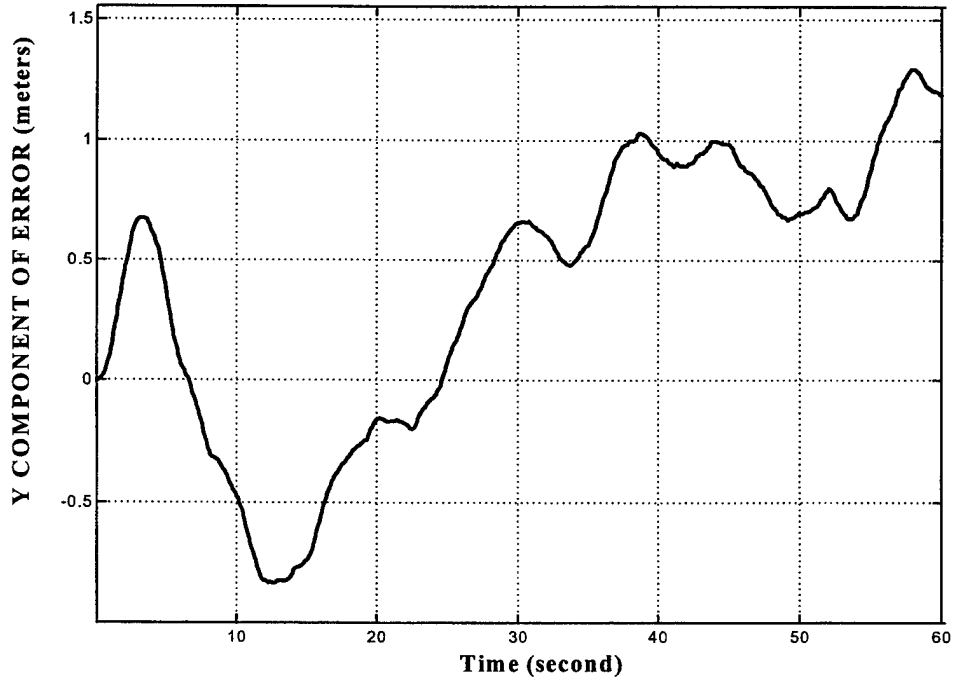
Figure 4.8: Seeker #1 position error in East/West direction
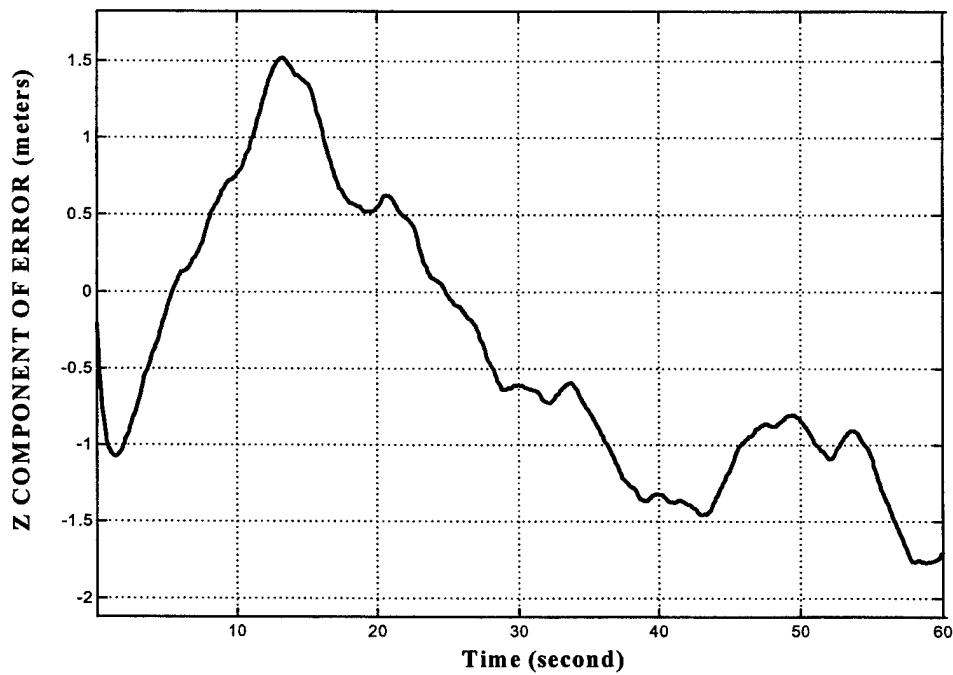
Figure 4.9: Seeker #1 position error in Up/Down direction

74
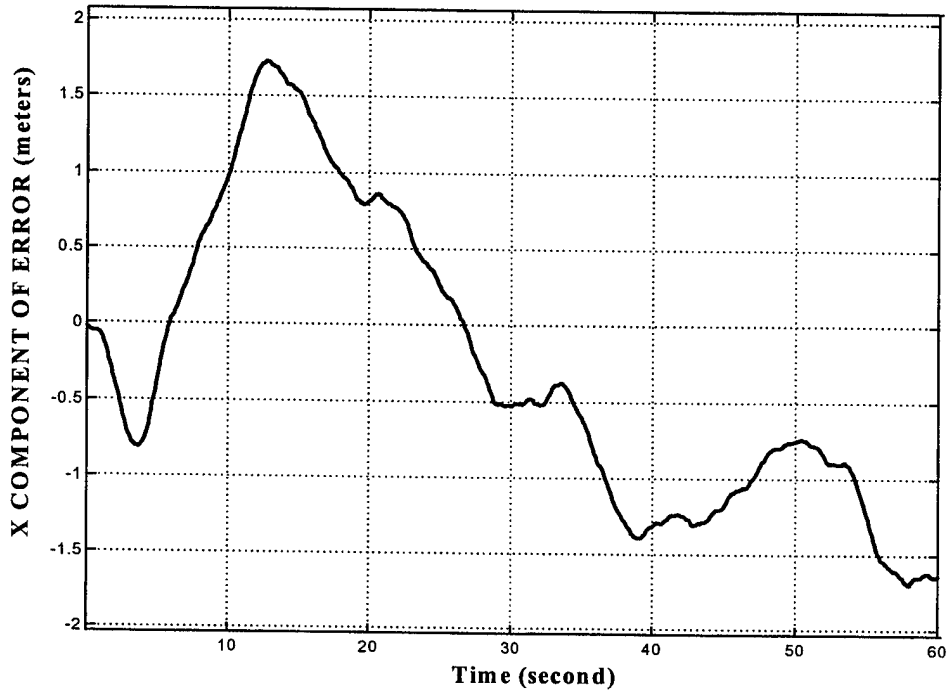
Figure 4.10: Seeker #2 position error in North/South direction
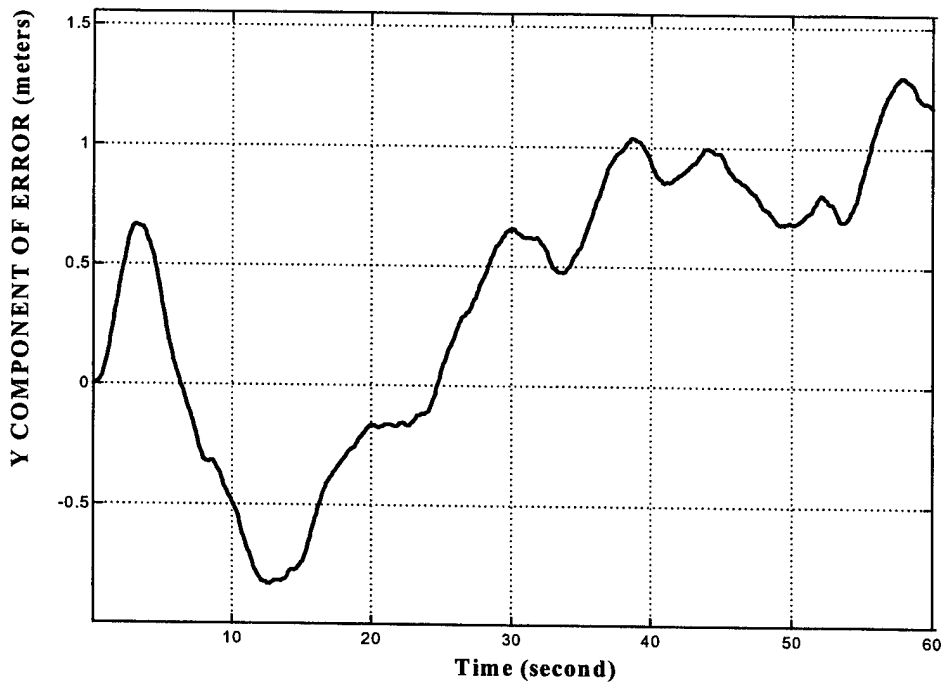
Figure 4.11: Seeker #2 position error in East/West direction

75
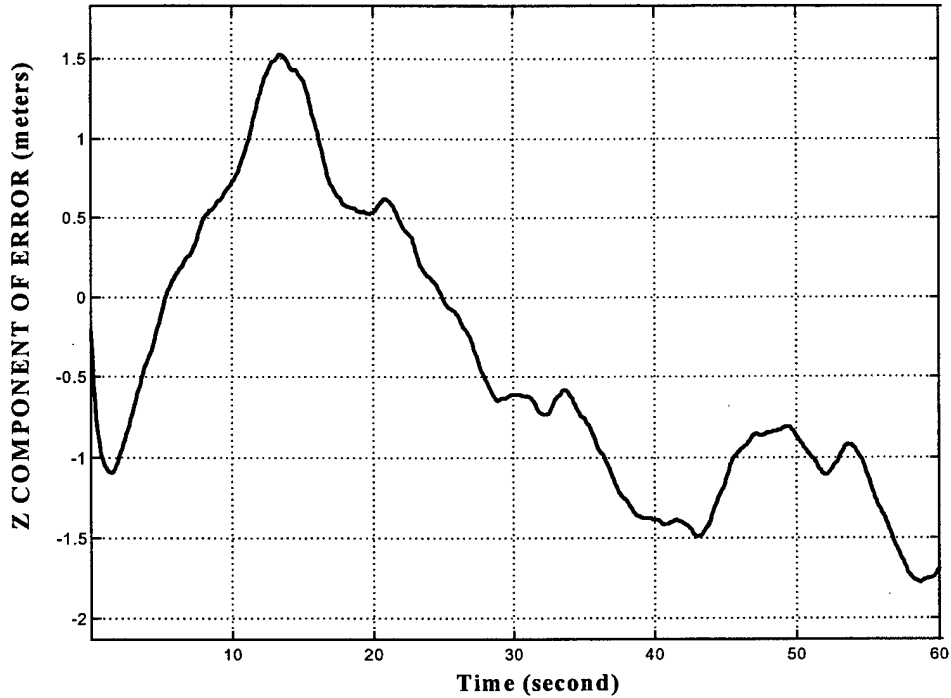
Figure 4.12: Seeker #2 position error in Up/Down direction

Figures 4.13 and 4.14 provide a comparison of the true and derived positions of seeker #1. In Figures 4.13 and 4.14 the initial displacement in the +y direction for the position of seeker #1 is due to the location of seeker #1 in body fixed coordinates relative to the center of the P-3. Additionally, the P-3 does not fly a straight line. The course variations are due to the **"P-3 FLIGHT PROFILER"** model. Because this model continuously tries to reduce the error between the ordered course and the actual course, the P-3 can not maintain a steady course but continuously hunts for the ordered course.

Figures 4.15 and 4.16 provide a comparison of the true and derived positions of seeker #2. The initial displacement in the -y direction is due to the placement of seeker #2 with in the body fixed coordinates.
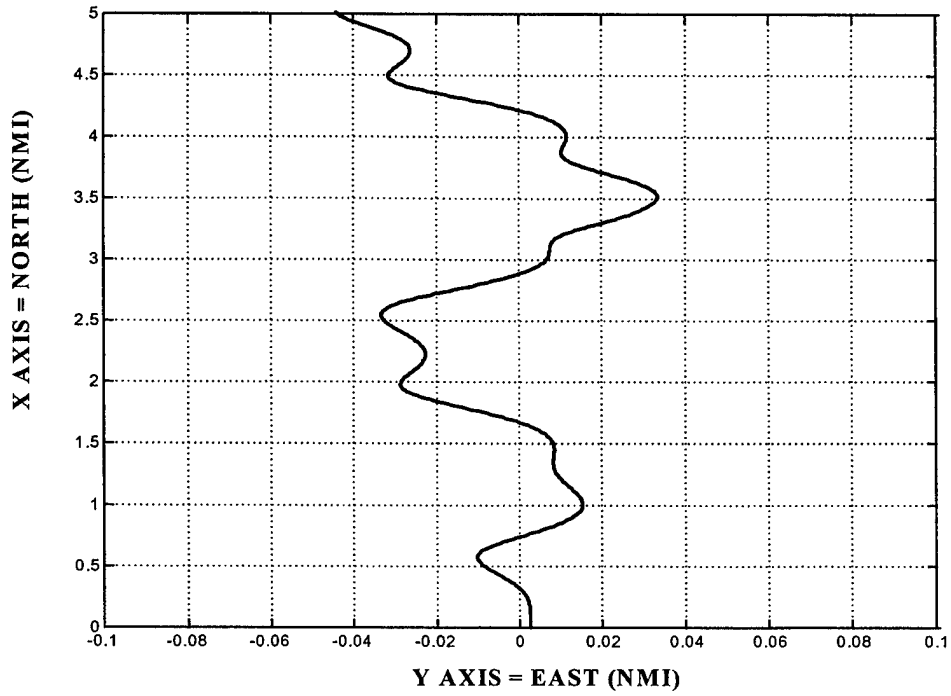
Figure 4.13: True position of seeker #1
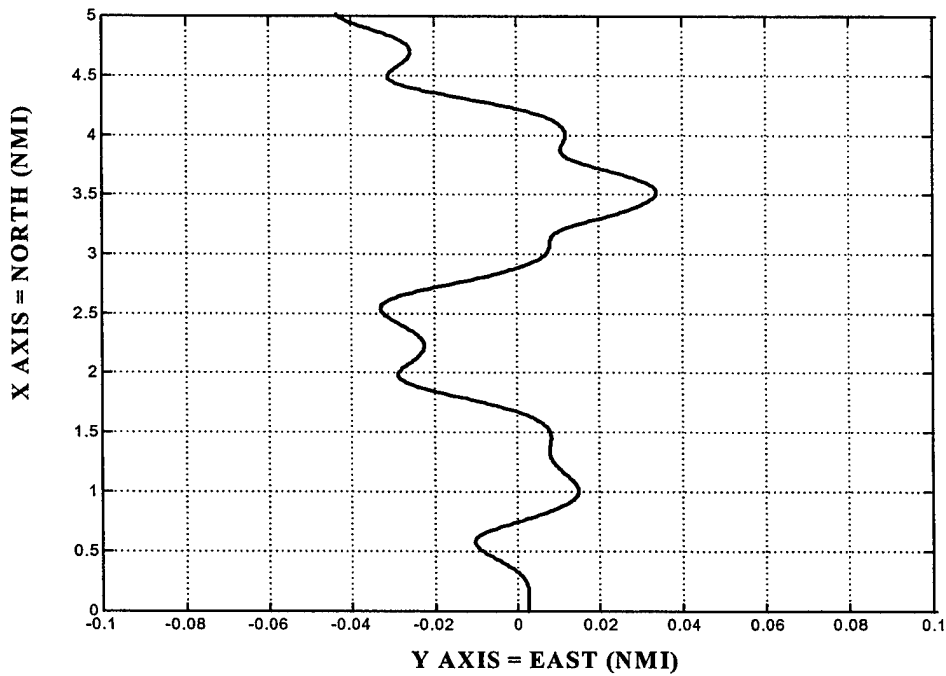
Figure 4.14: INS/GPS derived position of seeker #1
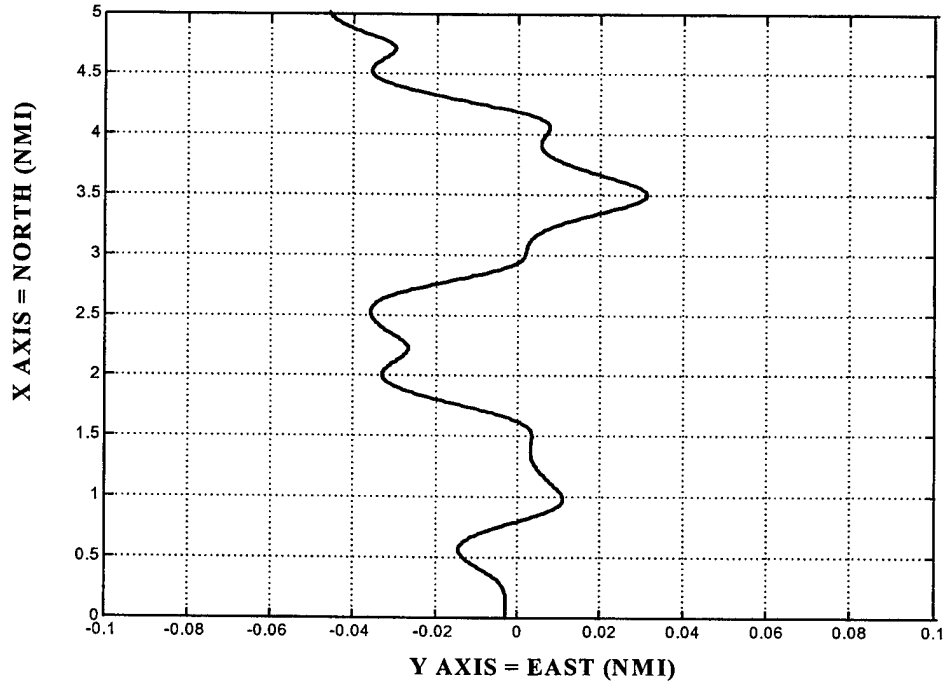
Figure 4.15: True position of seeker #2
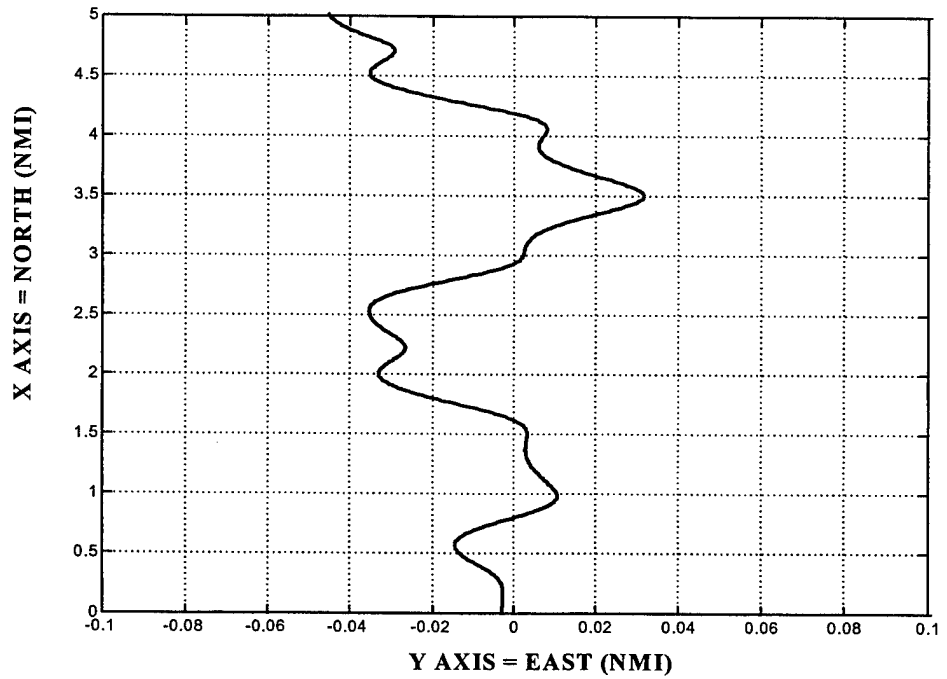
Figure 4.16: INS/GPS derived position of seeker #2

C. SEEKER CONTRIBUTED ERRORS

Figure 4.17 shows the error from the range resolution for the conical scan seeker model used in the simulation. Because the range resolution is modeled as 100 meters, an envelope of 50 meters is evident throughout the simulation. Notice that the range error does not decrease over the sample interval. This is due to the fact that the range resolution is a function of the seeker hardware and not the signal to noise ratio. The range resolution of this seeker model translates to down range errors in the derived target position as is seen in the following section.
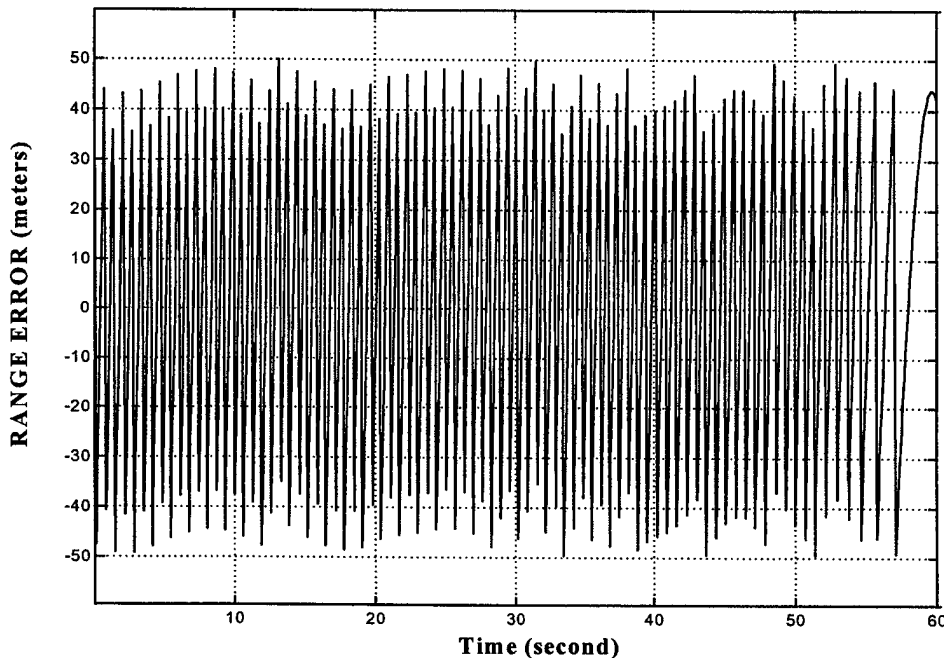
Figure 4.17: Range error from conical scan seeker (COSRO)

Figure 4.18 shows the precision in the measurement of azimuth and elevation angles from the conical scan radar. This precision is approximated as +/- 0.15 degrees over this data collection period. This precision in the measurement of the azimuth and

elevation remains relatively constant during this period because the aircraft is closing the target from 5 NMI. Because the signal to noise ratio diminishes the effects of the error slope and crossover loss in the conical scan seeker, at this range, the errors in the azimuth and elevation are dominated by the scintillation error.

An angular precision of +/- 0.15 degrees is expected to result in cross-range errors on the order of 25 meters when the seeker to target separation is 5 NMI.
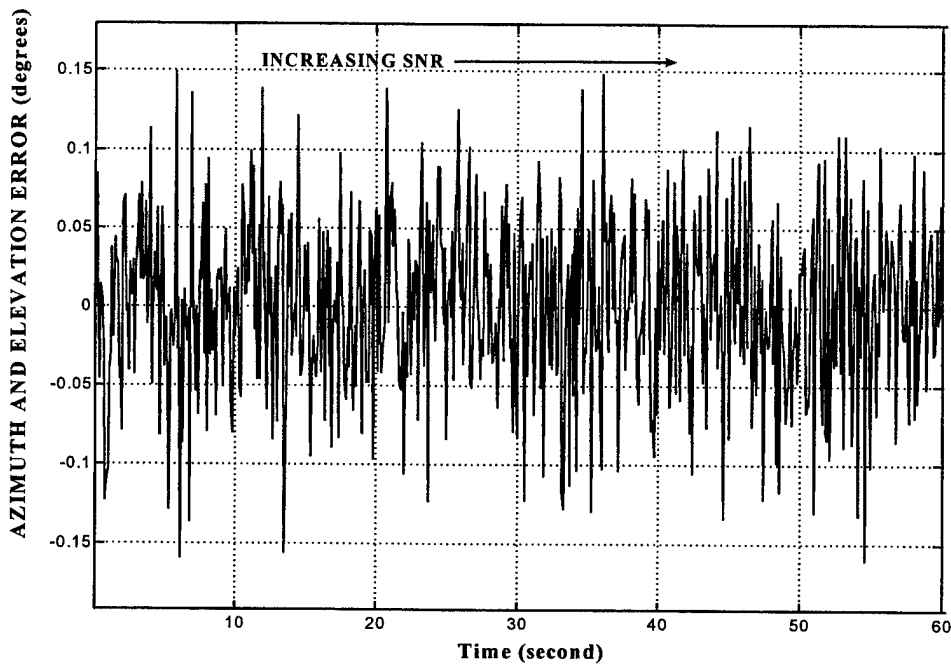
Figure 4.18: Azimuth and elevation error from conical scan seeker (COSRO)

Figure 4.19 shows the error in the range measurement for the monopulse seeker or seeker #2. Here the range resolution is 20 meters. As expected, the magnitude of the range error is +/- 10 meters. Notice the crossover rate for the range error is 5 times faster than for the crossover rate of the conical scan range error. This results from having a range resolution that is 5 times smaller in the case of the monopulse seeker. Again, the

80

range resolution of the monopulse seeker results in down range errors in the derived target position of roughly the same order magnitude.
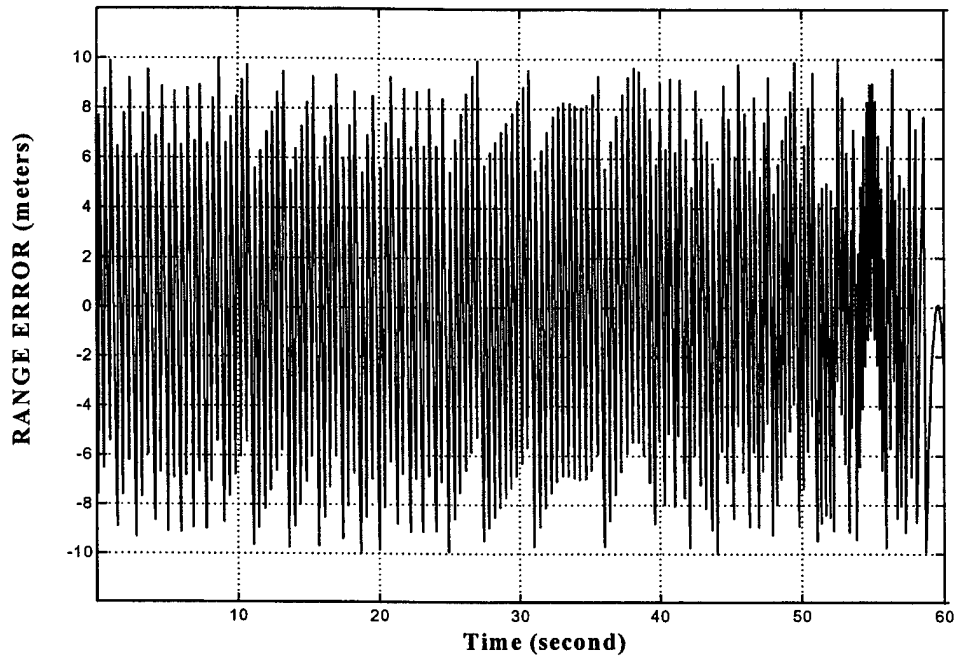
Figure 4.19: Range error from monopulse seeker

Figure 4.20 shows the azimuth and elevation measurement errors for the monopulse seeker. Because the monopulse seeker is not affected by scintillation errors, an increase in signal to noise ratio directly results in an increase in the precision of the measurement. As the range between the seeker and target decreases, the azimuth and elevation measurement errors decrease from +/- 0.05 degrees to a negligible amount. At 0.05 degrees the cross range error in the derived target position would be roughly 8 meters with a seeker to target separation of 5 NMI.
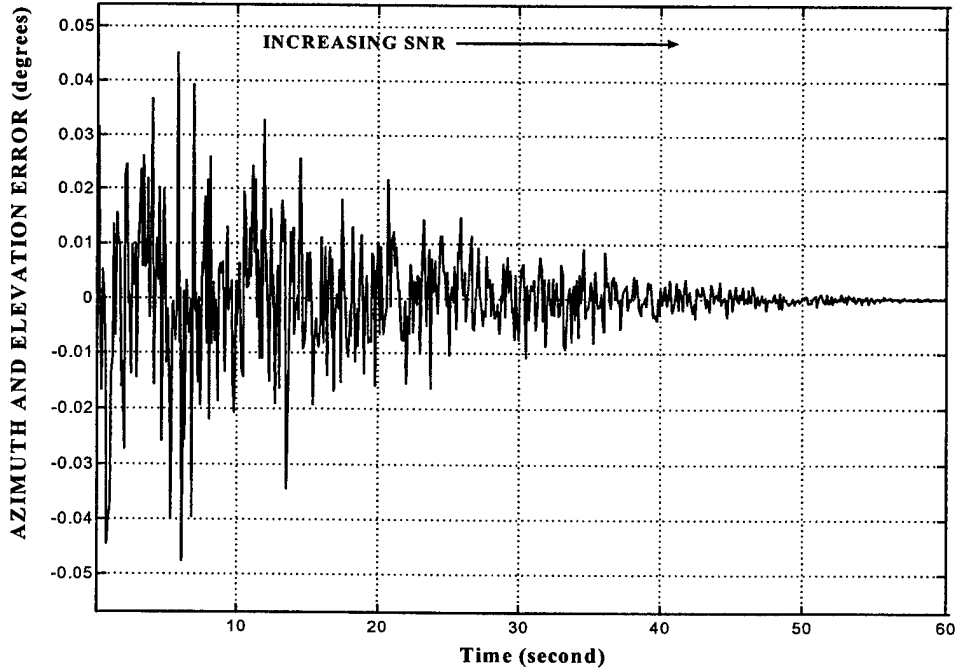
Figure 4.20: Azimuth and elevation error from monopulse seeker

D. DERIVED TARGET POSITION ERRORS

This section shows the true and derived target positions for each seeker type in the tangent plane coordinate system for several different types of target motion. In addition, this section shows the position errors that result from the DSTSPI algorithms for each case.

Figures 4.21 through 4.29 were generated with the target dead in the water. Figures 4.30 through 4.38 were generated with the target on a course of 270° true. Figures 4.39 through 4.47 were generated with the target on a course of 090° true. Figures 4.48 through 4.56 were generated with the target on a course of true North. Figures 4.57 through 4.65 were generated with the target on a course of 180° true. Figures 4.66 through 4.74 were generated with the target making a slow turn to port from 000° to 270° true.

Figures 4.75 through 4.83 were generated with the target making a slow turn to starboard from 000° to 090° true. Figures 4.84 through 4.93 were generated with the target making a slow turn to starboard from 180° to 270° true. Figures 4.94 through 4.101 were generated with the target making a slow turn to port from 180° to 090° true.

Table 4.1 is provided as a summary of the errors from the DSTSPI algorithms for seeker #1 and seeker #2 for each of the nine types of target motion.

TARGET MOTION TYPE	SEEKER #1 (C0SRO)			SEEKER #2 (MONOPULSE		
	X maximum error (meters)	Y maximum error (meters)	Z maximum error (meters)	X maximum error (meters)	Y maximum error (meters)	Z maximum error (meters)
Dead-In-Water	25	42	38	7.5	45	40
270° steady	25	48	38	7.5	46	40
090° steady	25	40	38	8.1	38	40
000° steady	22	43	39	11.5	45	41
180° steady	36	43	36	9	45	26
000° to 270°	25	42	39	10.5	45	40
000° to 090°	25	42	39	10.5	45	40
180° to 270°	32	42	41	10.5	45	40
180° to 090°	32	42	41	10.5	45	40
mean value	27.44	42.66	38.77	9.51	44.33	38.56
std deviation	4.66	2.18	1.56	1.51	2.39	4.72
variance	21.77	4.75	2.44	2.28	5.75	22.28
maximum	36	48	41	11.5	46	41

Table 4.1: Summary of DSTSPI derived target position errors

From Table 4.1 several conclusions are made. The errors between the derived target positions from both seekers and the true target position are essentially constant over

a wide range of target motions. The errors are greatest in the cross range direction. The errors from the COSRO seeker are larger than for the monopulse seeker. This is especially true when the seeker-to-target separation is small.

Assume that the errors that from the DSTSPI algorithms are roughly the same as the maximum values seen in Table 4.1. If this assumption is used, then the area of uncertainty in deriving a target's position is roughly a sphere of radius **40 meters** around the true target position. If the target's speed is **22 kts** or **11.3178 meters/sec**, then the elapsed time before any decoys are detected after launch is about **3.5 seconds**. This latency in detecting the decoy is defined as the time resolution, δt, of the DSTSPI algorithms. The time resolution, δt, decreases as the area of uncertainty of the target's position decreases. From the figures presented in this section, the general trend of the area of uncertainty of the target's position is that it decreases with a decreasing seeker-to-target separation.
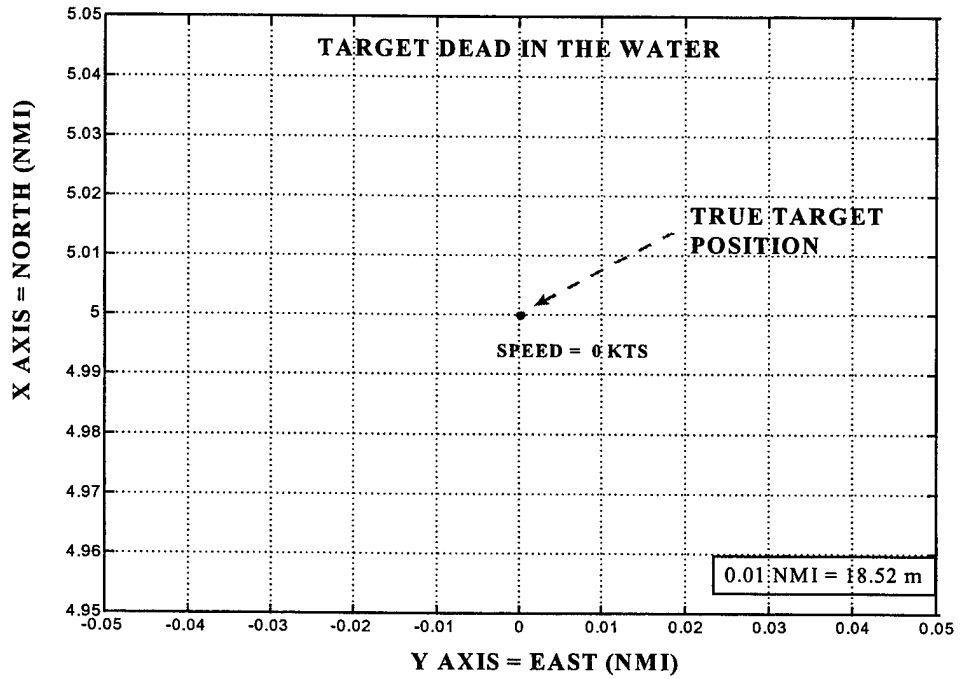
Figure 4.21: True target position - DIW
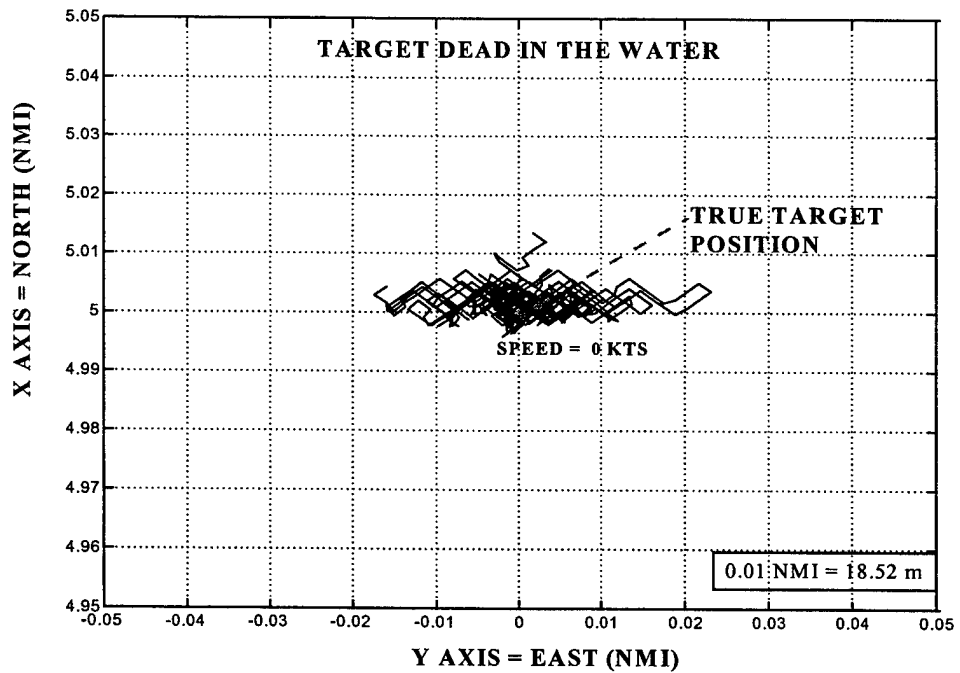
Figure 4.22: Simulator #1 DSTSPI derived target position - DIW

85
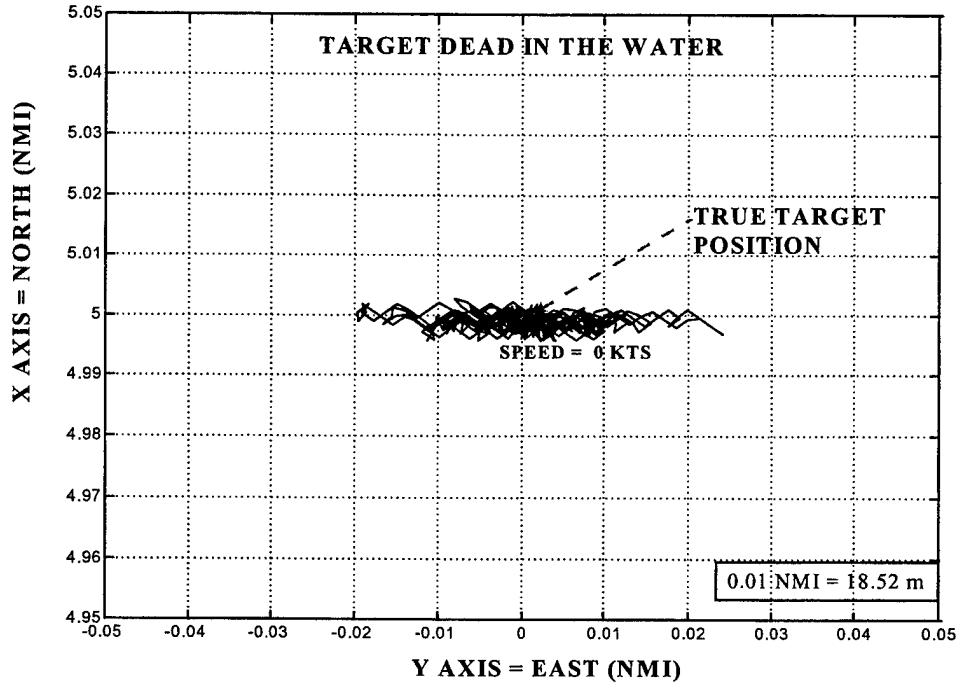
Figure 4.23: Simulator #2 DSTSPI derived target position - DIW
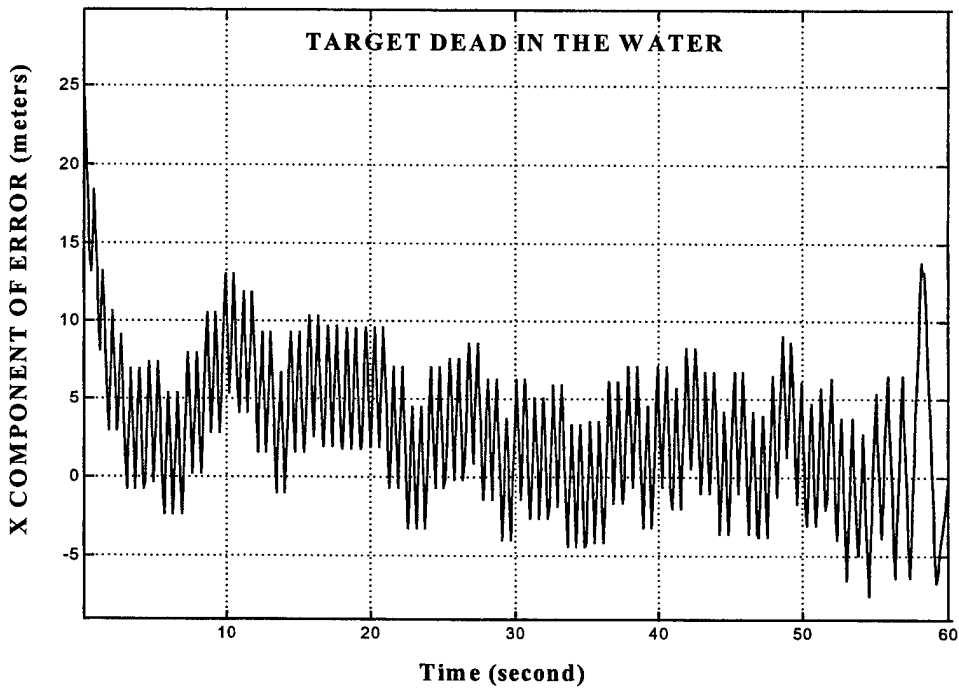
Figure 4.24: Simulator #1 derived target position error in the North/South direction - DIW
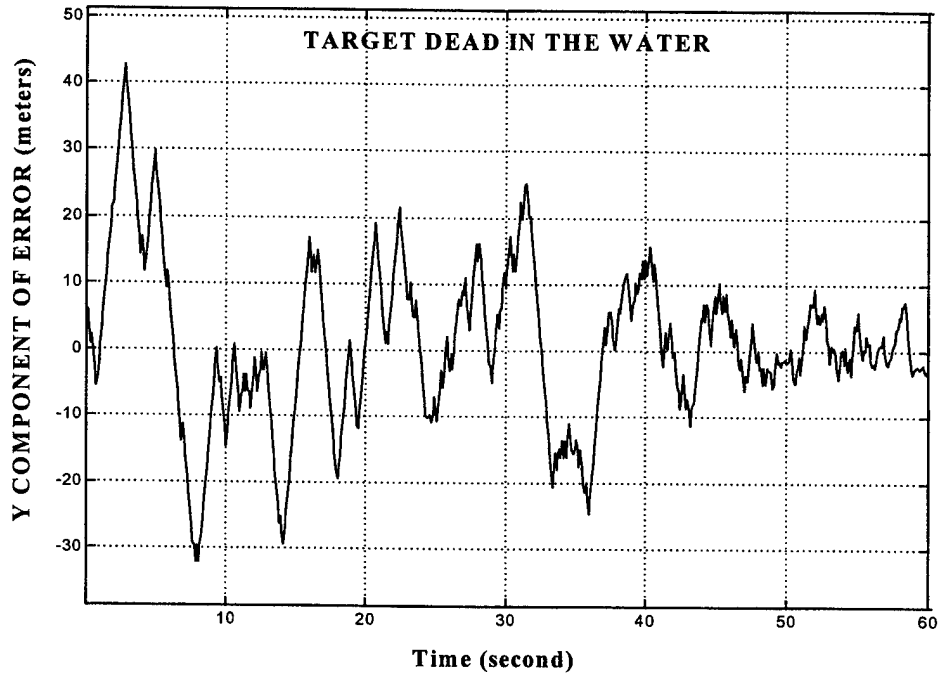
Figure 4.25: Simulator #1 derived target position error in the East/West direction - DIW
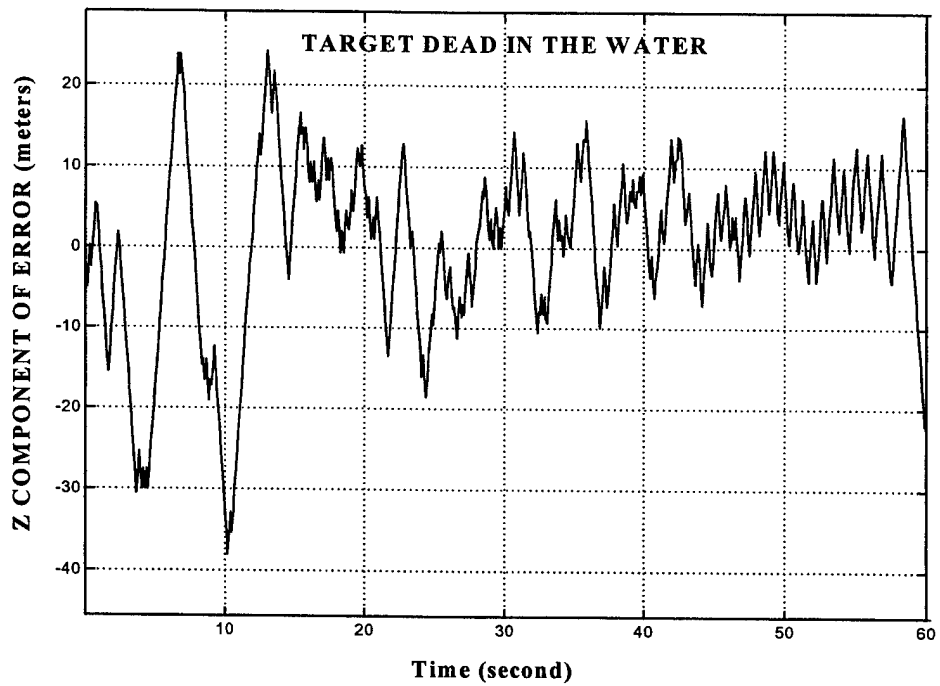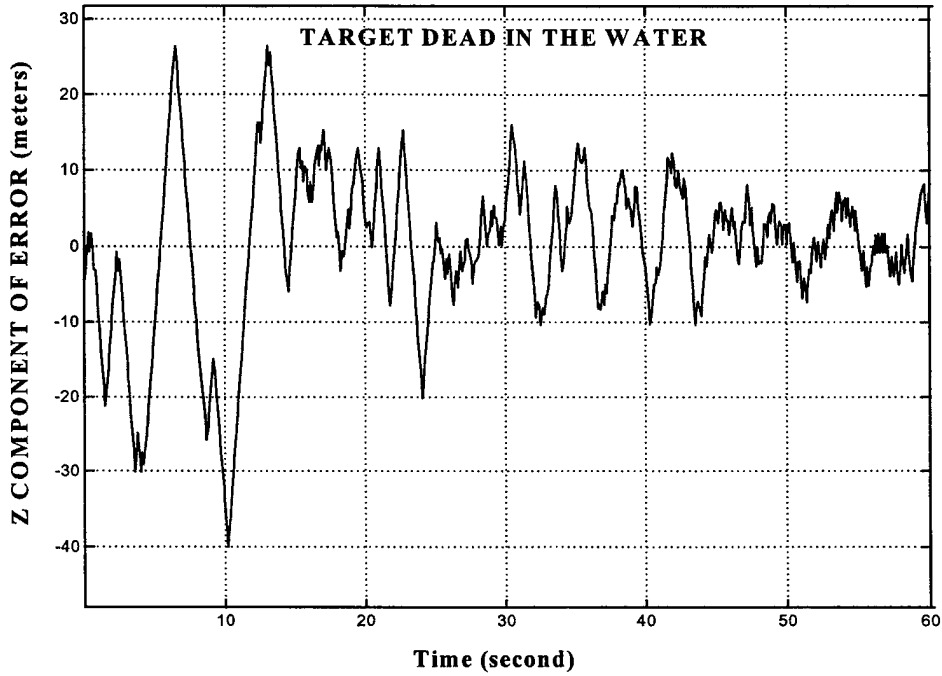

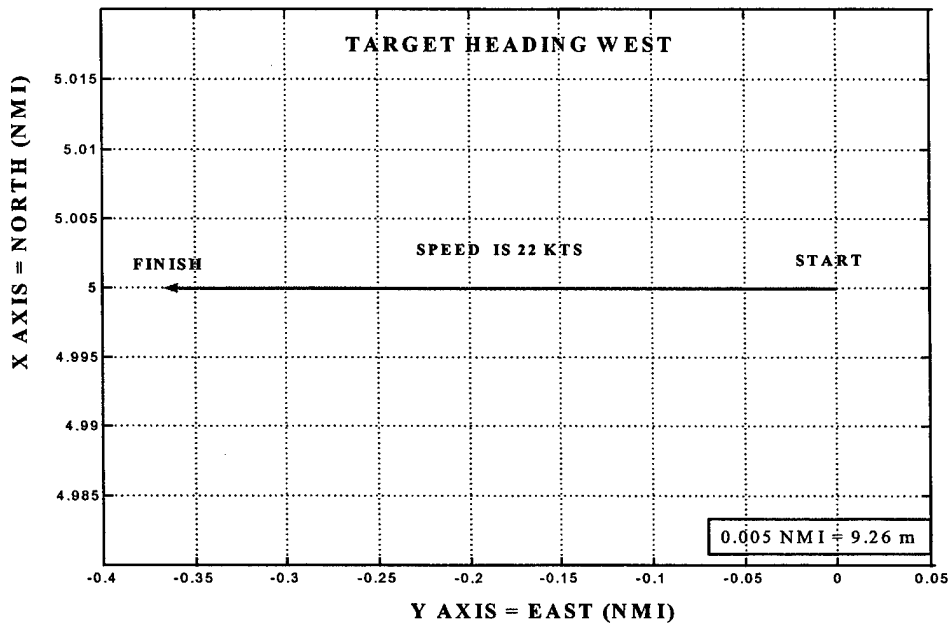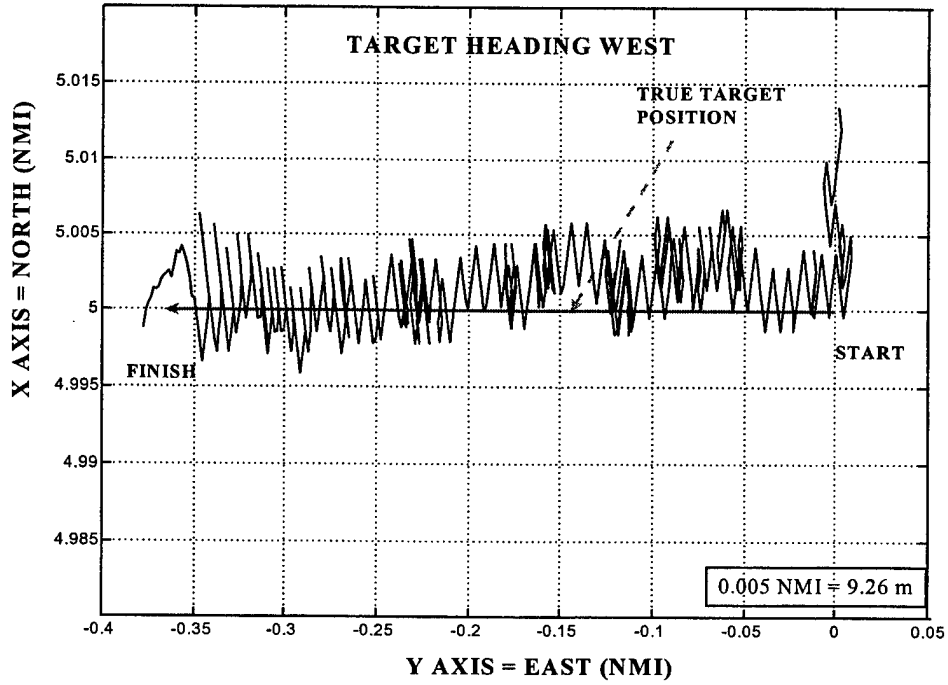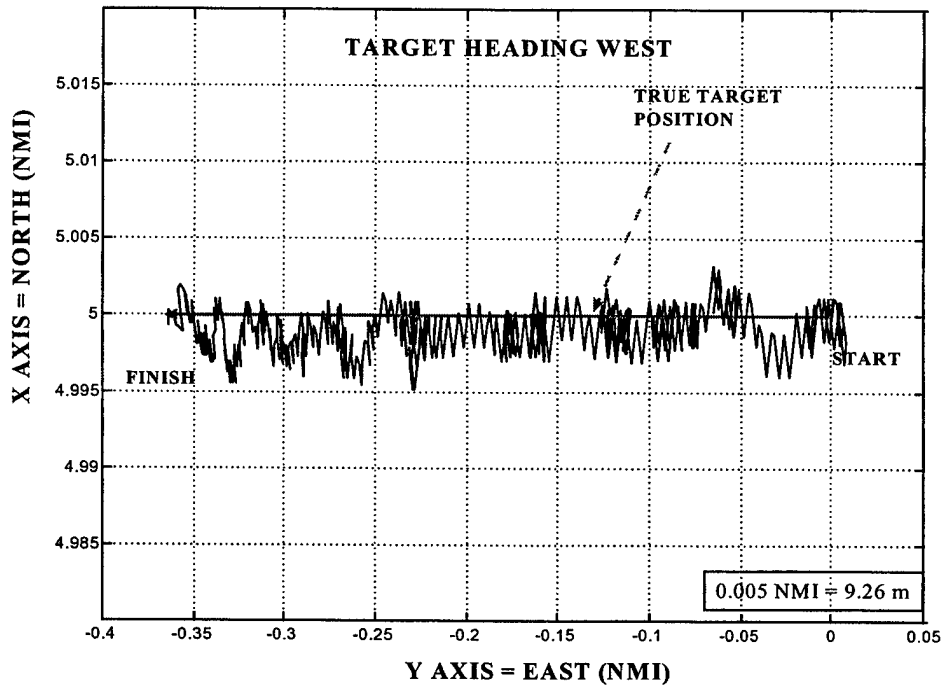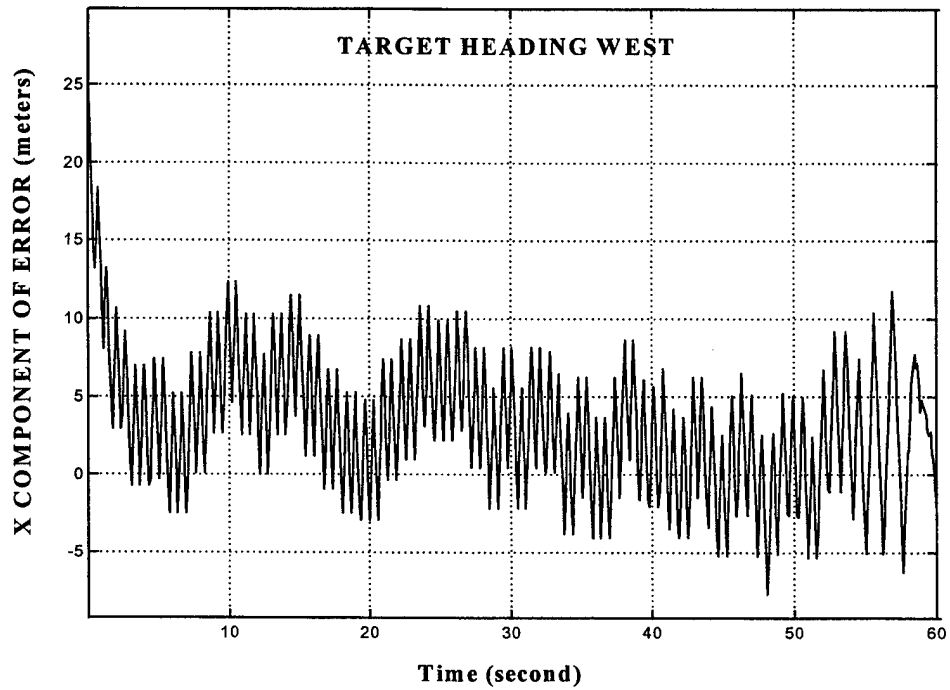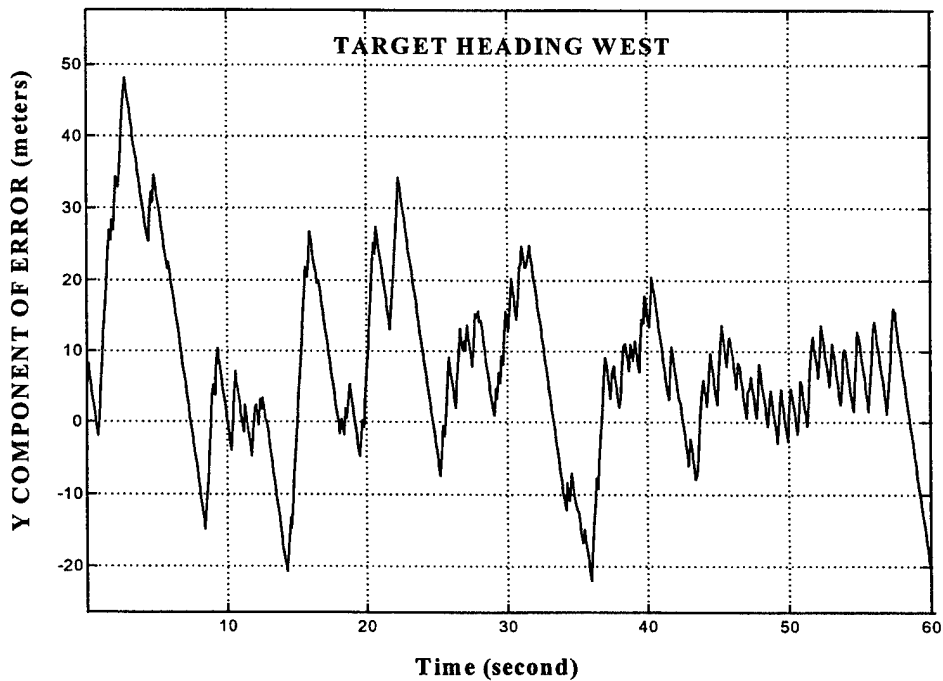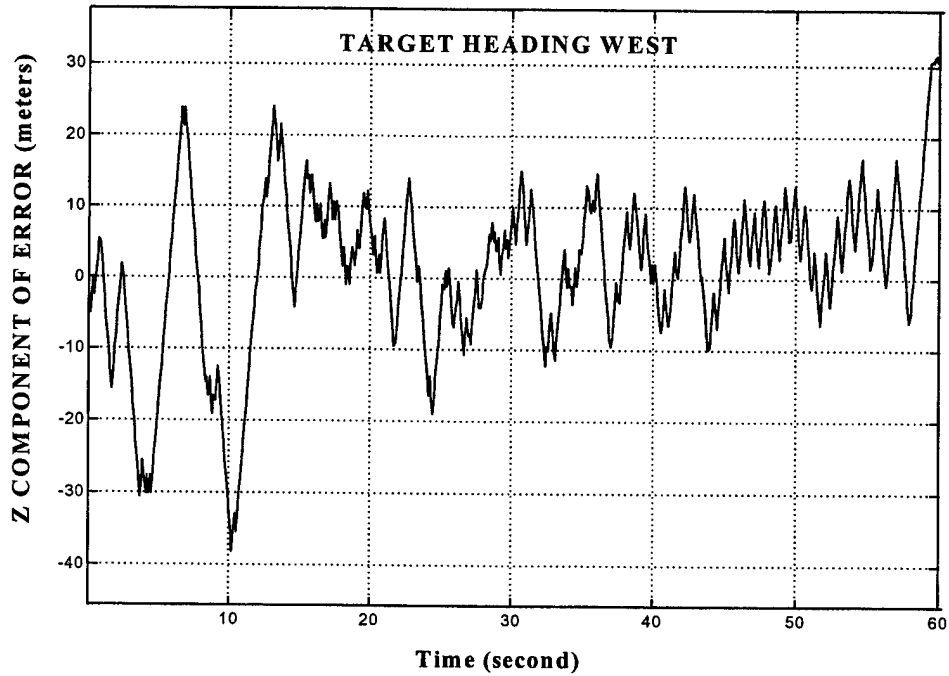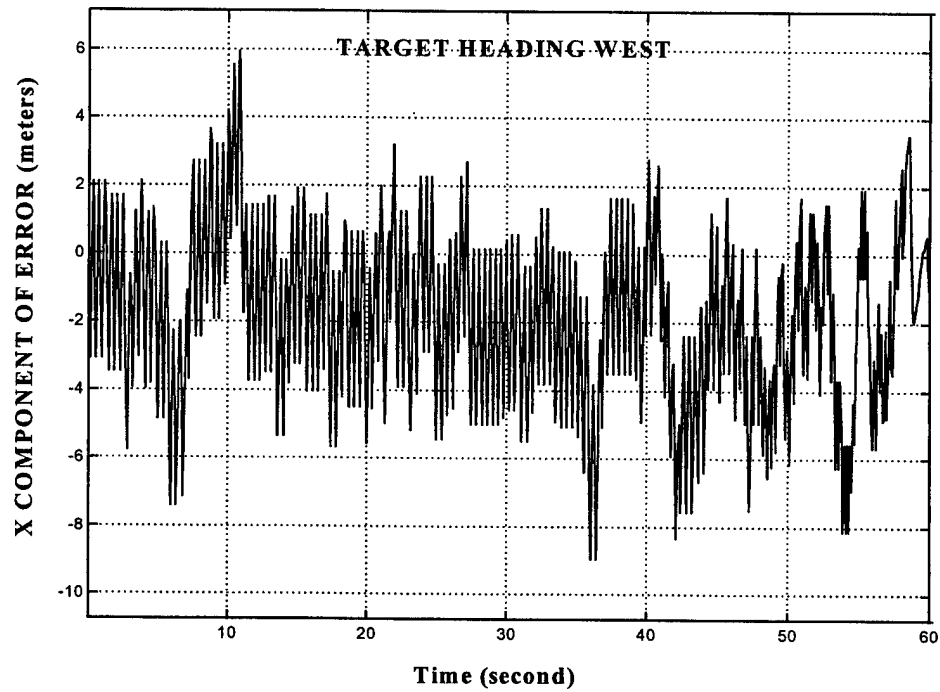**Figure 4.26: Simulator #1 derived target position error in the Up/Down direction - DIW**

87
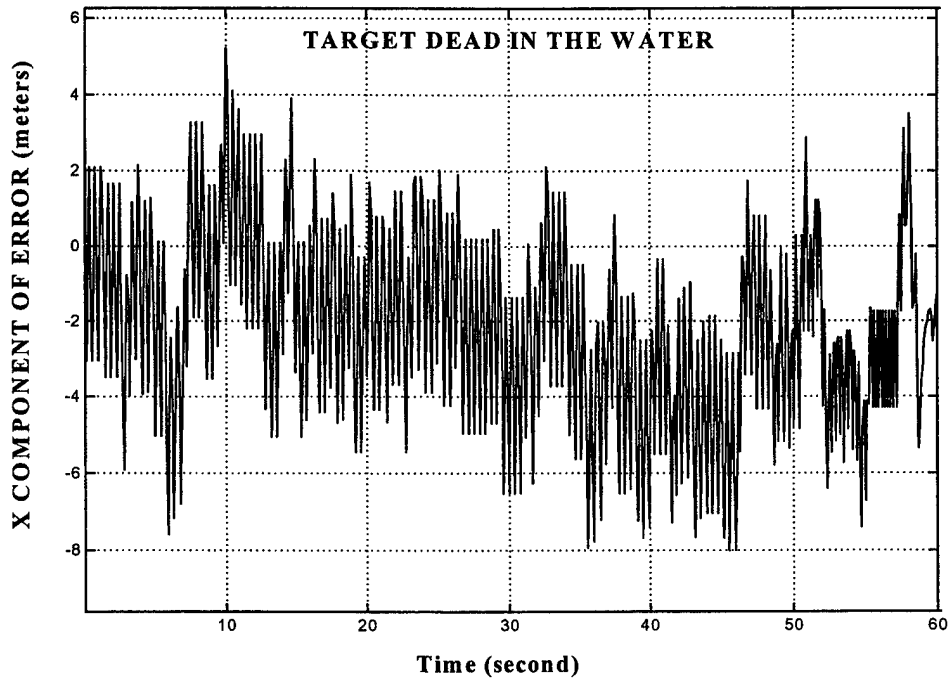
Figure 4.27: Simulator #2 derived target position error in the North/South direction - DIW
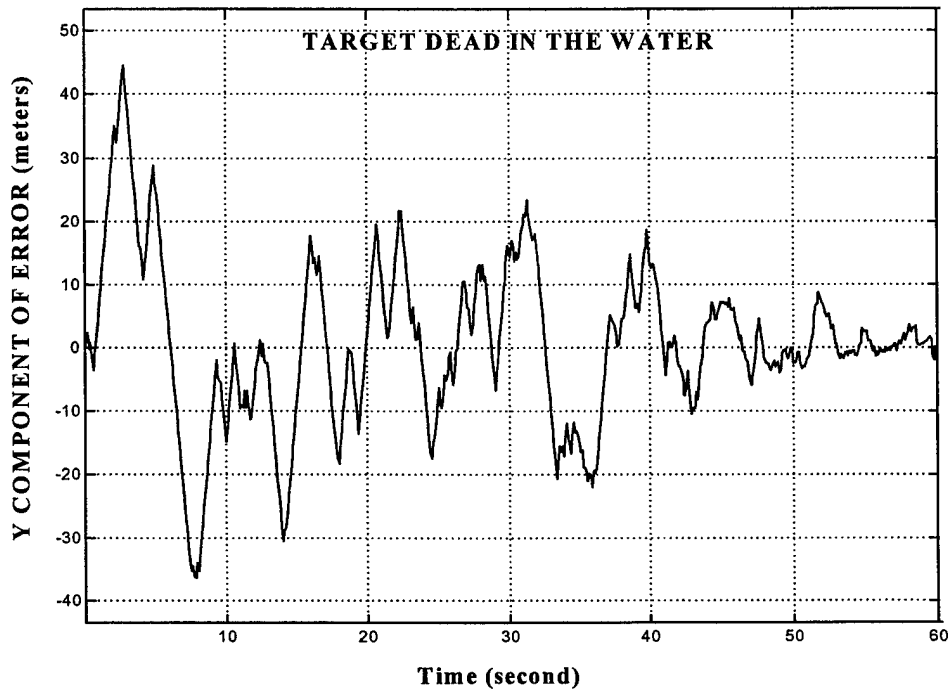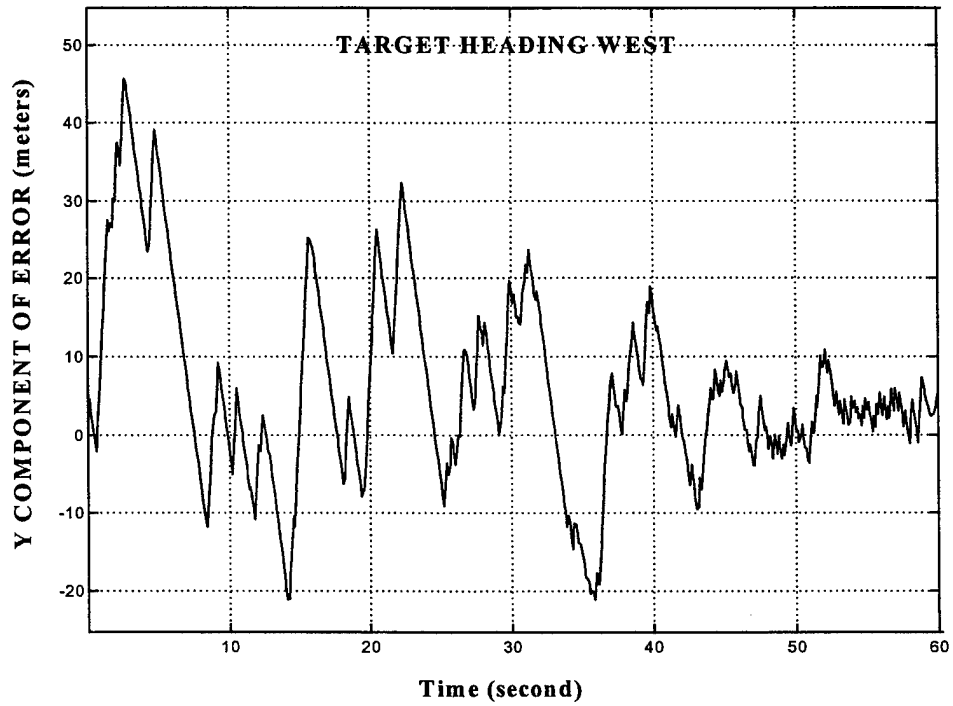

Figure 4.28: Simulator #2 derived target position error in the East/West direction - DIW

88

Figure 4.29: Simulator #2 derived target position error in the Up/Down direction - DIW

Figure 4.30: True target position - CSE 270°

Figure 4.31: Simulator #1 DSTSPI derived target position - CSE 270°

Figure 4.32: Simulator #2 DSTSPI derived target position - CSE 270°

Figure 4.33: Simulator #1derived target position error in the North/South direction - CSE 270°

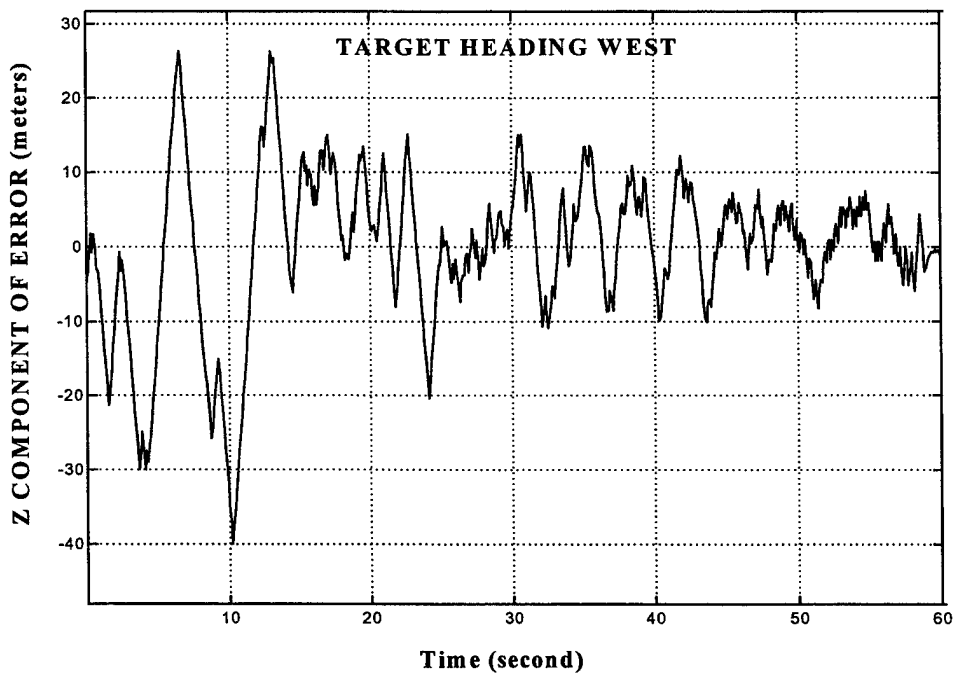**Figure 4.34: Simulator #1 derived target position error in the East/West direction - CSE 270°**

91

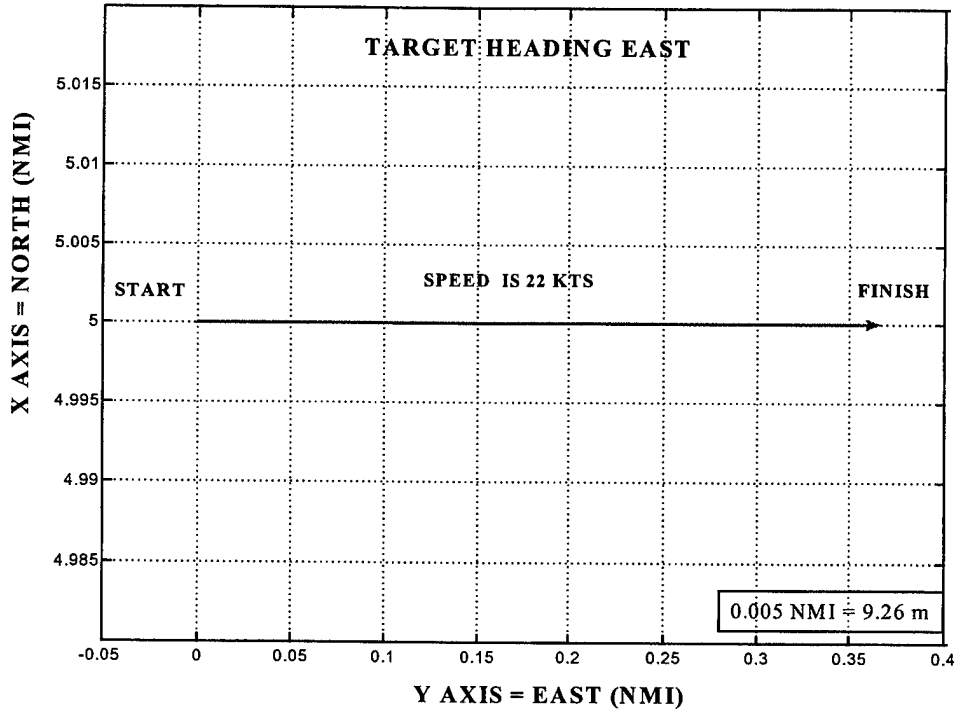**Figure 4.35: Simulator #1 derived target position error in the Up/Down direction - CSE 270°**

Figure 4.36: Simulator #2 derived target position error in the North/South direction - CSE 270°

Figure 4.37: Simulator #2 derived target position error in the East/West direction - CSE 270°

Figure 4.38: Simulator #2 derived target position error in the Up/Down direction - CSE 270°
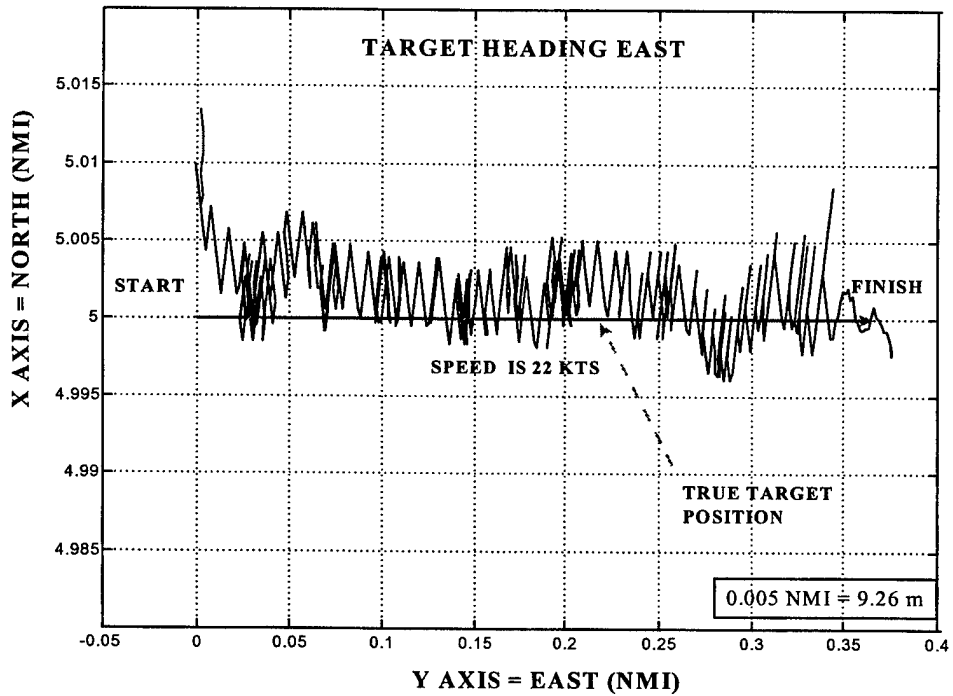
Figure 4.39: True target position - CSE 090°

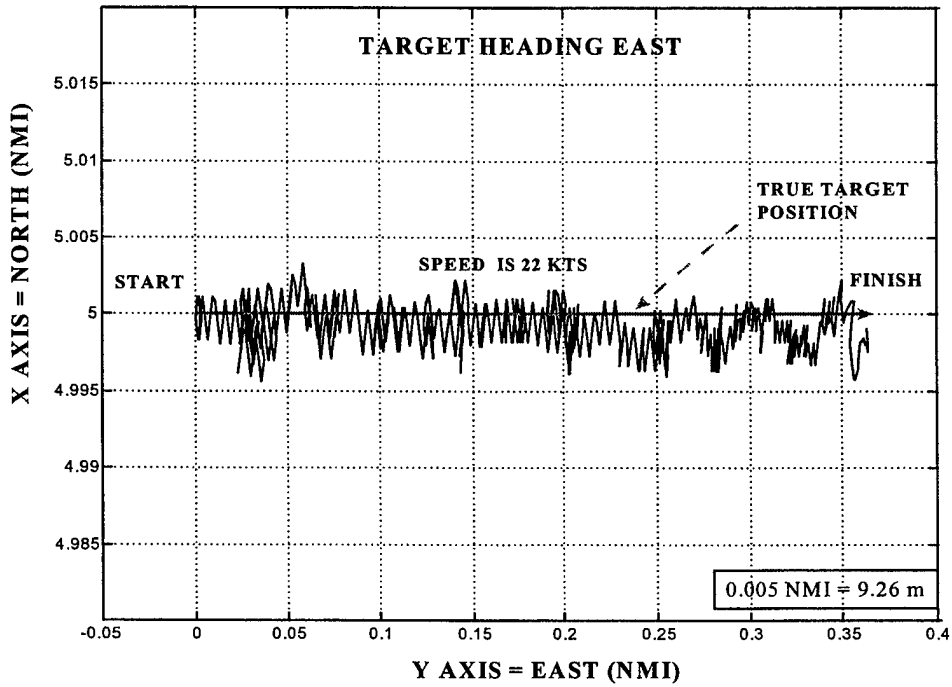**Figure 4.40: Simulator #1 DSTSPI derived target position - CSE 090°**

94

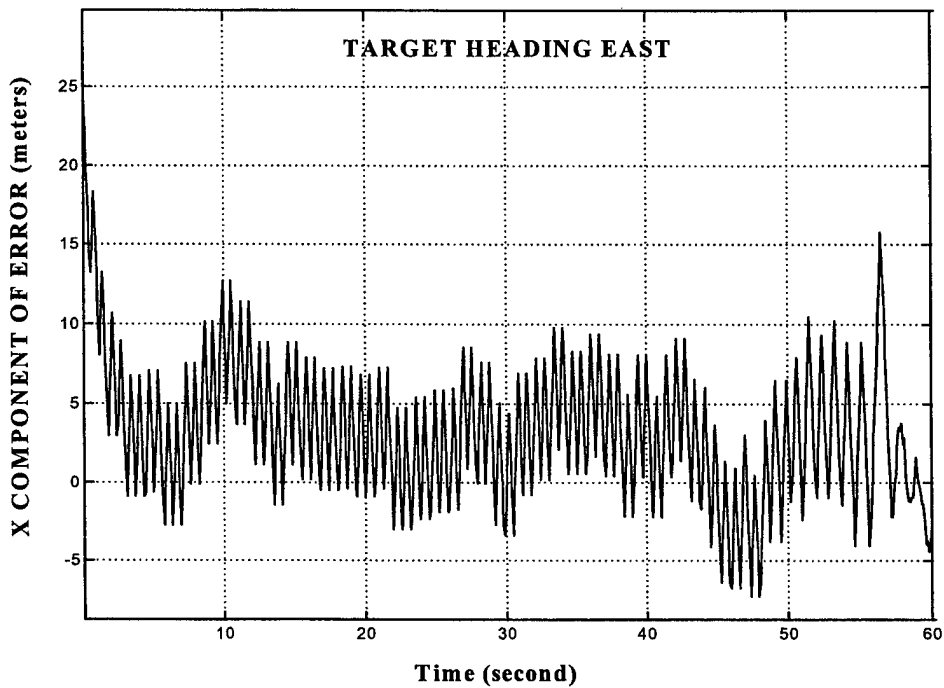**Figure 4.41: Simulator #2 DSTSPI derived target position - CSE 090°**

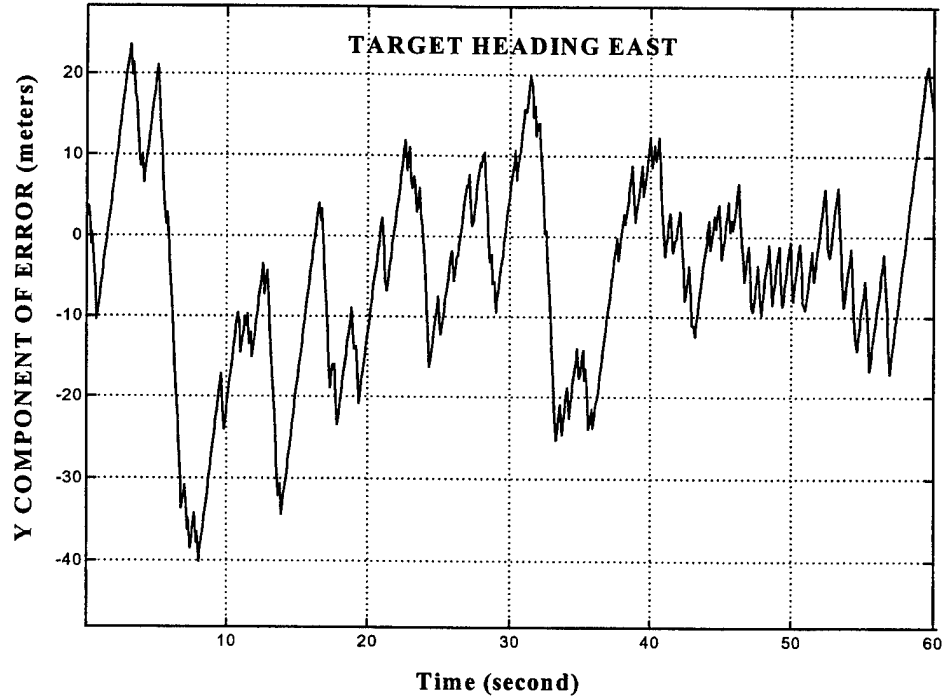**Figure 4.42: Simulator #1derived target position error in the North/South direction - CSE 090°**

Figure 4.43: Simulator #1 derived target position error in the East/West direction - CSE 090°
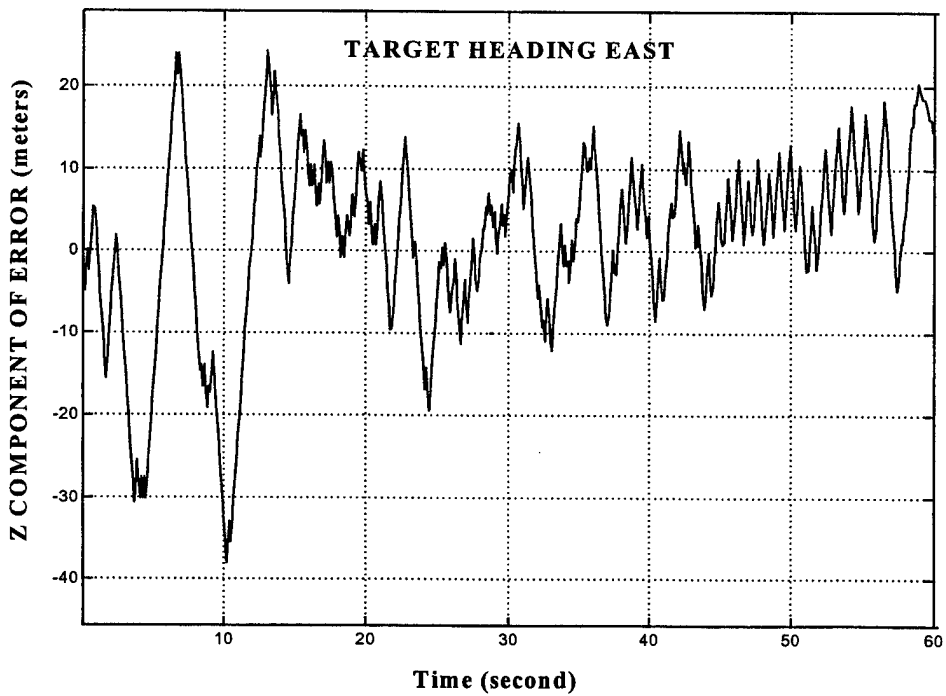

Figure 4.44: Simulator #1 derived target position error in the Up/Down direction - CSE 090°
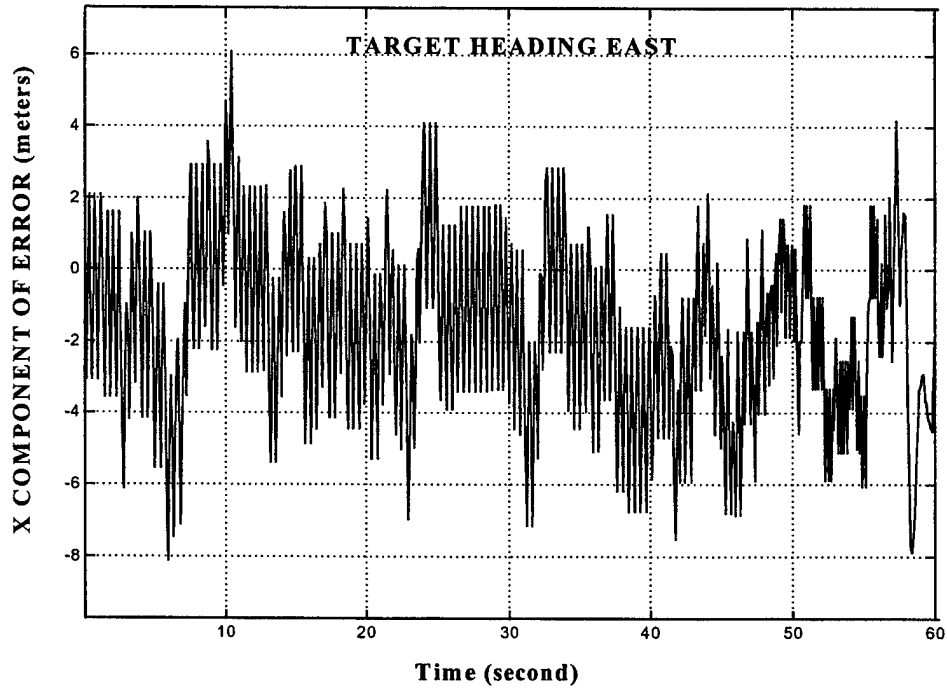
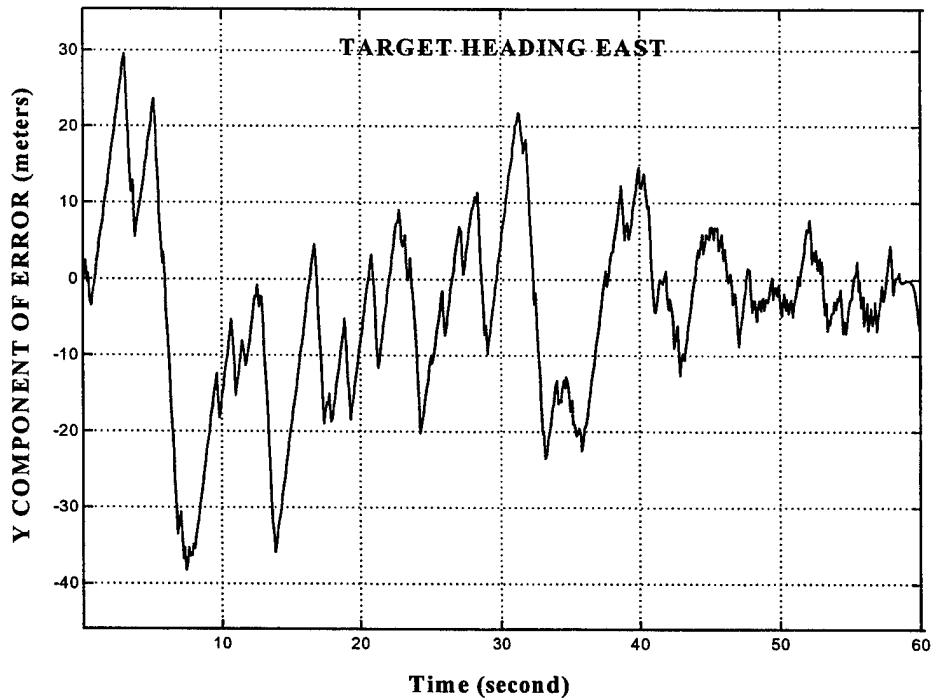**Figure 4.45: Simulator #2 derived target position error in the North/South direction - CSE 090°**

Figure 4.46: Simulator #2 derived target position error in the East/West direction - CSE 090°

Figure 4.47: Simulator #2 derived target position error in the Up/Down direction - CSE 090°

Figure 4.48: True target position - CSE 000°

Figure 4.49: Simulator #1 DSTSPI derived target position - CSE 000°

Figure 4.50: Simulator #2 DSTSPI derived target position - CSE 000°

99

Figure 4.51: Simulator #1 derived target position error in the North/South direction - CSE 000°

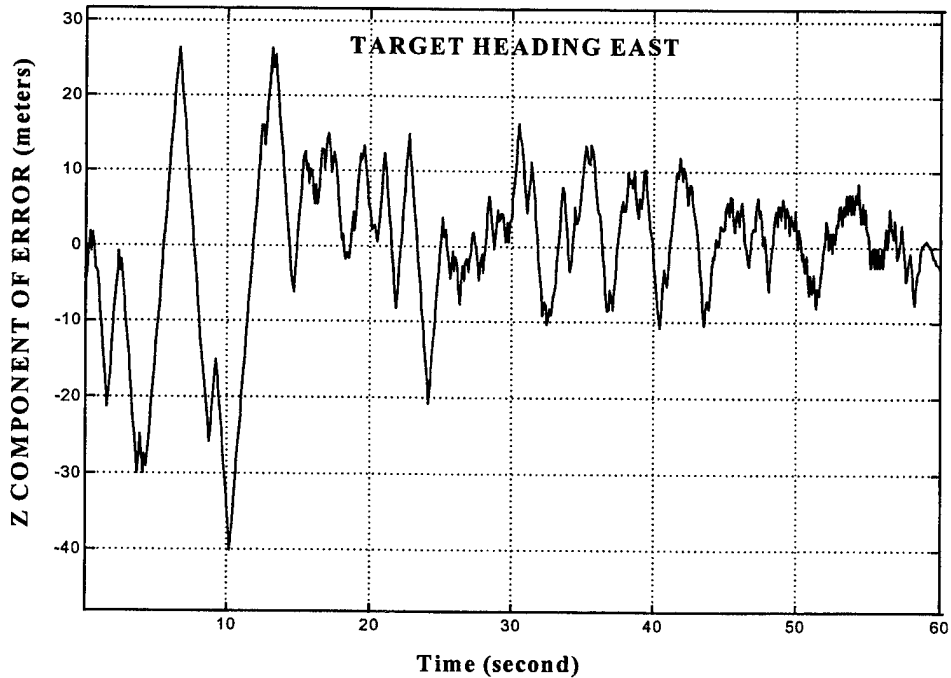**Figure 4.52: Simulator #1 derived target position error in the East/West direction - CSE 000°**

100

Figure 4.53: Simulator #1 derived target position error in the Up/Down direction - CSE 000°

Figure 4.54: Simulator #2 derived target position error in the North/South direction - CSE 000°

101

Figure 4.55: Simulator #2 derived target position error in the East/West direction-CSE 000°

Figure 4.56: Simulator #2 derived target position error in the Up/Down direction - CSE 000°
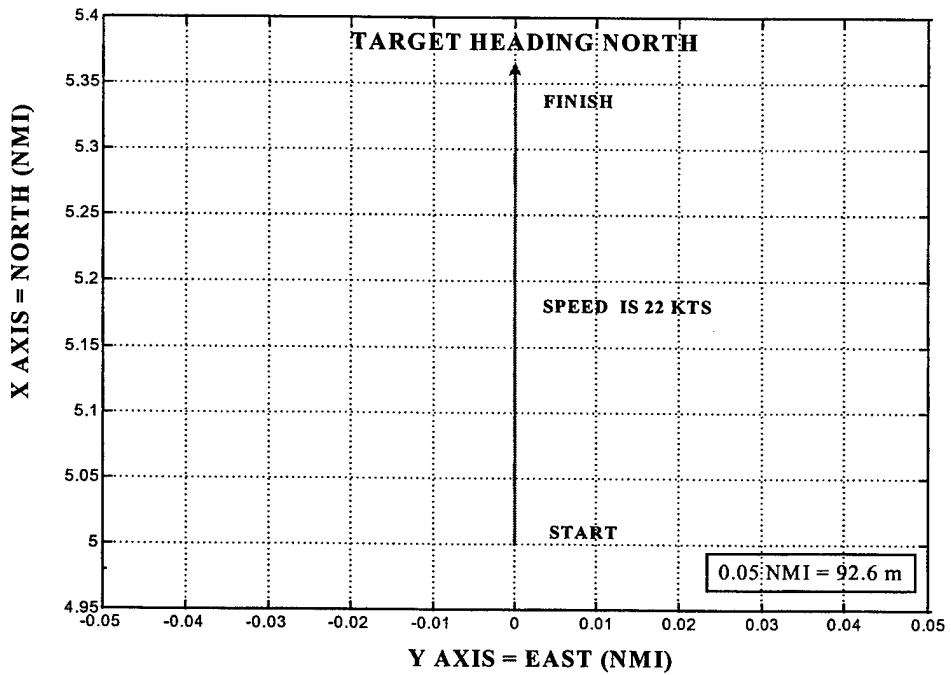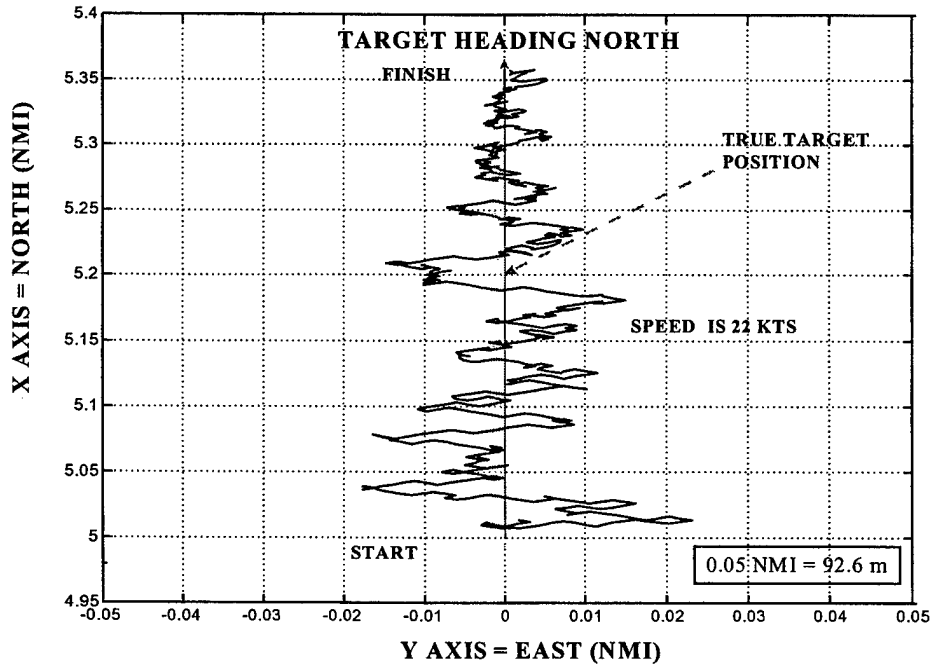
Figure 4.57: True target position - CSE 180°
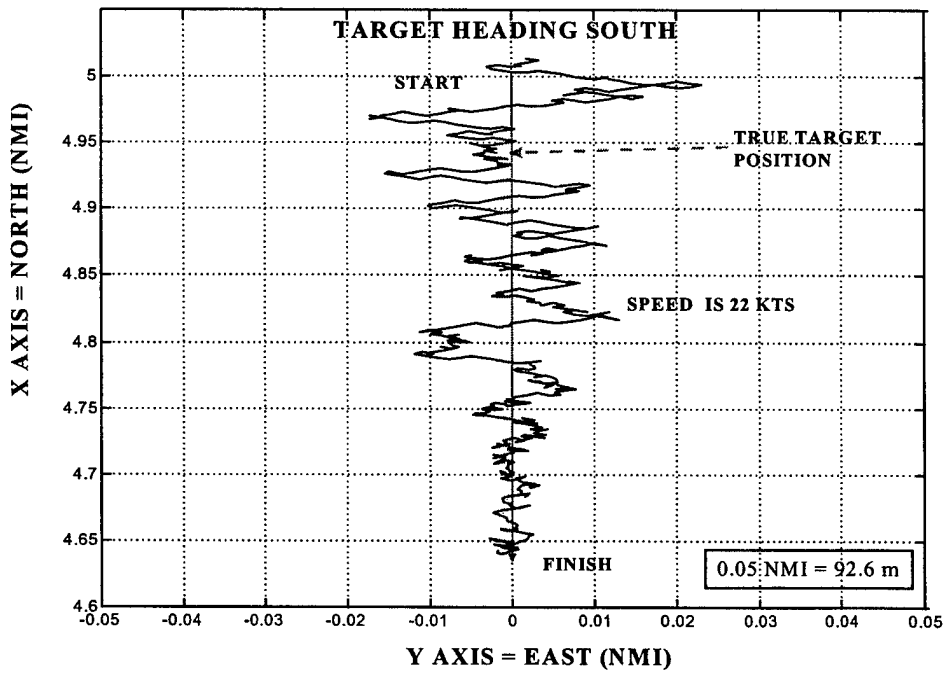
Figure 4.58: Simulator #1 DSTSPI derived target position - CSE 180°
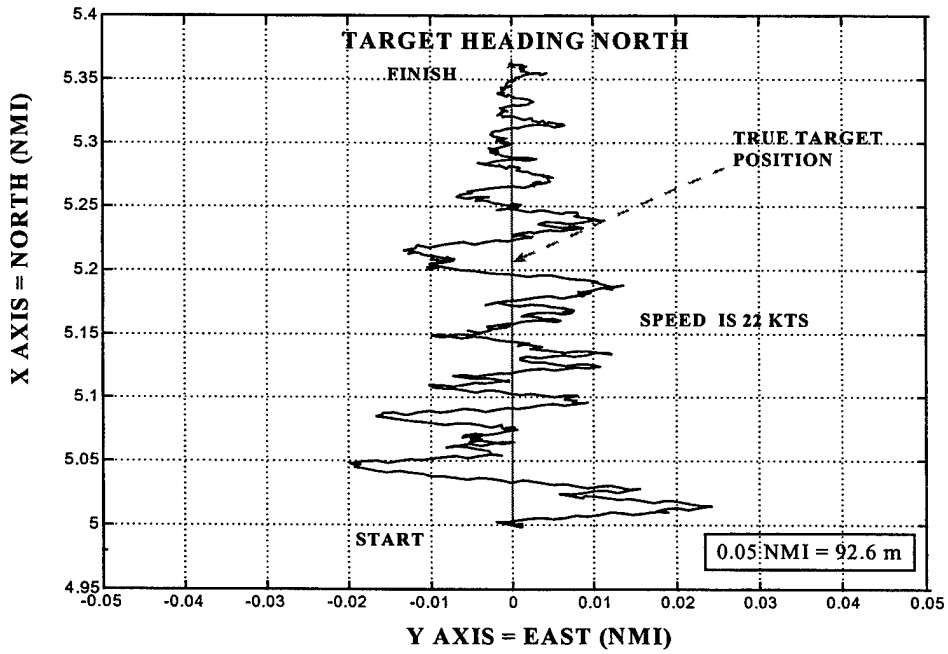
103

Figure 4.59: Simulator #2 DSTSPI derived target position - CSE 180°
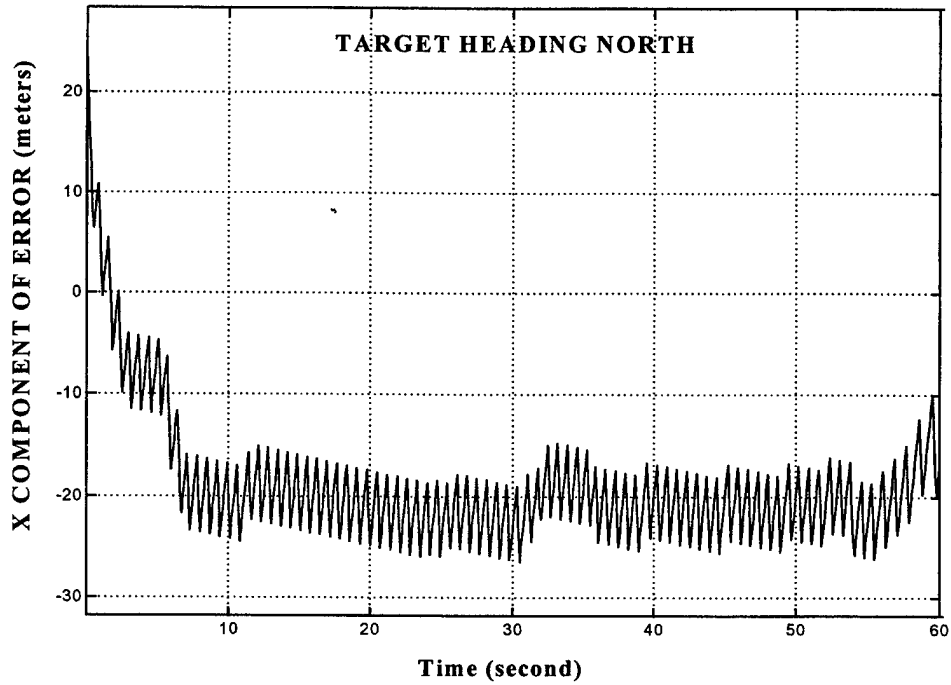

Figure 4.60: Simulator #1 derived target position error in the North/South direction - CSE 180°
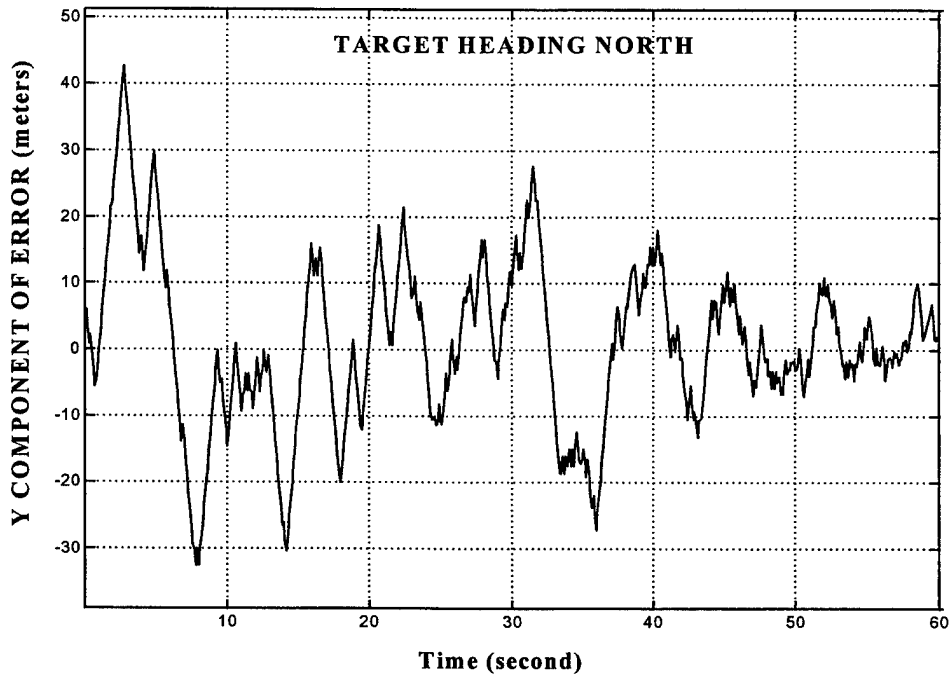
Figure 4.61: Simulator #1 derived target position error in the East/West direction - CSE 180°

Figure 4.62: Simulator #1 derived target position error in the Up/Down direction - CSE 180°

105

Figure 4.63: Simulator #2 derived target position error in the North/South direction - CSE 180°

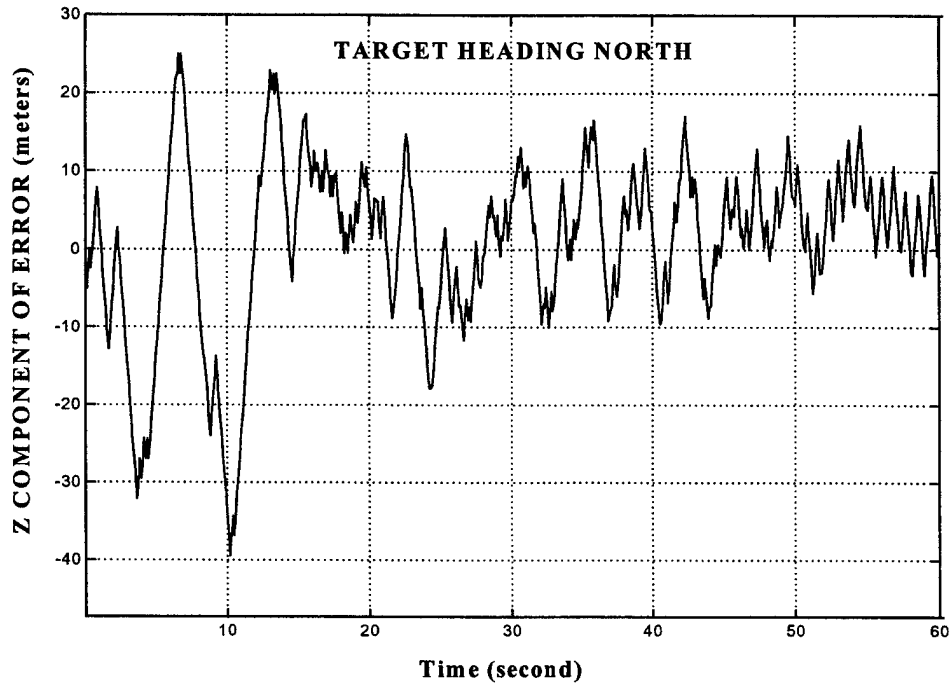**Figure 4.64: Simulator #2 derived target position error in the East/West direction - CSE 180°**

Figure 4.65: Simulator #2 derived target position error in the Up/Down direction - CSE 180°
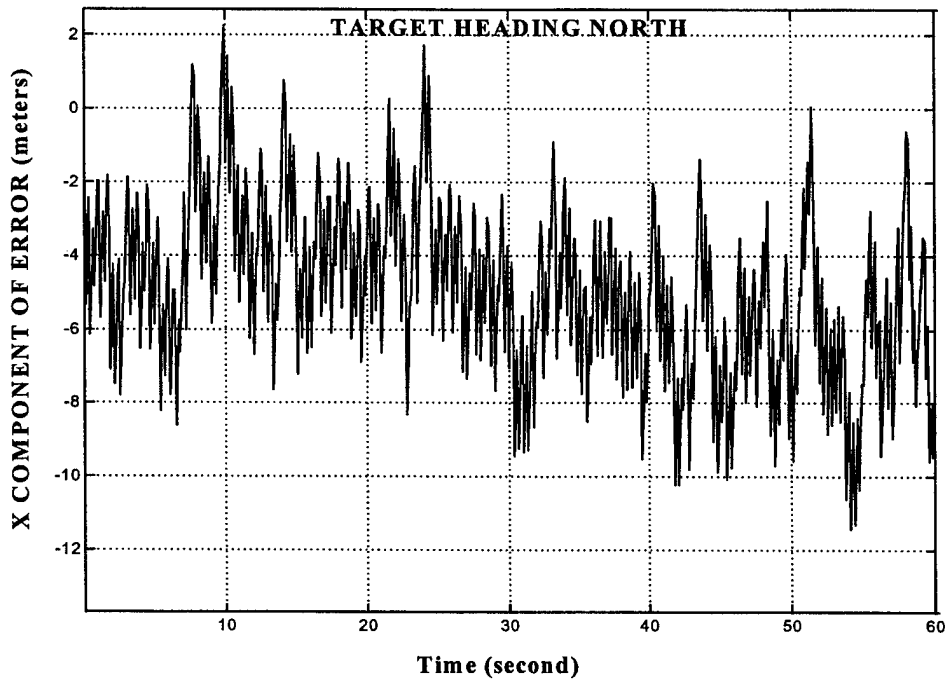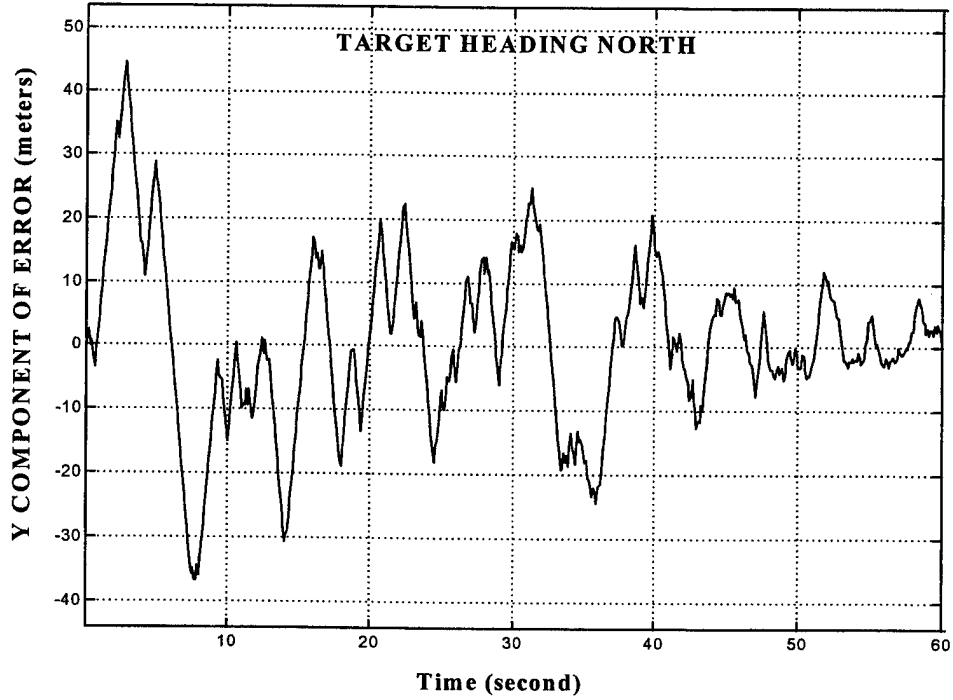

Figure 4.66: True target position - CSE 000° To 270°

Figure 4.67: Simulator #1 DSTSPI derived target position - CSE 000° To 270°

Figure 4.68: Simulator #2 DSTSPI derived target position - CSE 000° To 270°

Figure 4.69: Simulator #1derived target position error in the North/South direction - CSE 000° To 270°

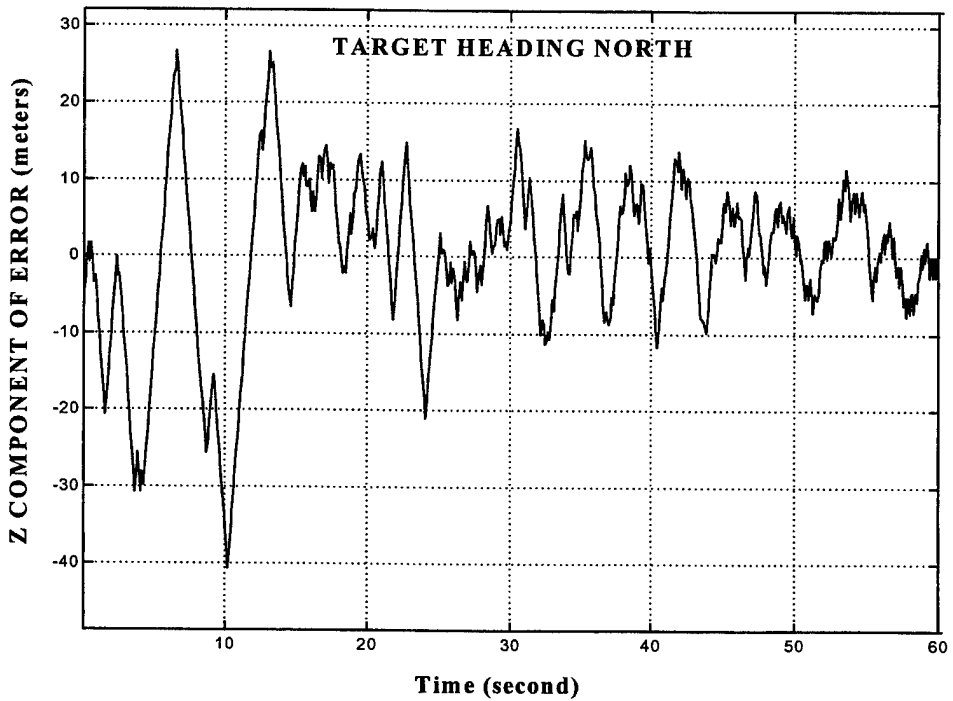**Figure 4.70: Simulator #1 derived target position error in the East/West direction - CSE 000° To 270°**

109
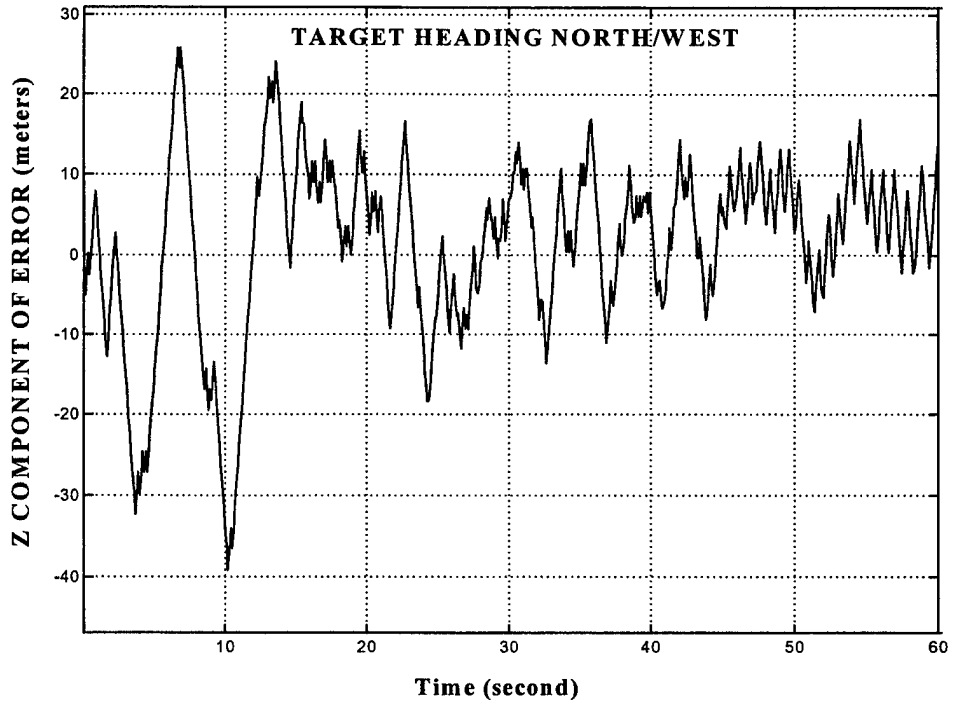
Figure 4.71: Simulator #1 derived target position error in the Up/Down direction - CSE 000° To 270°
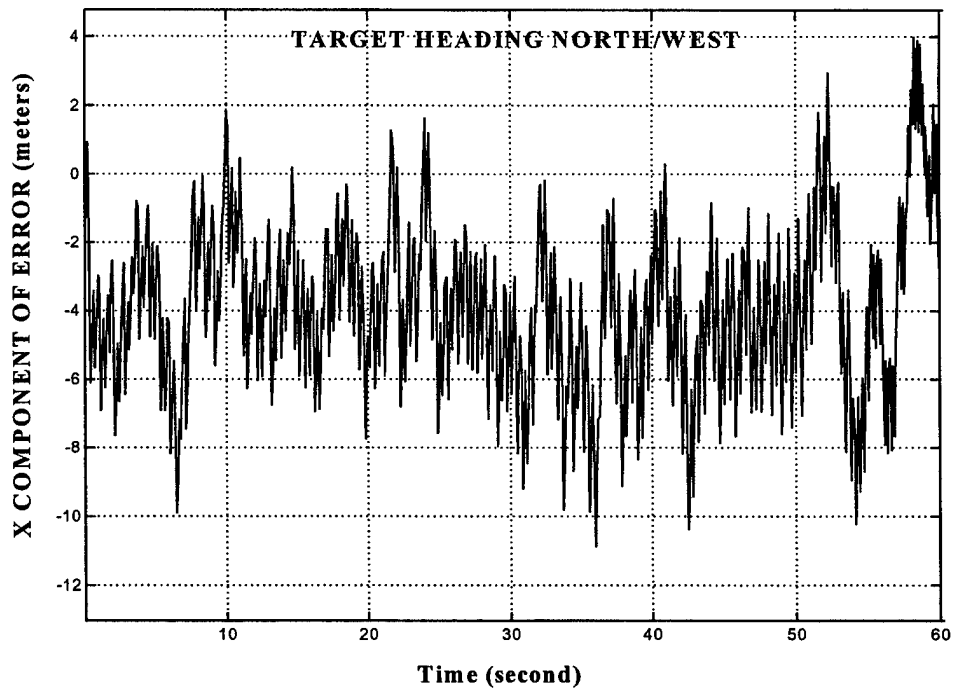
Figure 4.72: Simulator #2 derived target position error in the North/South direction - CSE 000° To 270°
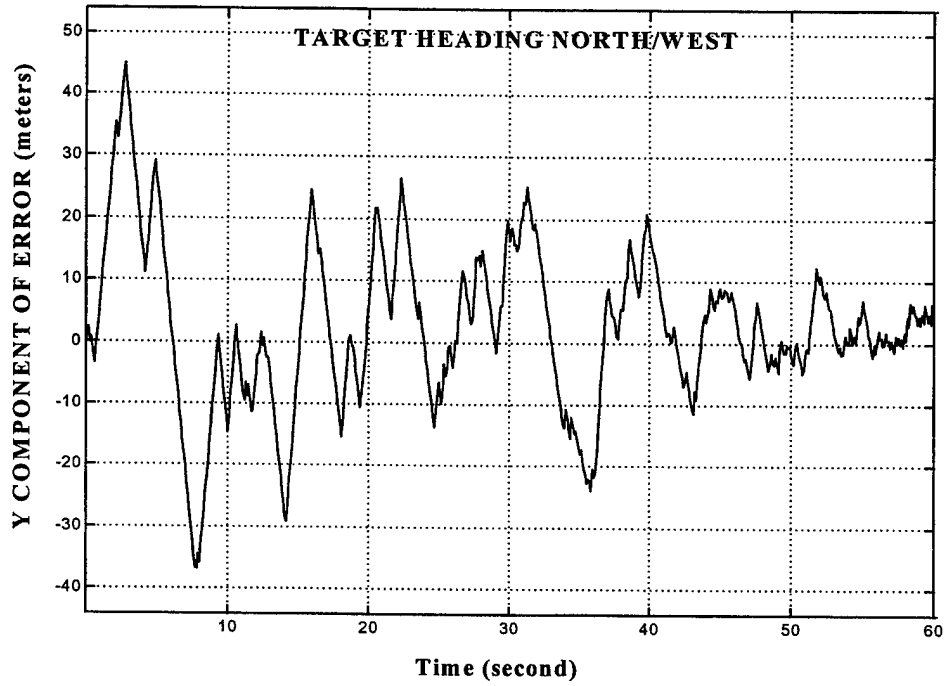
**Figure 4.73: Simulator #2 derived target position error in the East/West direction -
CSE 000° To 270°**
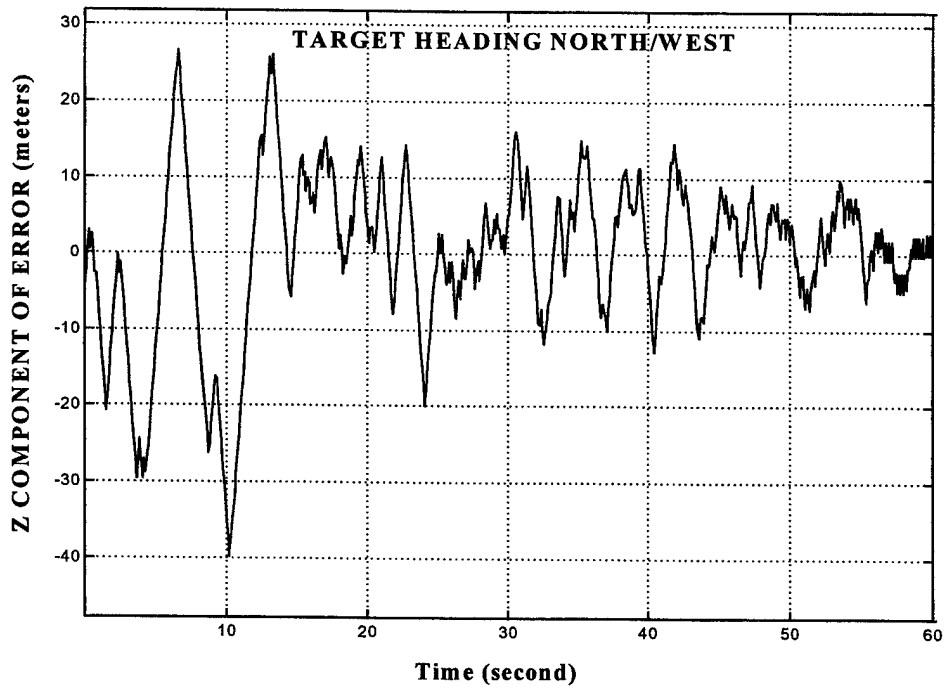
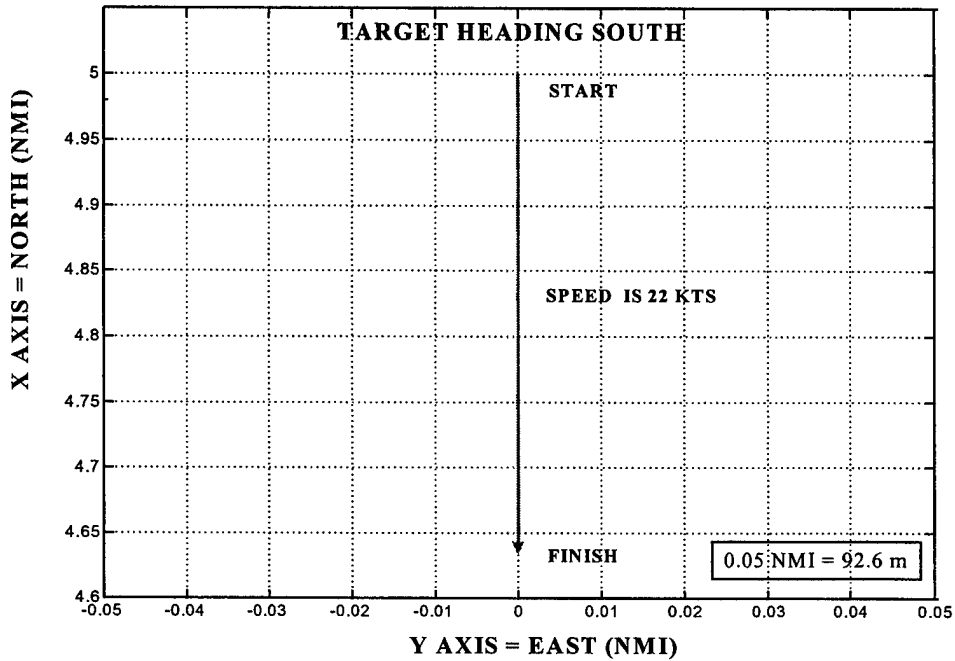**Figure 4.74: Simulator #2 derived target position error in the Up/Down direction -
CSE 000° To 270°**

111

Figure 4.75: True target position - CSE 000° To 090°
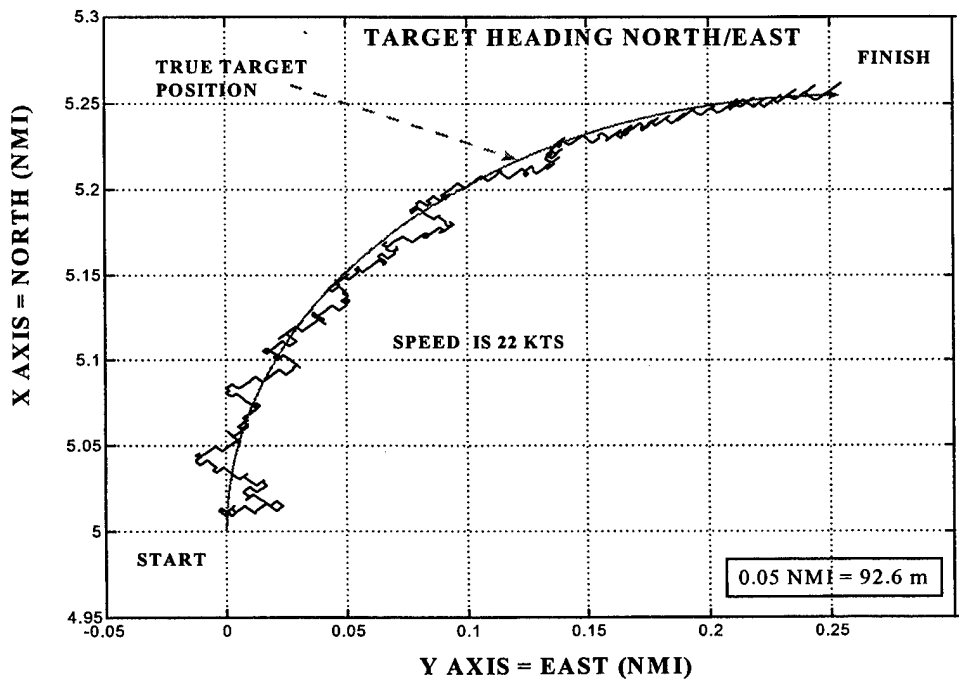
Figure 4.76: Simulator #1 DSTSPI derived target position - CSE 000° To 090°
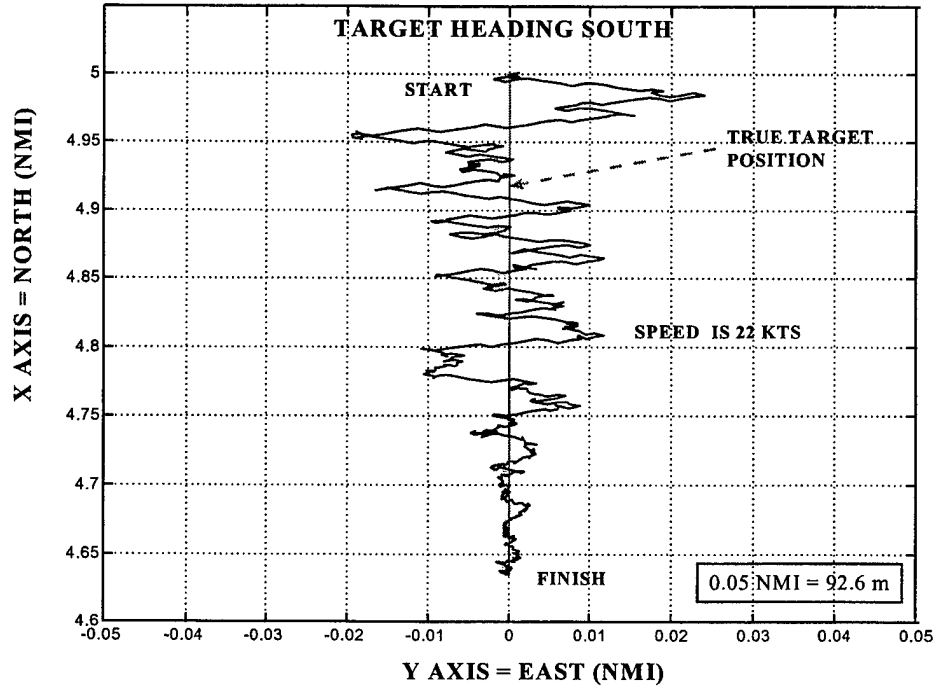
112
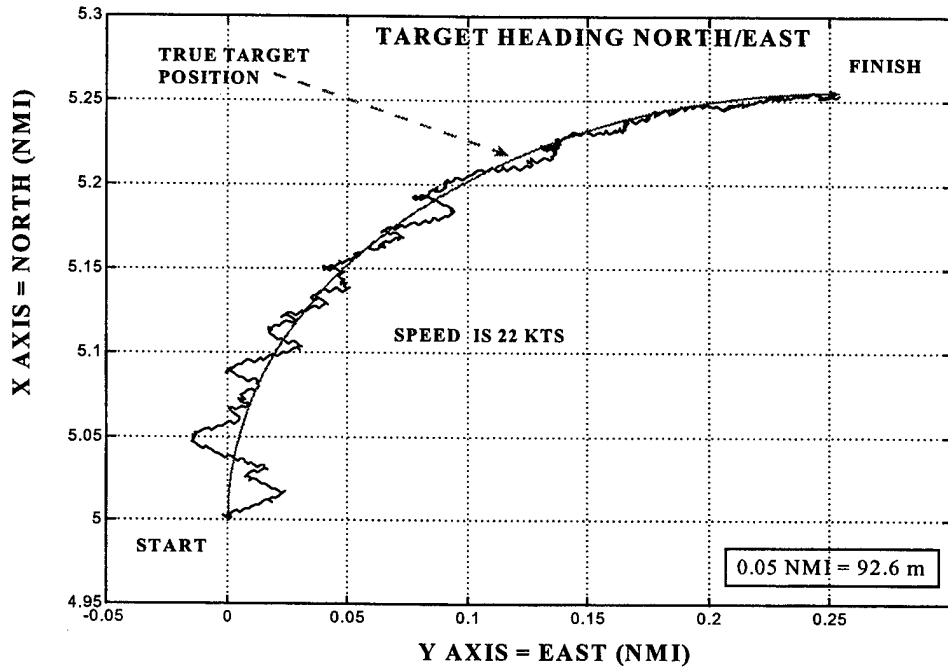
Figure 4.77: Simulator #2 DSTSPI derived target position CSE 000° To - 090°
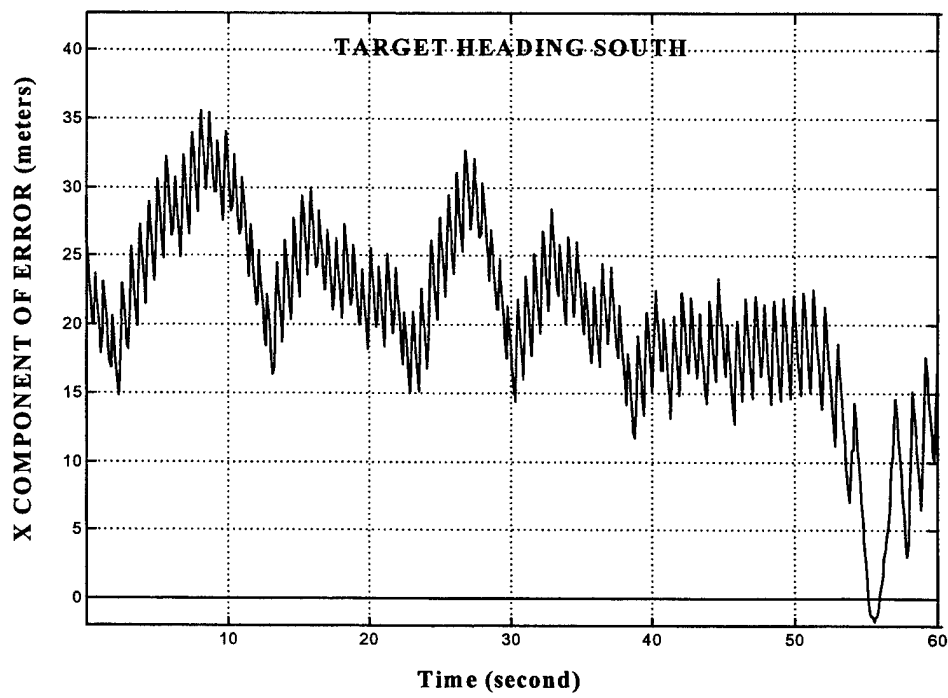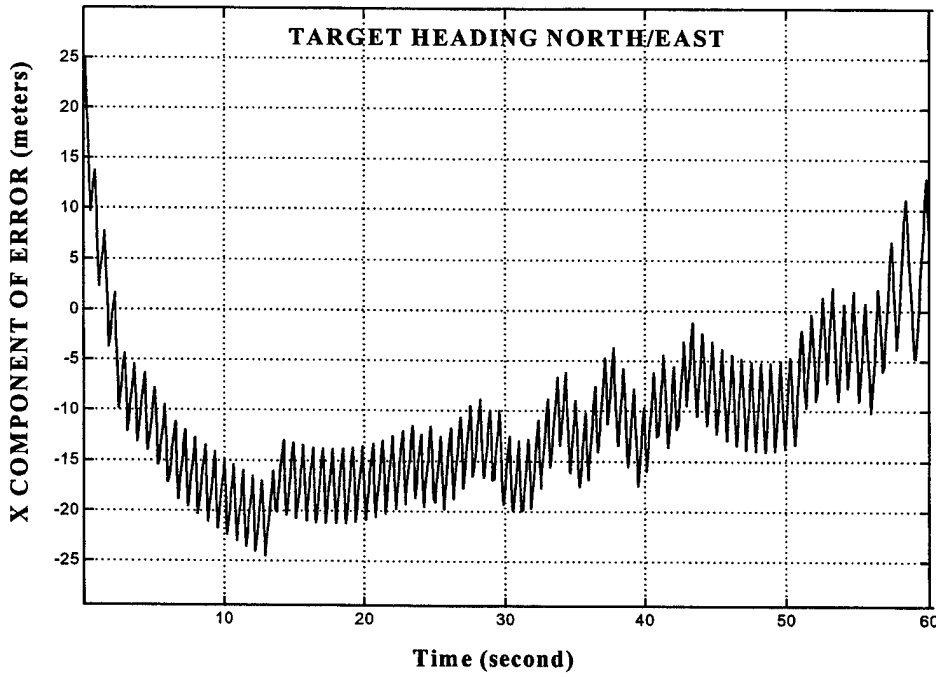

Figure 4.78: Simulator #1derived target position error in the North/South direction - CSE 000° To 090°
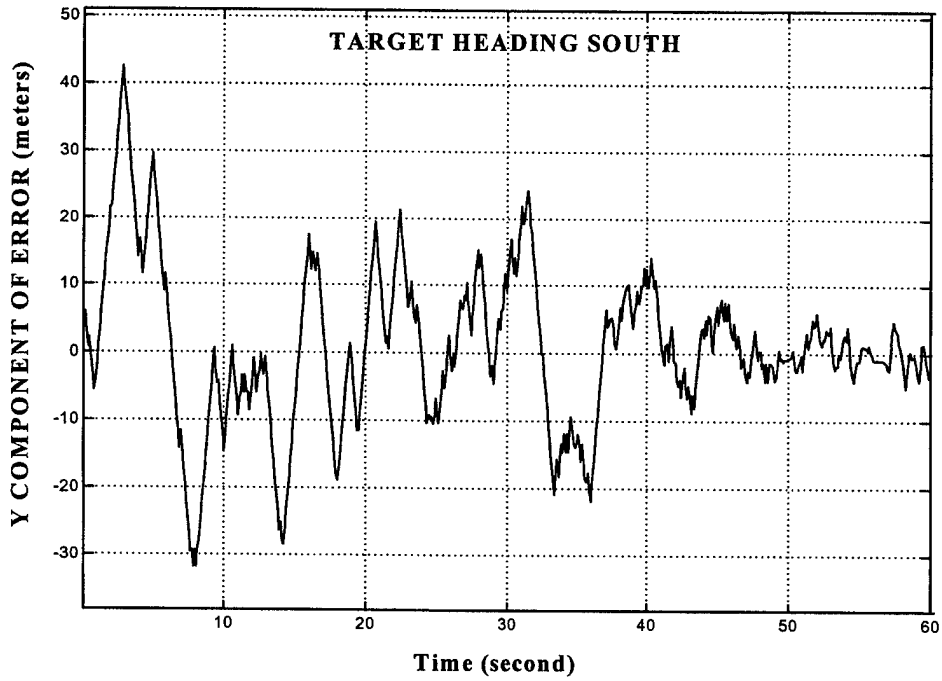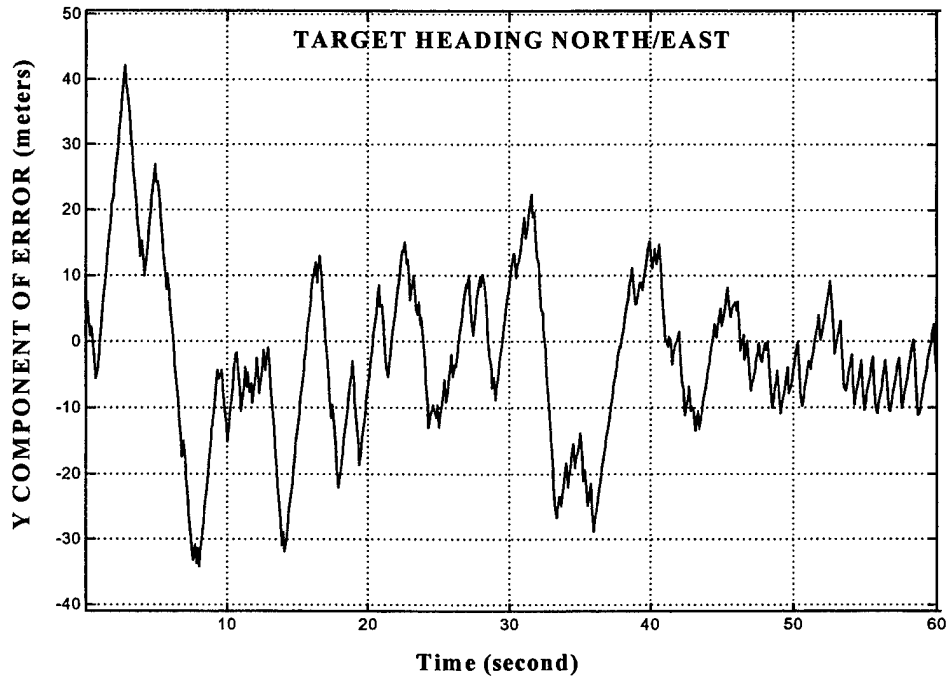
Figure 4.79: Simulator #1 derived target position error in the East/West direction - CSE 000° To 090°
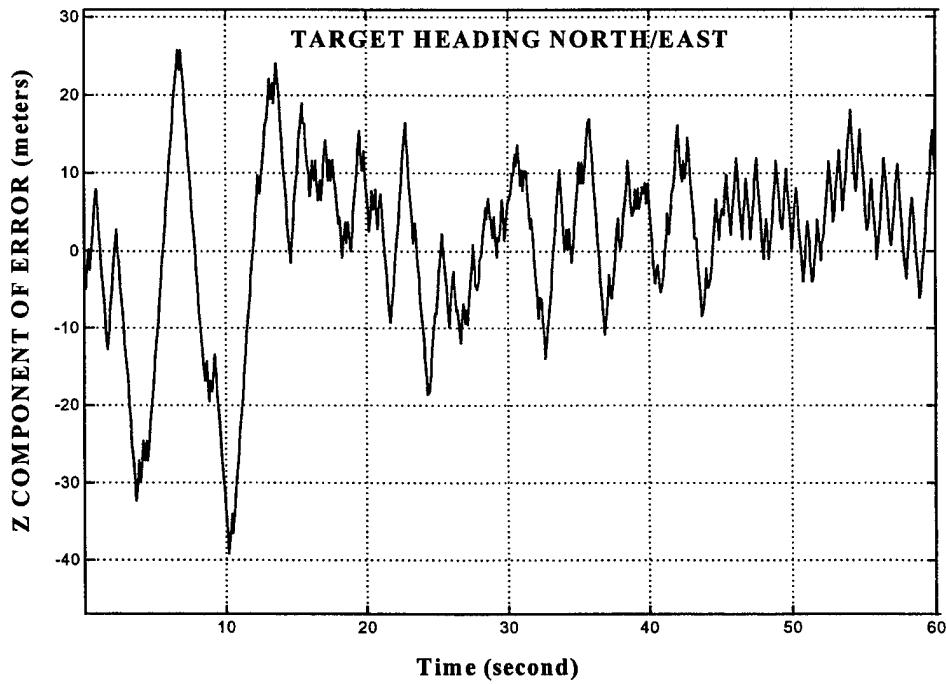
Figure 4.80: Simulator #1 derived target position error in the Up/Down direction - CSE 000° To 090°

114
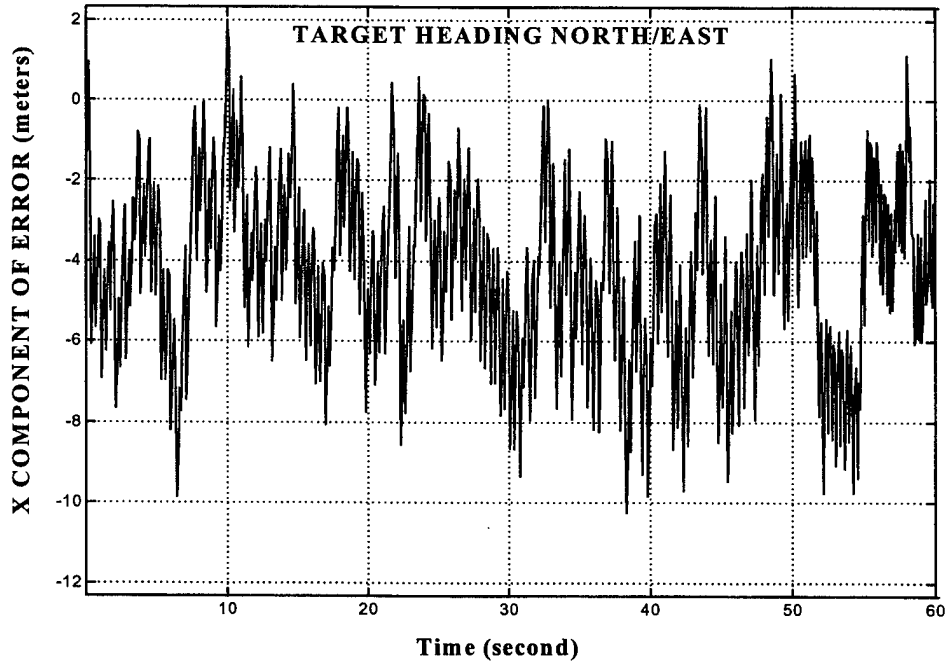
Figure 4.81: Simulator #2 derived target position error in the North/South direction - CSE 000° To 090°
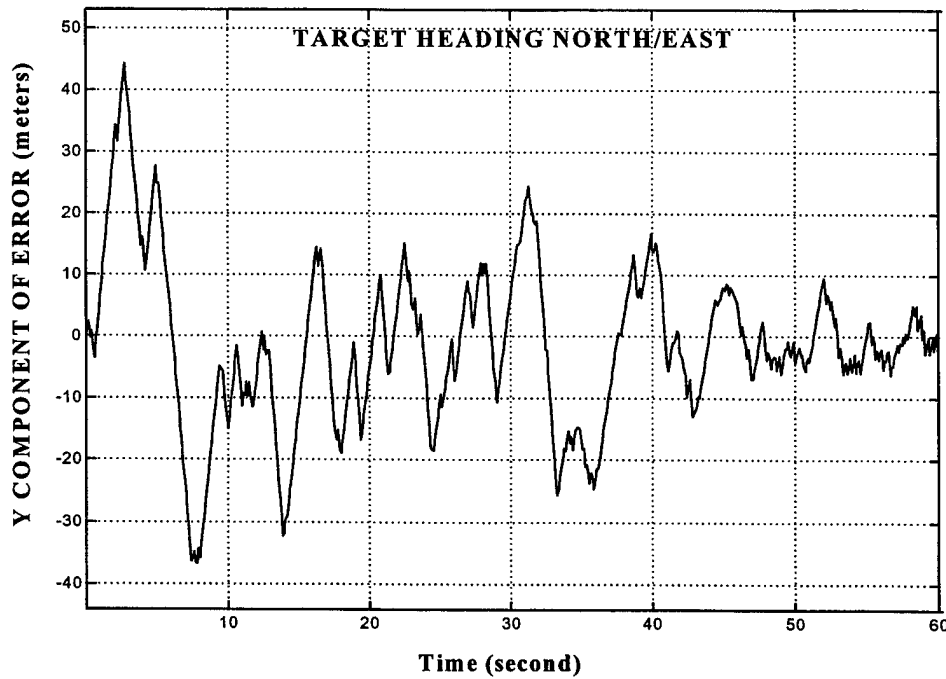
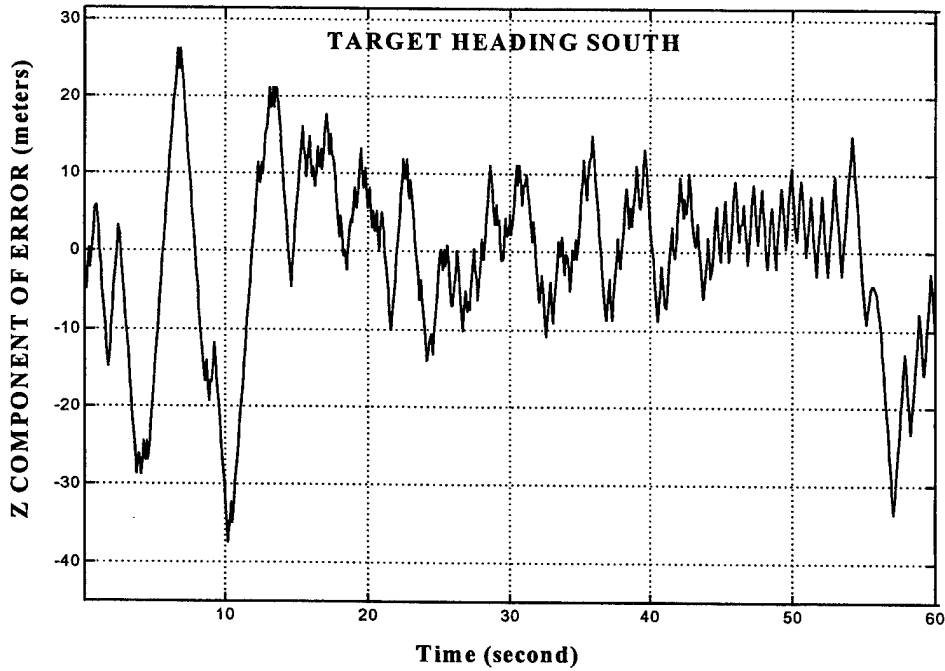**Figure 4.82: Simulator #2 derived target position error in the East/West direction - CSE 000° To 090°**

115
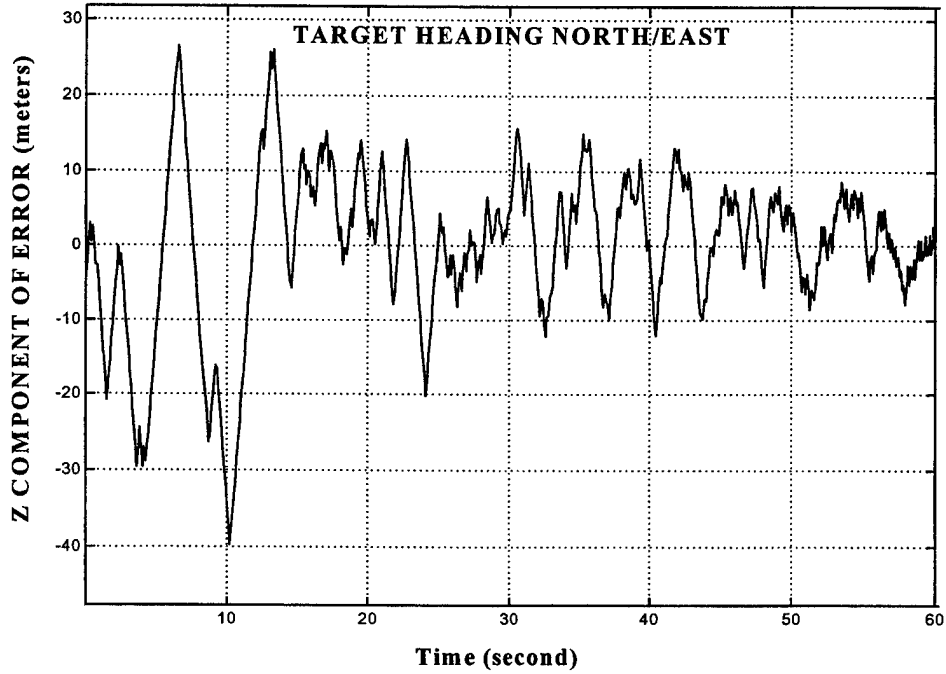
Figure 4.83: Simulator #2 derived target position error in the Up/Down direction - CSE 000° To 090°
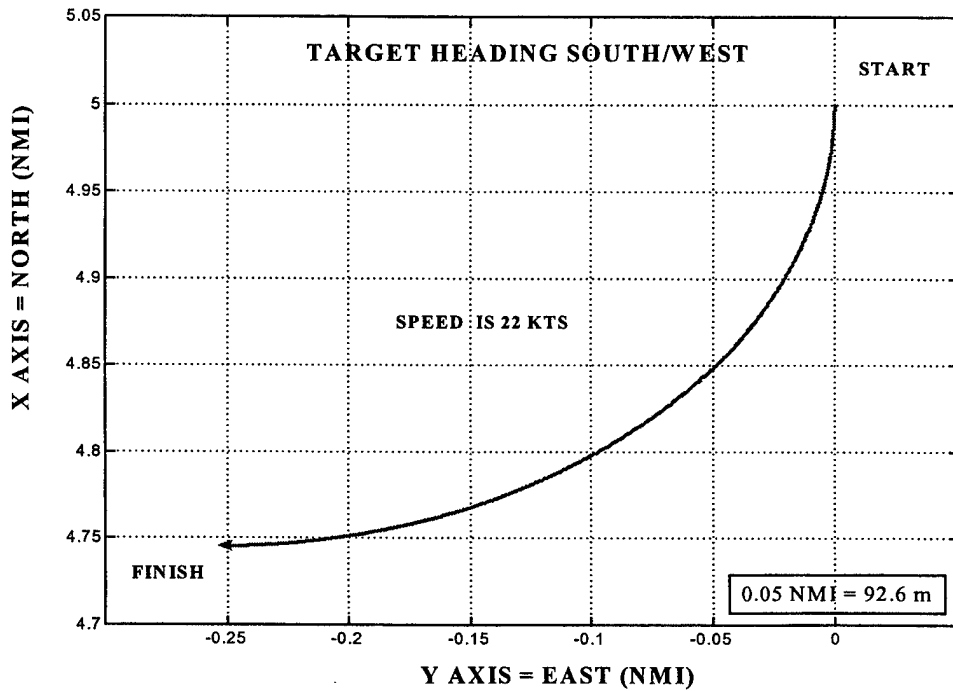
Figure 4.84: True target position - CSE 180° To 270°
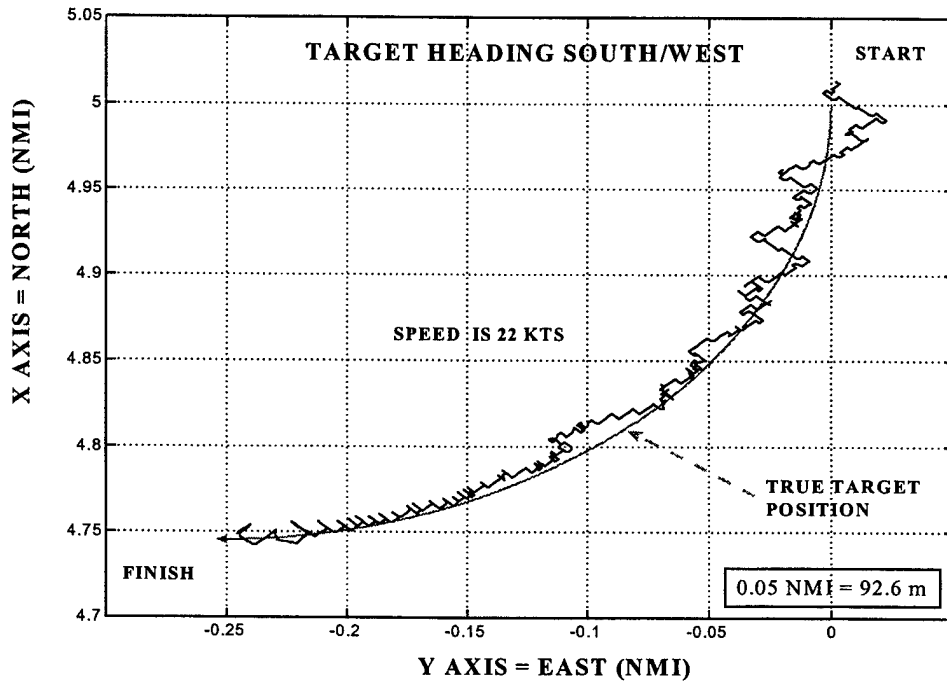
Figure 4.85: Simulator #1 DSTSPI derived target position - CSE 180° To 270°
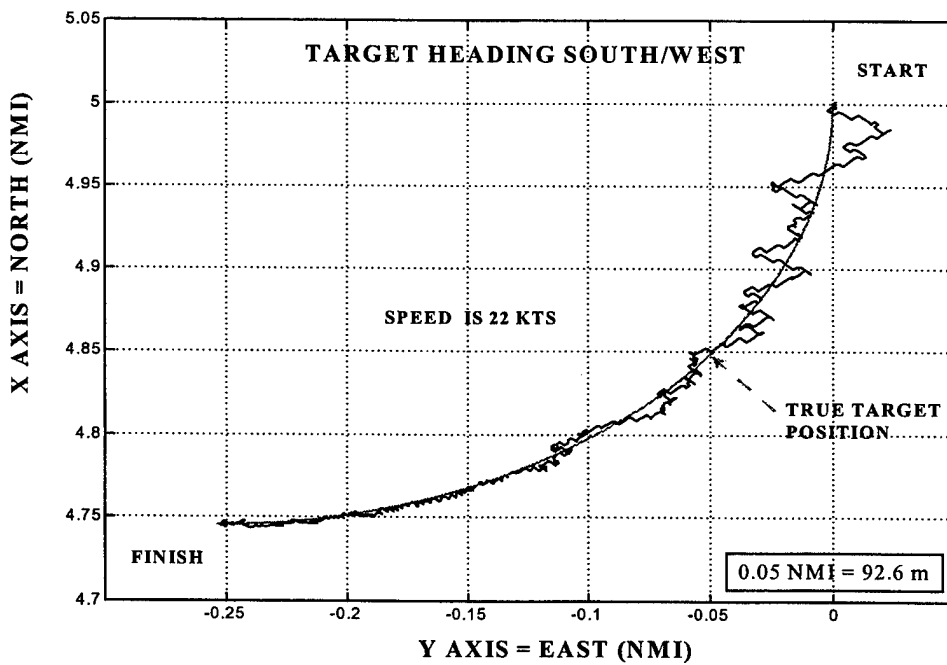
Figure 4.86: Simulator #2 DSTSPI derived target position - CSE 180° To 270°
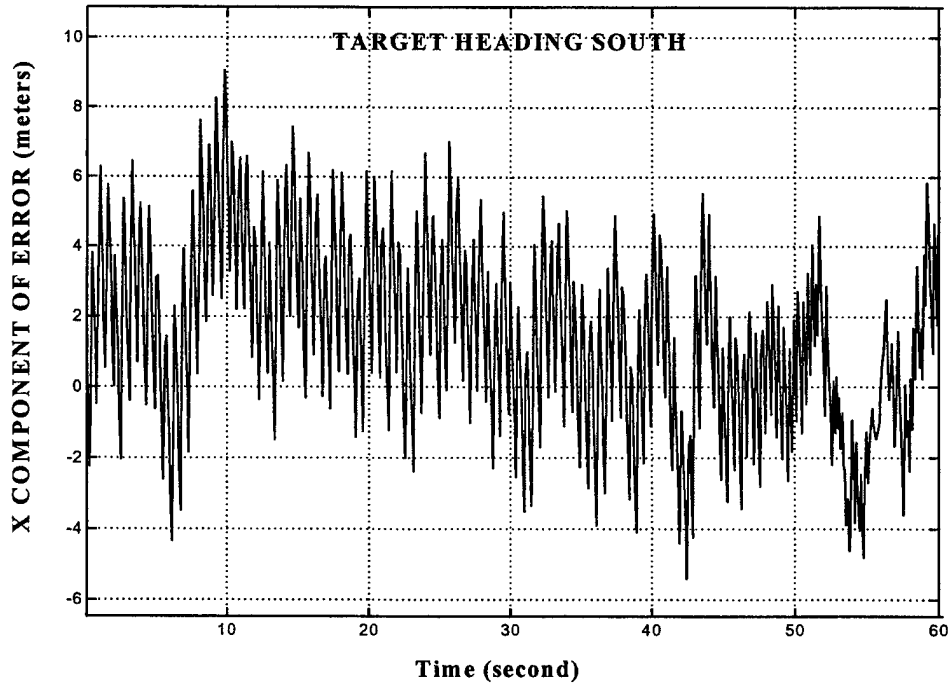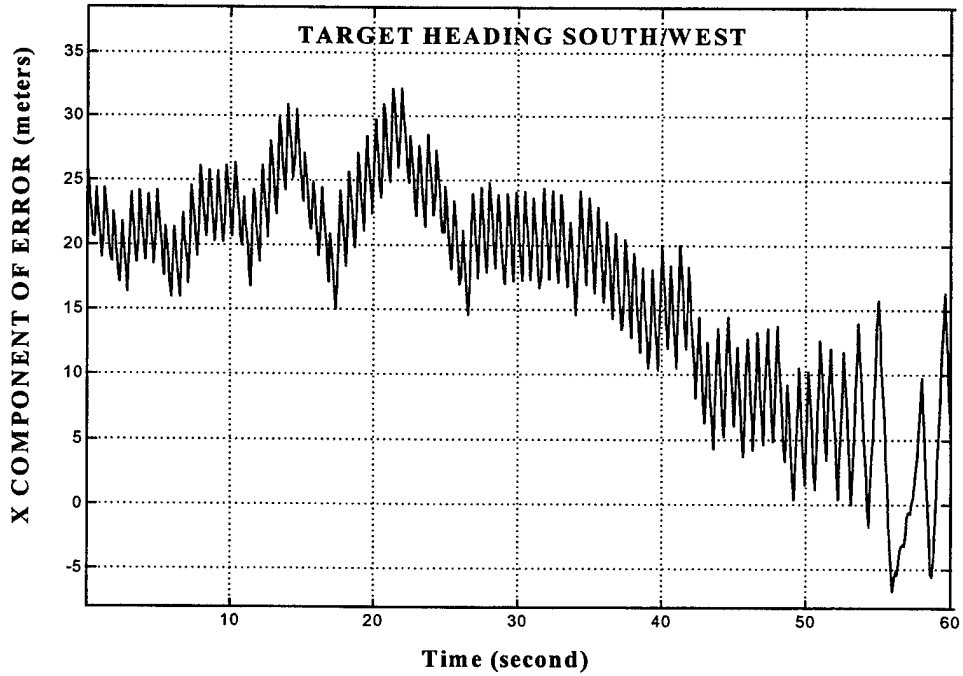
Figure 4.87: Simulator #1 derived target position error in the North/South direction -
CSE 180° To 270°
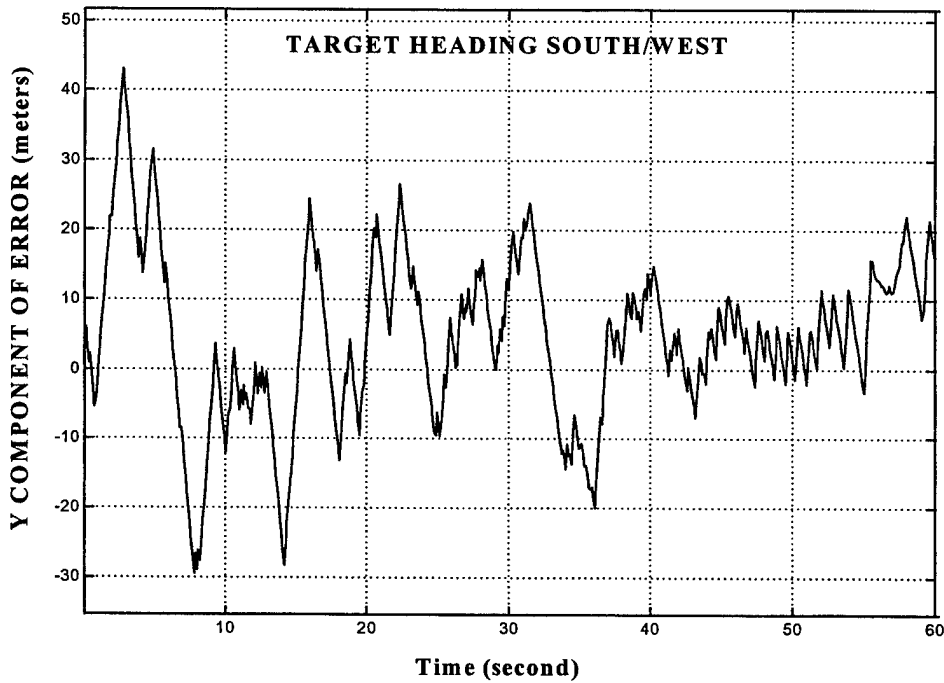
Figure 4.88: Simulator #1 derived target position error in the East/West direction -
CSE 180° To 270°
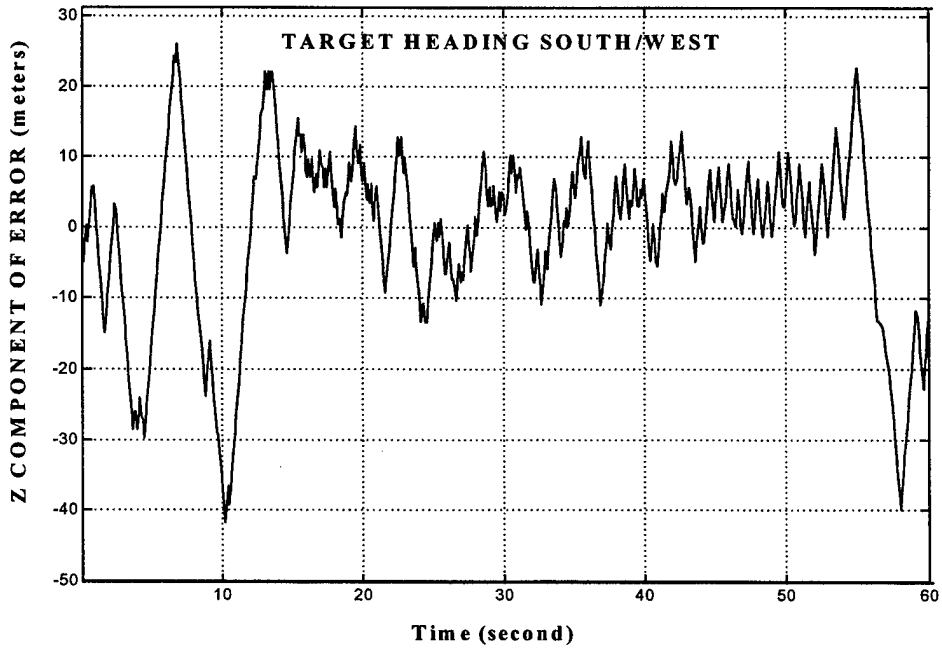
Figure 4.89: **Simulator #1 derived target position error in the Up/Down direction - CSE 180° To 270°**
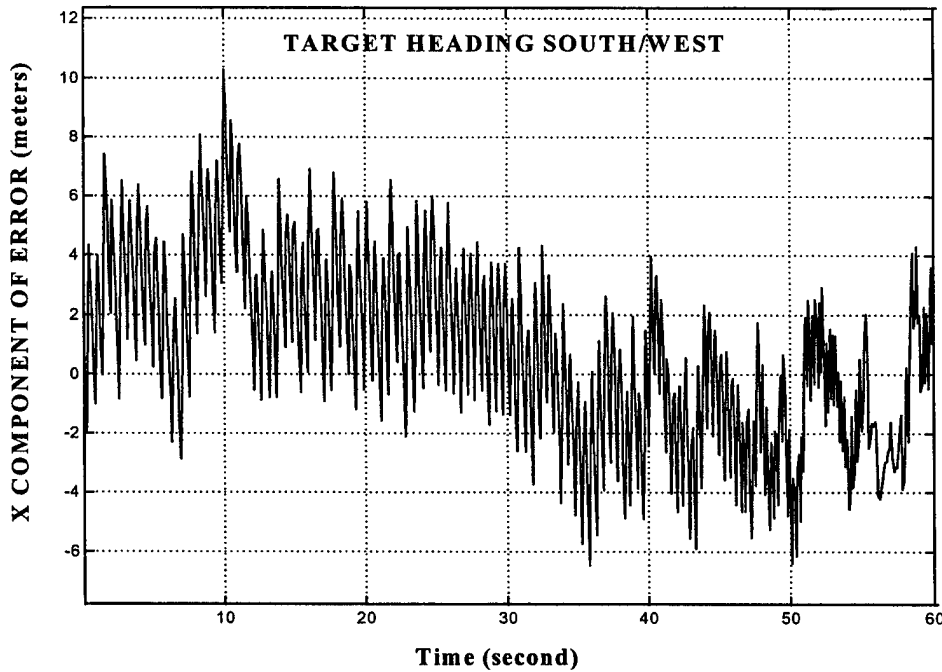
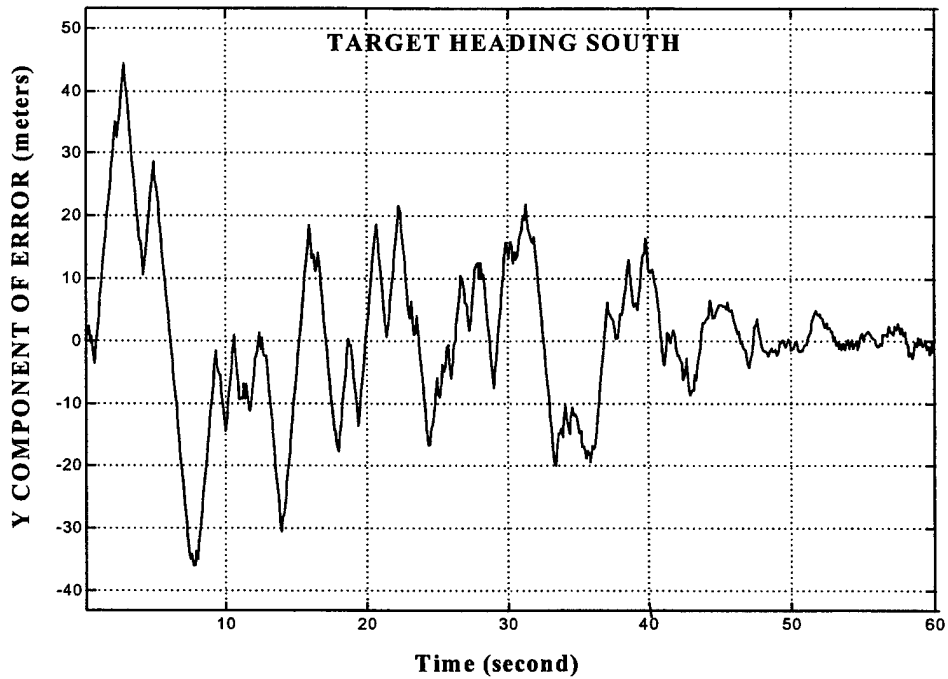**Figure 4.90:** **Simulator #2 derived target position error in the North/South direction - CSE 180° To 270°**
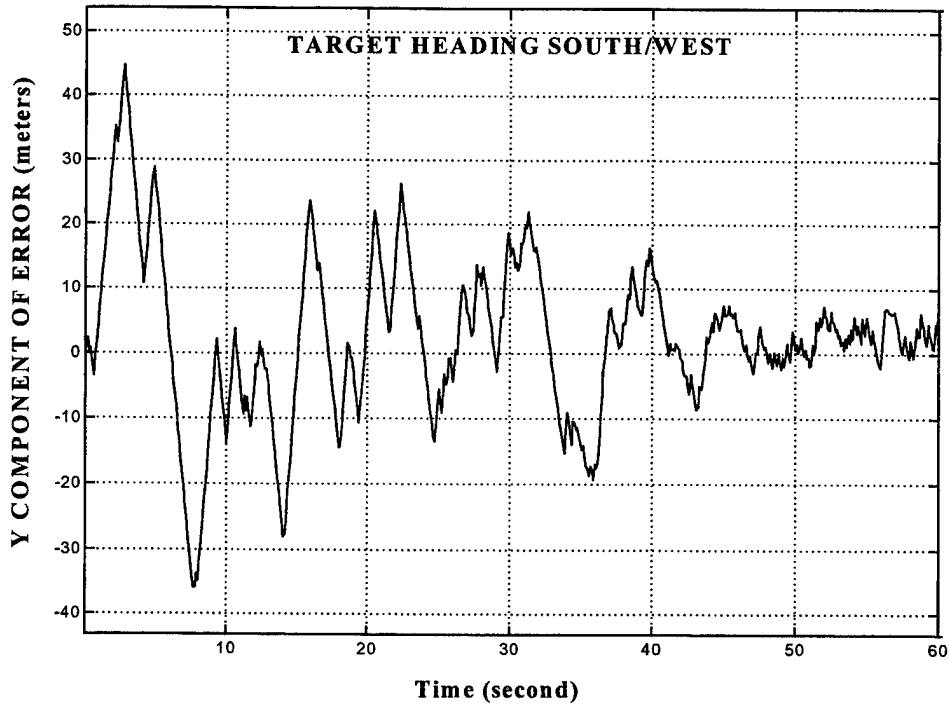
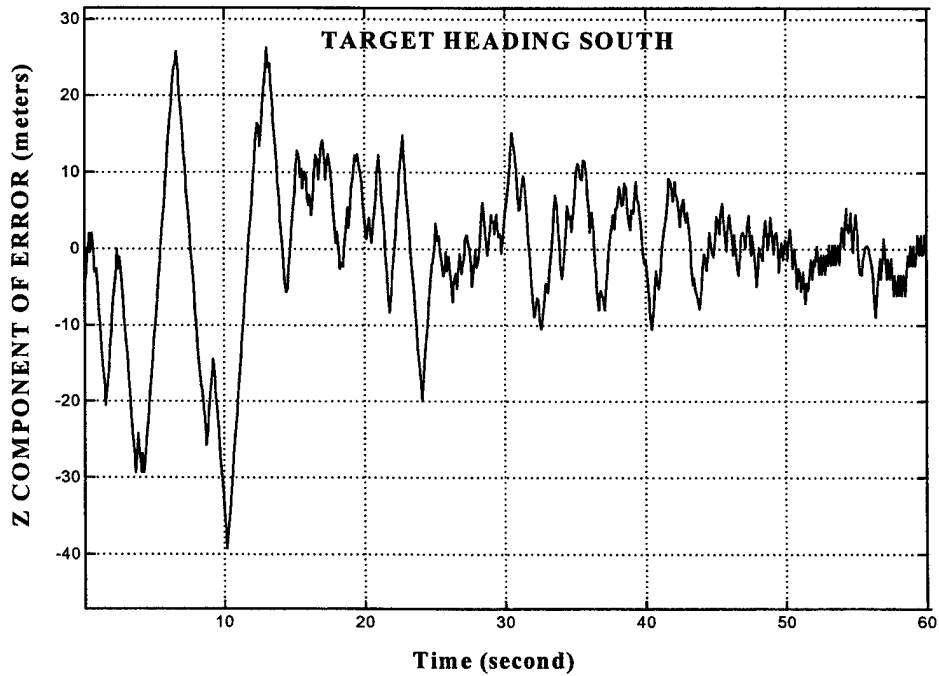**Figure 4.91:** **Simulator #2 derived target position error in the East/West direction -**
CSE 180° To 270°
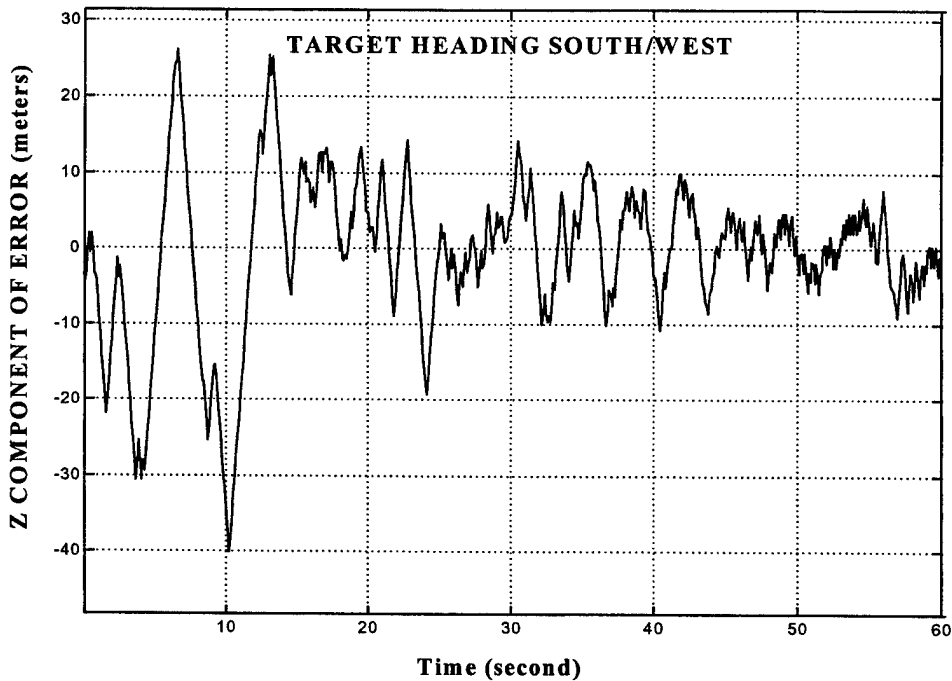
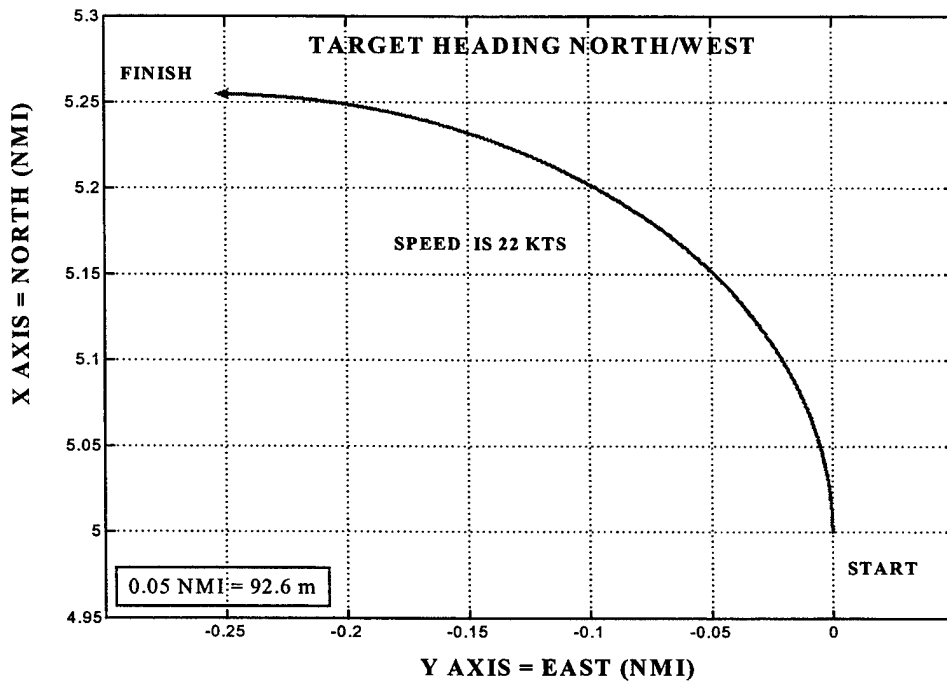**Figure 4.92:** **Simulator #2 derived target position error in the Up/Down direction -**
CSE 180° To 270°
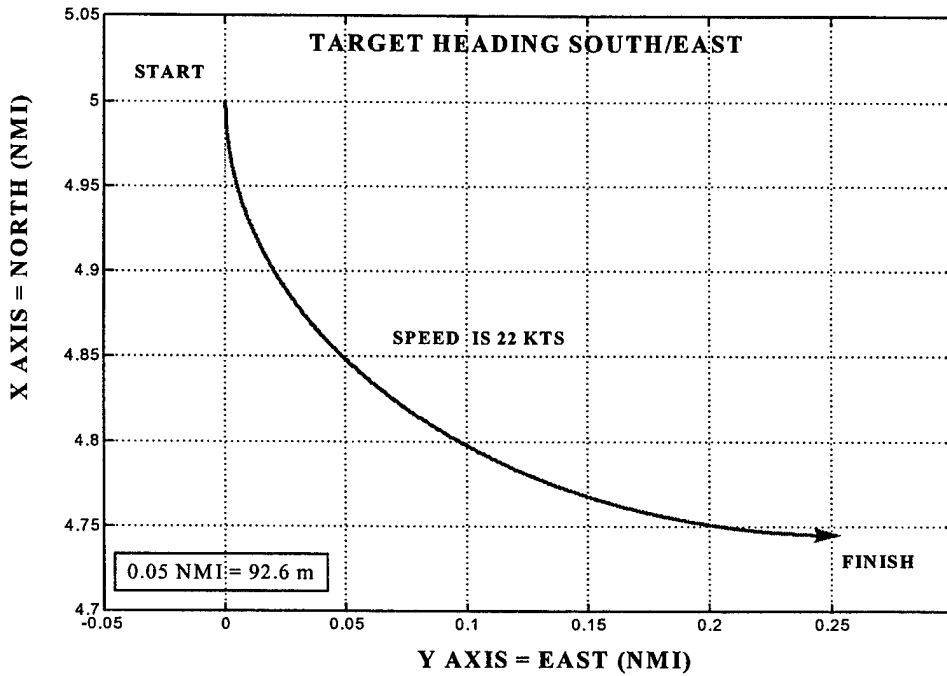
Figure 4.93: True target position - CSE 180° To 090°
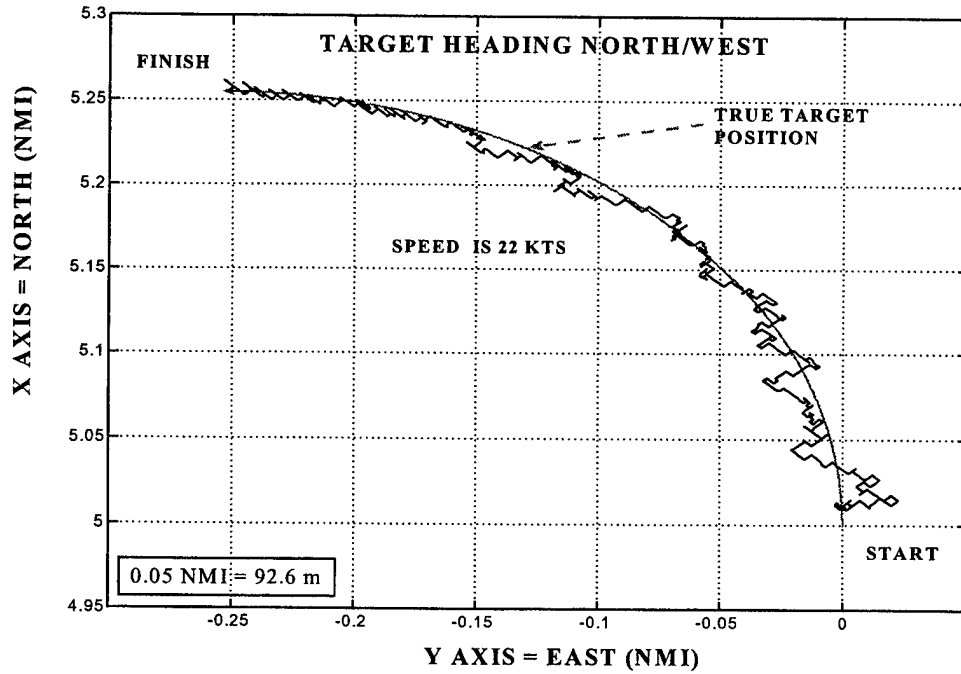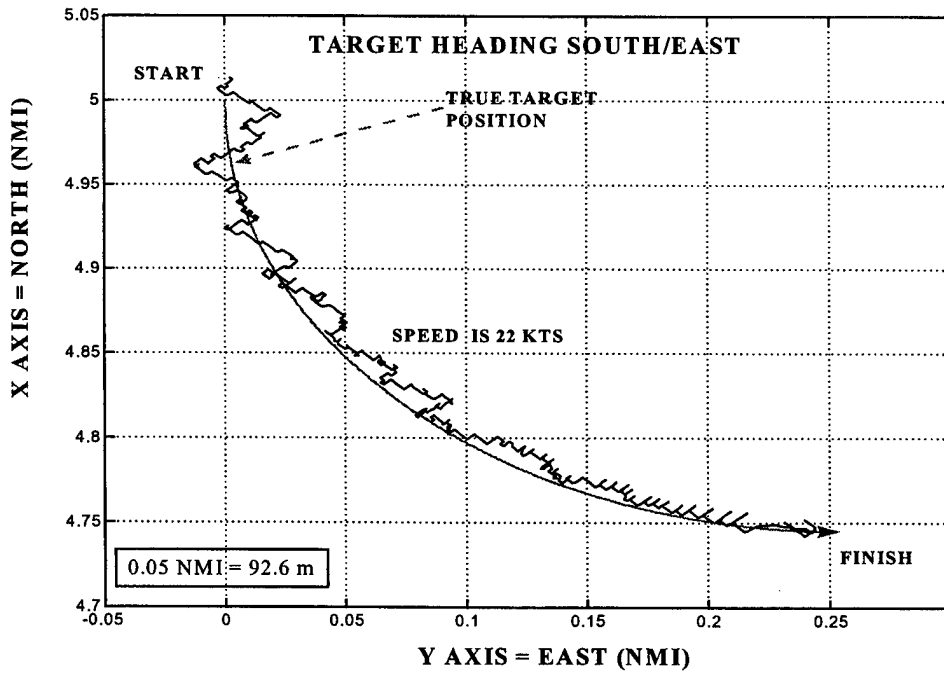

Figure 4.94: Simulator #1 DSTSPI derived target position - CSE 180° To 090°
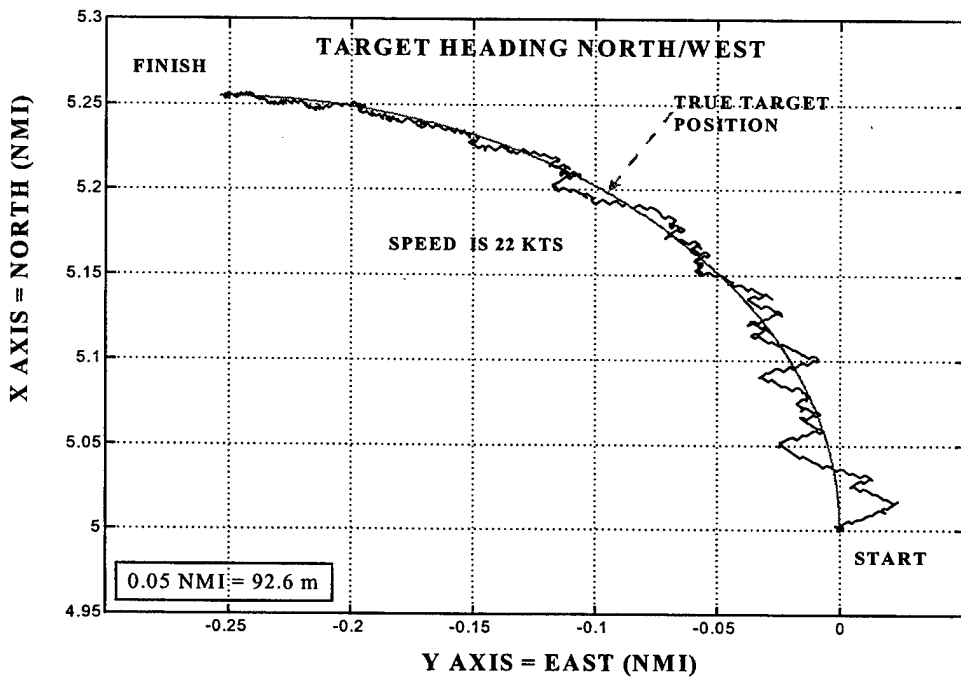
121
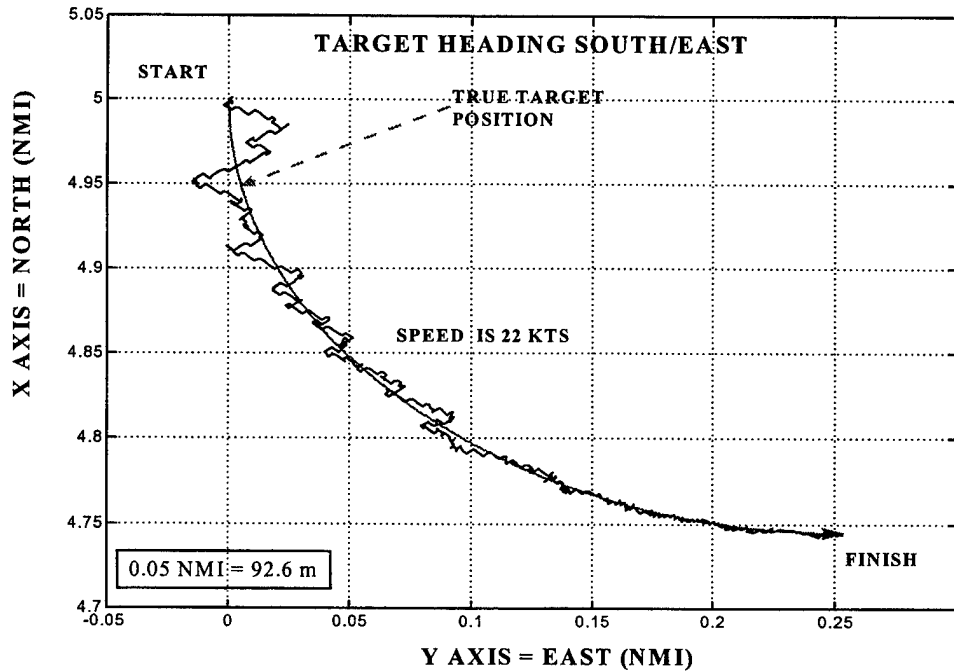
Figure 4.95: Simulator #2 DSTSPI derived target position - CSE 180° To 090°
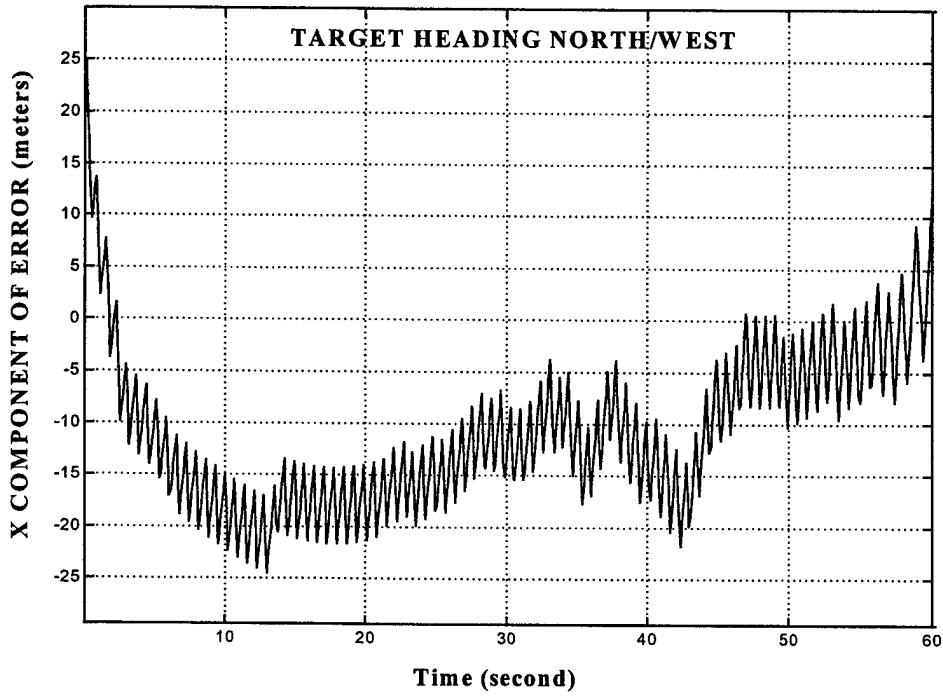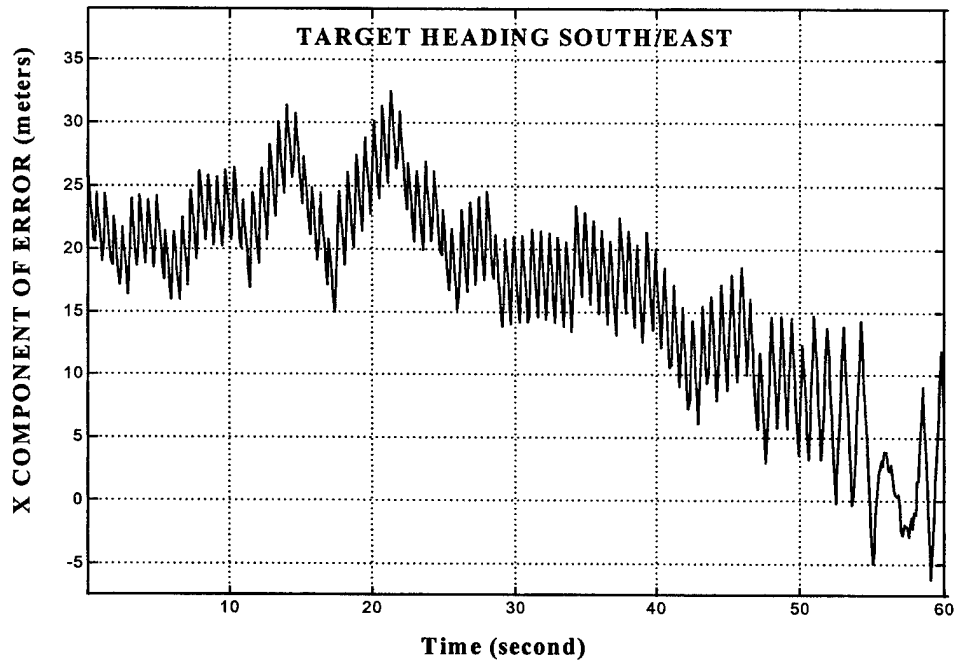

Figure 4.96: Simulator #1 derived target position error in the North/South direction - CSE 180° To 090°
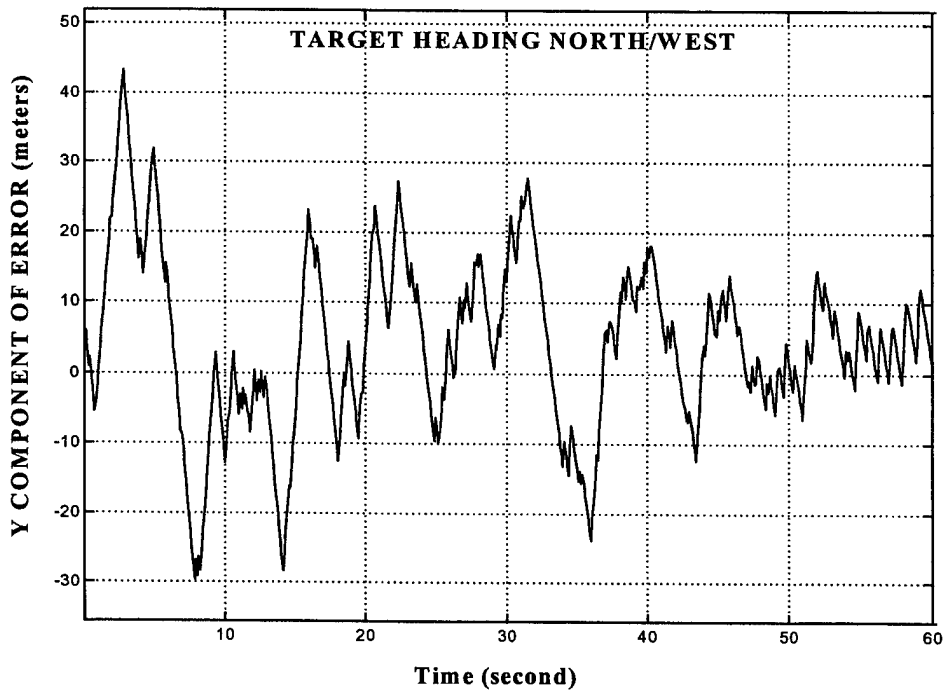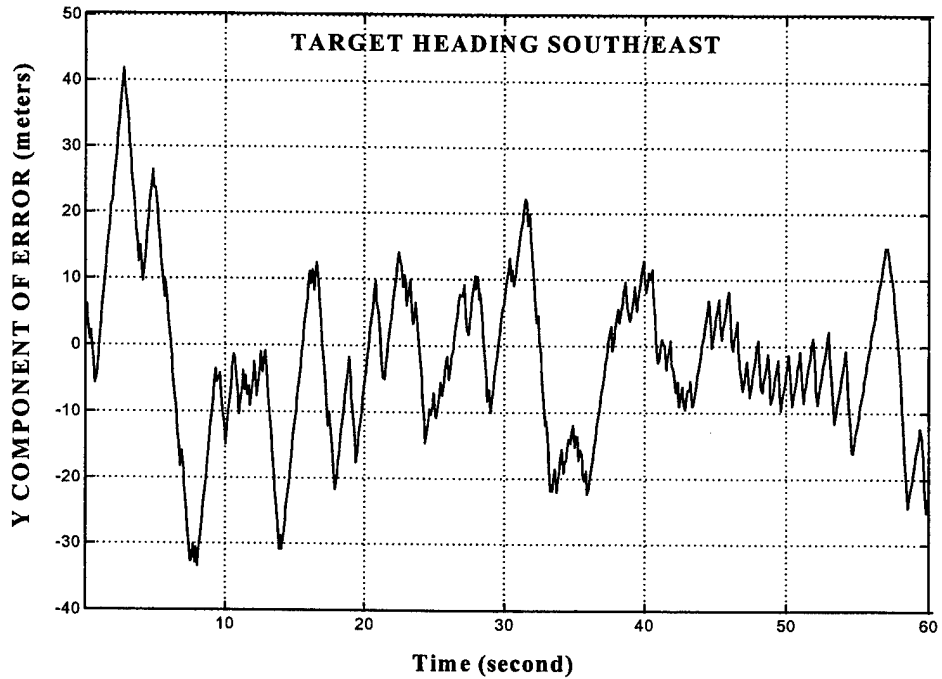
Figure 4.97: Simulator #1 derived target position error in the East/West direction - CSE 180° To 090°
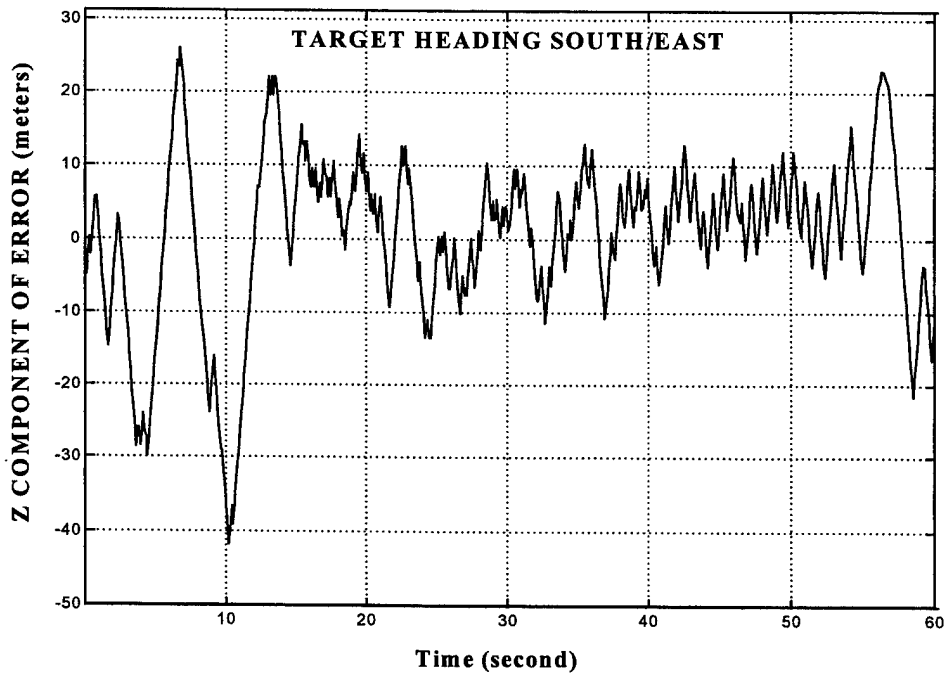
Figure 4.98: Simulator #1 derived target position error in the Up/Down direction - CSE 180° To 090°

123
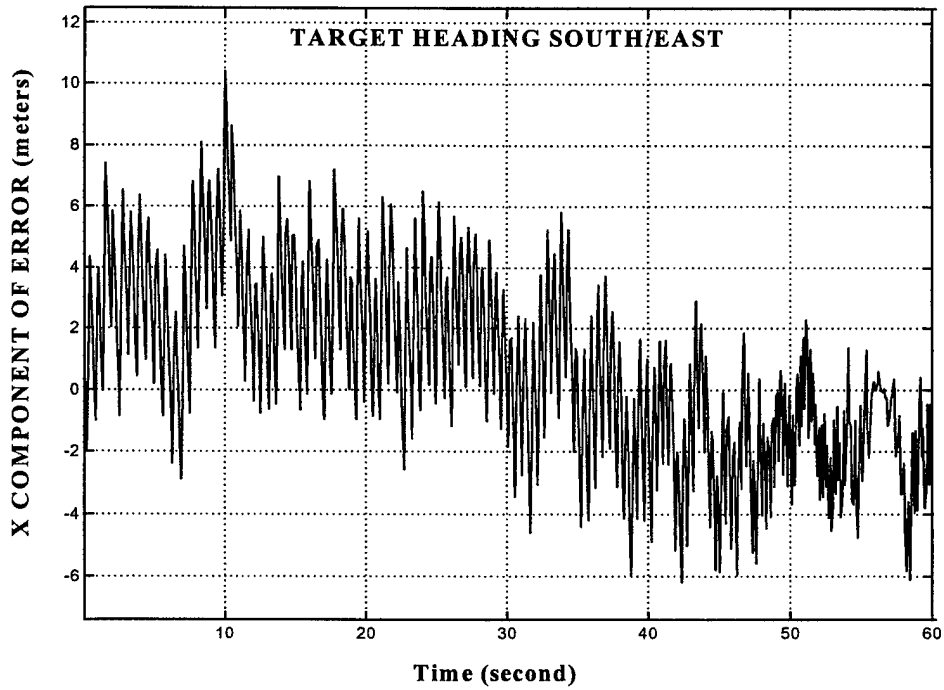
Figure 4.99: Simulator #2 derived target position error in the North/South direction - CSE 180° To 090°
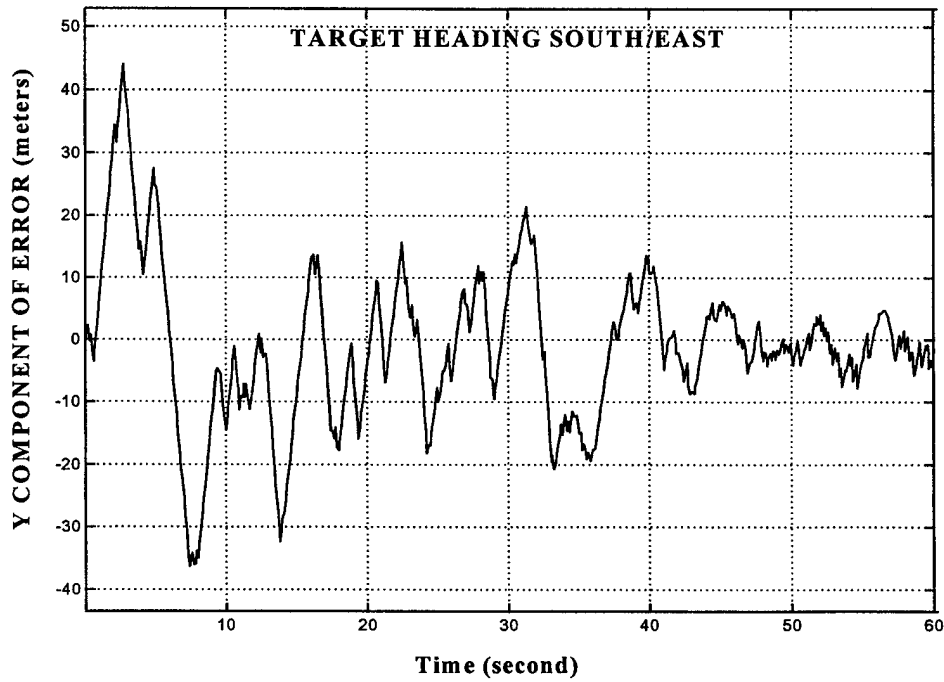
Figure 4.100: Simulator #2 derived target position error in the East/West direction - CSE 180° To 090°

124

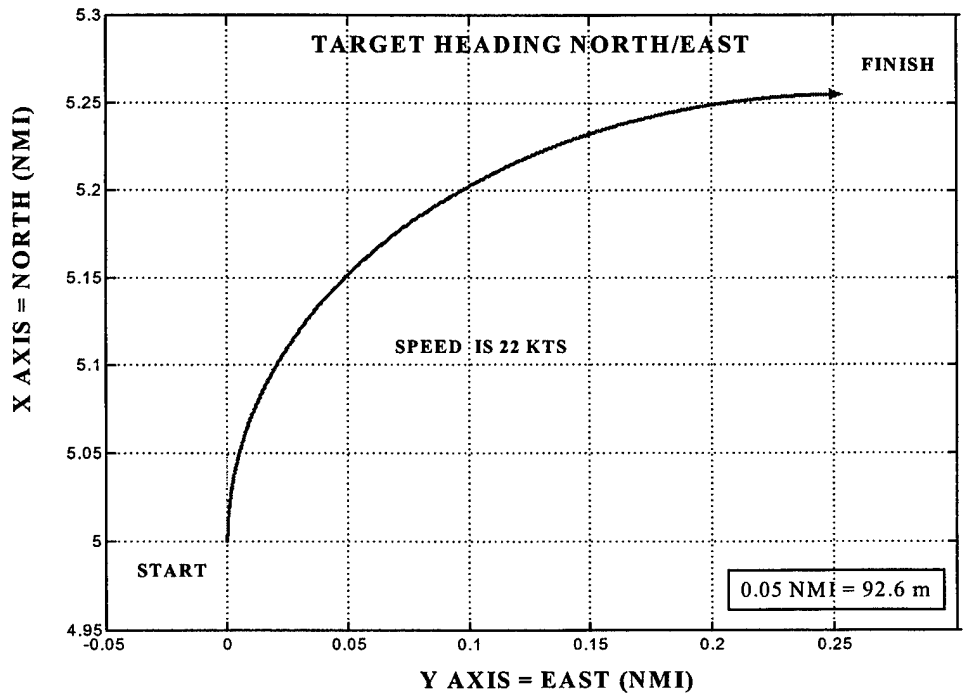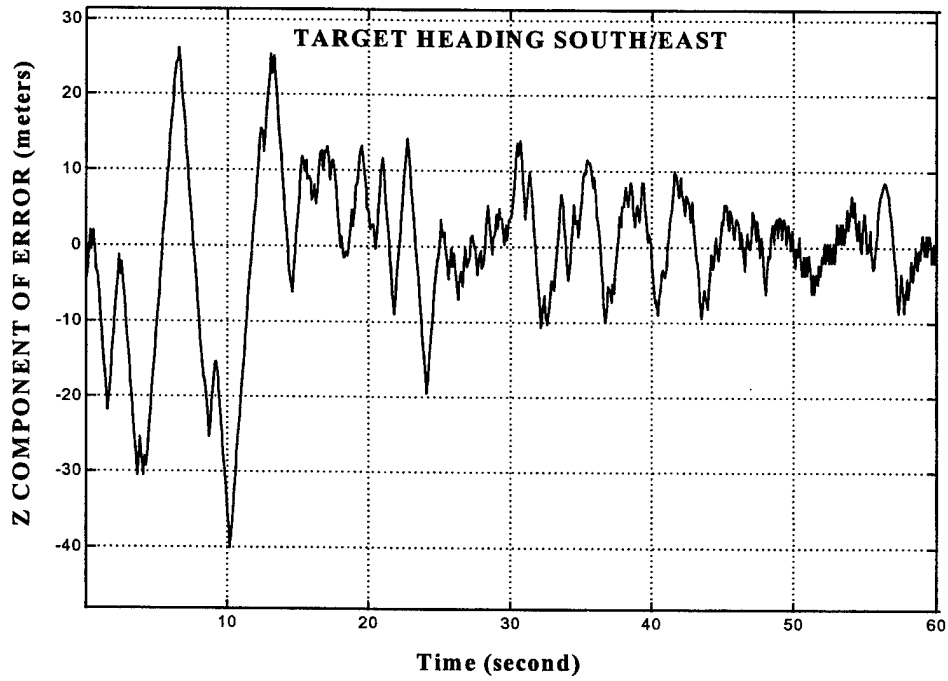**Figure 4.101: Simulator #2 derived target position error in the Up/Down direction - CSE 180° To 090°**

V. HARDWARE IMPLEMENTATION

As discussed in Chapter III, the DSTSPI algorithms require specific inputs. These inputs are a GPS position relative to the location of the GPS antenna, the pitch, roll and yaw of the aircraft that is given by the INS, and the azimuth, elevation and range between the seeker and the target. These inputs are shown in Figure 5.1. Of the three inputs, only the GPS position presents any real problems.
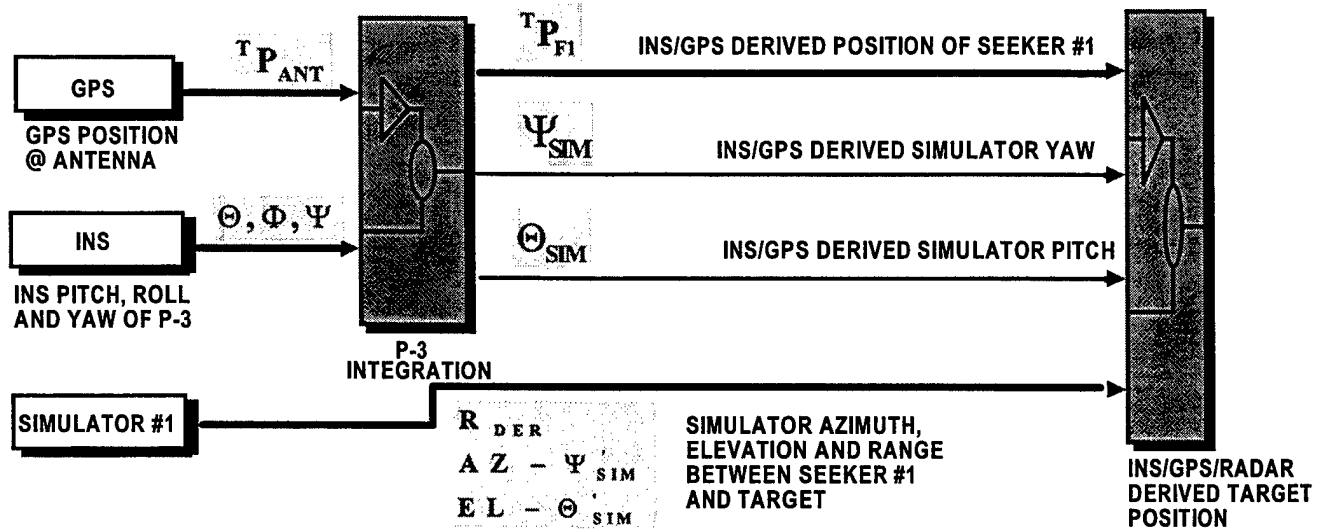
Figure 5.1: Hardware implementation of the DSTSPI algorithms

The algorithms presented in Chapter III assumed all fixed inertial positions are given in tangent plane coordinates. This is done as a matter of convenience. To continue to use the tangent plane coordinates in the hardware implementation, a fixed position located in geodetic coordinates must be defined somewhere in the ASW/EW engagement test scenario. This fixed point of reference could be located at the center of the operating area that is allocated prior to the test. This point is taken from the existing navigational

127

chart, the coordinates of which are given in the geodetic sense of Latitude and Longitude. The actual location is arbitrary.

To locate the P-3 in tangent plane coordinates we must take the position of the origin of the tangent plane coordinate system given in geodetic coordinates and perform a coordinate transformation from geodetic to ECEF coordinates. This position now becomes the origin of the tangent plane coordinate system given in ECEF coordinates.

The geodetic to ECEF coordinate transformation is easily computed. First, three quantities must be defined. The first of these quantities is the flattening factor, **f**, which represents the relative flatness of the reference ellipsoid. The mathematical definition for **f** is defined as [Ref. 1, p. 118-119]

$$f = \frac{a - b}{a} \qquad (5\text{-}1)$$

where **a** and **b** are the semi-major and semi-minor axes of the reference ellipsoid, respectively. The next quantity that must be defined is the eccentricity, ε. The eccentricity of the reference ellipsoid is defined as

$$\varepsilon^2 = 2f - f^2. \qquad (5\text{-}2)$$

The last quantity that must be defined is the normal, **N**, which represents the length of the ellipsoidal normal from the ellipsoidal surface to the intersection of the polar axis (Z_{ECEF}). Mathematically, **N** is defined as

$$N = \frac{a}{\sqrt{1 - \varepsilon^2 \sin^2 \phi}}, \qquad (5\text{-}3)$$

where ϕ is the geodetic latitude. Now, by using these three quantities, the geodetic to ECEF transformation is defined by the following equations

128

$$X_{ECEF} = (N + h)\cos\phi\cos\lambda \qquad (5\text{-}4)$$

$$Y_{ECEF} = (N + h)\cos\phi\sin\lambda \qquad (5\text{-}5)$$

$$Z_{ECEF} = \left[N(1 - \varepsilon^2) + h\right]\sin\phi \qquad (5\text{-}6)$$

where **h** is the geodetic height or height above reference ellipsoid and λ is the geodetic longitude. Equations (5-4) through (5-6) are incorporated into the MATLAB function "LL2ECEF.M" found in Appendix A.

Now, the next step is to find the position of the P-3 relative to the tangent plane coordinates. To do this we take the GPS position given in ECEF coordinate and subtract it from the origin of the tangent plane given in ECEF coordinates. This results in a position vector that has the correct orientation, NED.

Another option is to use a DGPS reference station. Here a portable DGPS reference station is located as near as possible to the testing location (this location must be on land). This station provides the necessary differential corrections to the local receiver. The advantage of using a portable DGPS reference station is that they usually provide better corrections than the Coast Guard differential stations. Another advantage is that these remote stations have the ability to record the GPS data. This would allow for further reductions in the errors from GPS. [Ref. 3] A typical system is found in Appendix B. The problem is that these reference stations must be setup and in operation 24 hours prior to the test scenario. Another problem is the cost. A typical reference station costs approximately twenty thousand dollars.

Since the algorithms presented in Chapter III are not intended for real time use, an actual hardware implementation only involves recording the three inputs for post-test

analysis. The difficulty in doing this is to ensure the data is saved in a format that is compatible with a particular post analysis software. To make the process easier, several GPS receiver manufacturers provide software packages that provide a post analysis capability. To this end it behooves the user to pick a GPS system that comes with a complete software package.

Another potential hazard in the recording of the data for post-test analysis is to ensure that all the recorded times are properly synchronized. Any clock differences translate directly into position errors. This is especially true for the time-tagged data of the INS and the Simulators since the angular rates can be quite large.

Perhaps the most difficult problem is the determination of the actual target position as a function of time given noisy data from the DSTSPI algorithms. The goal of the post-test analysis is to provide sufficient accuracy in the determination of the target's position so as to allow for the recognition of any launched decoys. To help attain this goal it is possible to take the raw data from the DSTSPI algorithms and in some way make an educated guess about the true target position. A first order approximation in obtaining the target's true position might be a simple least-squares fit of the data, but because of the cross range errors which are a consequence of the INS and seeker errors, a simple least-squares fit on the data does not provide any useful information. This is especially true for a maneuvering target. A better method in determining the target's true position given the noisy data might involve an iterative process by which the errors in all directions are minimized at the same rate.

VI. CONCLUDING REMARKS

The effectiveness of the at sea Anti-Ship Missile/Electronic Warfare engagement test scenario is heavily dependent upon the results of this thesis. By knowing the target's position in a fixed inertial coordinate system, the post analysis problem of distinguishing between target and decoy is made easier. Any launched decoys during the test scenario show up as an instantaneous deviation in the target track. This allows the test engineers determine if the seeker broke lock on the target and tracked an offboard decoy (e.g., chaff). By improving the method by which the at sea ASM/EW test scenario evaluation is performed, the war-fighting capabilities of the U. S. Navy improve.

Also, by knowing a target's position relative to a fixed inertial coordinate system, a target's position can be sent to any platform and be understood immediately without being specific to the platform's Fire Control System. Target positions that are fixed in a fixed inertial coordinate system allow for ease of processing because the information is sensor independent.

Considering the results obtained in this simulation, it is feasible to derive a target's position in a fixed inertial coordinate system from the integration of INS, GPS and radar. The precision to which the target's position is derived depends heavily upon the quality of the navigation equipment used in the integration process.

With the advent of more and more sophisticated weaponry, it becomes increasingly more important to provide the best available means by which an evaluation of these weapons is made. Of particular significance is the foreign missile threat. It is here that a great deal of time and money is spent in determining the effectiveness of our shipboard

self defense systems against these threats. The validation of a shipboard self defense

system against a missile threat usually involves modeling and simulation.

LIST OF REFERENCES

1. Kaminer, I. I. and Howard, R. M. "Avionics Technology Development For CR And VTOL UAV," Technical Report, Department Of Aeronautics, Naval Post Graduate School, Monterey, CA, December, 1993.

2. Herrington, J. B. "Uniform Framework For IMU/GPS Integration Using Kalman Filtering," Master's Thesis, Department Of Aeronautics, Naval Post Graduate School, Monterey, CA, June, 1995.

3. Clynch, J., "A Global Positioning System (GPS) Users Seminar," Department of Oceanography, Naval Post Graduate School, Monterey, CA, March, 1996.

4. Barton, D. K., *MODERN RADAR SYSTEMS*, Artech House, Inc., 1988.

5. Gates, P. J., *SURFACE WARSHIPS Vol. III*, Brassey's Sea Power: Naval Weapons Systems and Technology Series, Volume 3, 1987

6. Gill, C., "AA4276 Design Project - A Guidance, Navigation, and Control System for the Boeing 747," Department Of Aeronautics, Naval Post Graduate School, Monterey, CA, December, 1995.

7. Harney, R. C., Class Notes for TS3003, U. S. Naval Post Graduate School, Monterey, CA, 1996

8. White, C. And Reiber, C. "Navy Technical Assessment of LTN-72 Inertial Navigation Software Program 72-9-20," Technical Report, Naval Air Test Center Patuxent River, Maryland, June 1985

APPENDIX A

MATLAB FILES:

AZIMUTH.M

```
function out = azimuth(theta);
%ANDREW ROWE
%THIS FUNCTION COMPUTES THE AZIMUTH ANGLE
%RELATIVE TO TRUE NORTH FROM THE THETA GIVEN
%FROM CARTESIAN TO SPHERICAL COORDINATE
%TRANSFORMATION
%10/10/96
x = theta;
y=450-x;
if y >= 360
y=y-360;
end;
out = y;
```

B2NANT.M

```
function out = b2nant(vec);
% ANDREW ROWE
% THIS FUNCTION CONVERTS A VECTOR GIVEN IN THE BODY FIXED FRAME COORDINATE
% SYSTEM INTO THE NAVIGATION FRAME
% ROLL=PHI PITCH=THETA YAW=PSI
% p1 IS THE POSITION VECTOR OF THE GPS ANTENNA IN BODY FIXED FRAME
% COORDINATES RELATIVE TO THE CENTER OF THE AIRCRAFT
% 10/10/96
phi = vec(1);
theta = vec(2);
psi = vec(3);
Tphi = [1 0 0; 0 cos(phi) -sin(phi); 0 sin(phi) cos(phi)];
Ttheta = [cos(theta) 0  sin(theta); 0 1 0; -sin(theta) 0 cos(theta)];
Tpsi =  [ cos(psi) -sin(psi) 0; sin(psi) cos(psi) 0;0 0 1];
p1=[-5;0;0];
out = inv(Tpsi*Ttheta*Tphi)*p1;
```

B2NCEN.M

```
function out = b2ncen(vec);
% ANDREW ROWE
% THIS FUNCTION CONVERTS A VECTOR GIVEN IN THE BODY FIXED FRAME COORDINATE
% SYSTEM INTO THE NAVIGATION FRAME
% p1 IS THE POSITION VECTOR OF THE CENTER OF THE AIRCRAFT RELATIVE TO THE
% POSITION OF THE GPS ANTENNA
% ROLL=PHI PITCH=THETA YAW=PSI
% 10/10/96
phi = vec(1);
theta = vec(2);
```

```
psi = vec(3);
Tphi = [1 0 0; 0 cos(phi) -sin(phi); 0 sin(phi) cos(phi)];
Ttheta = [cos(theta) 0  sin(theta); 0 1 0; -sin(theta) 0 cos(theta)];
Tpsi =  [ cos(psi) -sin(psi) 0; sin(psi) cos(psi) 0;0 0 1];
p1=[5;0;0];
out = inv(Tpsi*Ttheta*Tphi)*p1;
```

B2NP1.M

```
function out = b2np1(vec);
% ANDREW ROWE
% THIS FUNCTION CONVERTS A VECTOR GIVEN IN THE BODY FIXED FRAME COORDINATE
% SYSTEM INTO THE NAVIGATION FRAME
% p1 IS THE POSITION VECTOR OF THE AFT PART OF THE SIMULATOR #1 RELATIVE TO
% THE CENTER OF THE AIRCRAFT IN BODY COORDINATES
% ROLL=PHI PITCH=THETA YAW=PSI
% 10/10/96
phi = vec(1);
theta = vec(2);
psi = vec(3);
Tphi = [1 0 0; 0 cos(phi) -sin(phi); 0 sin(phi) cos(phi)];
Ttheta = [cos(theta) 0  sin(theta); 0 1 0; -sin(theta) 0 cos(theta)];
Tpsi =  [ cos(psi) -sin(psi) 0; sin(psi) cos(psi) 0;0 0 1];
p1=[-2;5;0];
out = inv(Tpsi*Ttheta*Tphi)*p1;
```

B2NP12.M

```
function out = b2np12(vec);
% ANDREW ROWE
% THIS FUNCTION CONVERTS A VECTOR GIVEN IN THE BODY FIXED FRAME COORDINATE
% SYSTEM INTO THE NAVIGATION FRAME
% p1 IS THE POSITION VECTOR OF THE AFT PART OF THE SIMULATOR #2 RELATIVE TO
% THE CENTER OF THE AIRCRAFT IN BODY COORDINATES
% ROLL=PHI PITCH=THETA YAW=PSI
% 10/10/96
phi = vec(1);
theta = vec(2);
psi = vec(3);
Tphi = [1 0 0; 0 cos(phi) -sin(phi); 0 sin(phi) cos(phi)];
Ttheta = [cos(theta) 0  sin(theta); 0 1 0; -sin(theta) 0 cos(theta)];
Tpsi =  [ cos(psi) -sin(psi) 0; sin(psi) cos(psi) 0;0 0 1];
p1=[-2;-5;0];
out = inv(Tpsi*Ttheta*Tphi)*p1;
```

B2NP2.M

```
function out = b2np2(vec);
% ANDREW ROWE
% THIS FUNCTION CONVERTS A VECTOR GIVEN IN THE BODY FIXED FRAME COORDINATE
% SYSTEM INTO THE NAVIGATION FRAME
% p1 IS THE POSITION VECTOR OF THE FORWARD PART OF THE SIMULATOR #1
% RELATIVE TO THE CENTER OF THE AIRCRAFT IN BODY COORDINATES
```

% ROLL=PHI PITCH=THETA YAW=PSI
% 10/10/96
phi = vec(1);
theta = vec(2);
psi = vec(3);
Tphi = [1 0 0; 0 cos(phi) -sin(phi); 0 sin(phi) cos(phi)];
Ttheta = [cos(theta) 0 sin(theta); 0 1 0; -sin(theta) 0 cos(theta)];
Tpsi = [cos(psi) -sin(psi) 0; sin(psi) cos(psi) 0;0 0 1];
p1=[2;5;0];
out = inv(Tpsi*Ttheta*Tphi)*p1;

B2NP22.M

function out = b2np22(vec);
% ANDREW ROWE
% THIS FUNCTION CONVERTS A VECTOR GIVEN IN THE BODY FIXED FRAME COORDINATE
% SYSTEM INTO THE NAVIGATION FRAME
% p1 IS THE POSITION VECTOR OF THE FORWARD PART OF THE SIMULATOR #2
% RELATIVE TO THE CENTER OF THE AIRCRAFT IN BODY COORDINATES
% ROLL=PHI PITCH=THETA YAW=PSI
% 10/10/96
phi = vec(1);
theta = vec(2);
psi = vec(3);
Tphi = [1 0 0; 0 cos(phi) -sin(phi); 0 sin(phi) cos(phi)];
Ttheta = [cos(theta) 0 sin(theta); 0 1 0; -sin(theta) 0 cos(theta)];
Tpsi = [cos(psi) -sin(psi) 0; sin(psi) cos(psi) 0;0 0 1];
p1=[2;-5;0];
out = inv(Tpsi*Ttheta*Tphi)*p1;

CONTHETA.M

function out = contheta(component);
% ANDREW ROWE
% THIS FUNCTION COMPUTES THE ANGULAR PRECISION FOR A CONICAL SCAN RADAR
% SEEKER. THIS IS USED IN THE SEEKER MODEL
% 10/10/96
R = component(1); %range in meters
Pt = 250e3;   %power in watts 250 Kw
sigma = 3000;   %radar cross section square meters
f = 9e9;   %radar frequency of 9 Ghz
alpha = .055;   %attenuation dB/km page279 Barton
Gain = 1995.26;   % antenna gain 33 dB
c = 2.9979e8;   %speed of light
lambda = c/f;   %wavelenght in meters
B = 10e6;   %noise bandwidth
F = 10;   %noise figure
kT = 4.14e-21;   %joules at 300 K
bw = .0785398;   %3dB transmitter beam width (uniform illumination) 4.5 degrees
SN = Pt*Gain*Gain*sigma*10^(-0.2*alpha*R/1000)*lambda*lambda/4/pi/kT/B/F/4/4/pi/pi/R/R/R/R;
sigma_s=0.0125*bw;   %scintillation error at optimized squint angle
                        %Barton page 390
SN = 100*SN;   % 100 pulse integration improvement

137

thetasig = bw/(SN)^0.5 + sigma_s;   %radians

THETAD.M

```
function thetasig = thetad(component);
% ANDREW ROWE
% THIS FUNCTION COMPUTES THE ANGULAR PRECISION FOR A MONOPULSE
% SEEKER.  THIS IS USED IN THE SEEKER MODEL
% 10/10/96
R = component(1);          %range in meters
Pt = 30e3;                 %power in watts 30 Kw
sigma = 3000;              %radar cross section square meters
f = 17e9;                  %radar frequency of 17 Ghz
alpha = .055;              %attenuation dB/km page279 Barton
Gain = 218.77;             % antenna gain 23.4 dB
c = 2.9979e8;              %speed of light
lambda = c/f;              %wavelenght in meters
B = 10e6;                  %noise bandwidth
F = 8.9;                   %noise figure
kT = 4.14e-21;             %joules at 300 K
bw = .13962;               %3dB transmitter beam width (uniform illumination) 8 degrees
SN = Pt*Gain*Gain*sigma*10^(-0.2*alpha*R/1000)*lambda*lambda/4/pi/kT/B/F/4/4/pi/pi/R/R/R/R;
km = 1.9;                  %error slope for monopulse radar dual horn
thetasig = bw/km/(100*2*SN)^0.5;          %radians
```

HEAD.M

```
function out = head(direc);
% ANDREW ROWE
% THIS FUNCTION DETERMINES THE HEADING BASED ON NOT EXCEEDING 180 DEGREE
% TURN DURING AIRCRAFT MANEUVERS
% 10/10/96
x = direc(1);
y = direc(2);
        if (x > y) & ((x-y) < pi),
                direction = 1;
        elseif (x < y) & ((y-x) < pi),
                direction = -1;
        elseif (x > y) & ((x-y) >= pi),
                direction = -1;
        elseif (x < y) & ((y-x) >= pi),
                direction = 1;
        elseif x==y,
                direction = 1;
        end;
out = direction;
```

OVER2PI.M

```
function out = over2pi(direc);
% ANDREW ROWE
% THIS FUNCTION ENSURES THAT THE HEADING FALLS BETWEEN 0 AND 2PI
% 10/10/96
```

```
x = direc;
if x >= 2*pi
        x=x-2*pi;
end;
if x < 0,
        x=x+2*pi;
end;
out = x;
```

LL2ECEF.M

```
function ecef=112ecef(x)
% converts from geodetic latitude, longitude, elevation to % earth-centered earth-fixed Cartesian
coordinates
phi = x(1); lambda = x(2);h = x(3);
% define semi-major and semi-minor earth axes a=6378137;b=6356000;
% define auxiliary quantities f,e, and N
f=(a-b)/a; e = f*(2-f); N = a/sqrt(1-(e*sin(phi))-2);
% convert to Cartesian
ecef = [(N + h)*cos(phi) * cos(lambda)
        (N + h)*cos(phi) * sin(lambda)
         (N*(1-e^2)+h) * sin(phi)];
```

APPENDIX B

The following Pages include manufacturer data-sheets from the *DEL NORTE Technology, Inc.*

DEL NORTE Technology, Inc. e-mail: dnti@delnorte.com

1) FLYING FLAGMAN® Global Positioning System Measuring Unit

FEATURES/BENEFITS:
- 12-Channel GPS Receiver
- Flow Rate/Temp/Humidity Monitoring
- 10 Home Points
- 100 Field Memory
- Polygon Field Entry
- Racetrack, Parallel Line and Squeeze to Middle Functions
- 10 Position/Sec Updates
- Ground Speed in MPH, m/sec or knots
- Serial Port for control/logging
- Break Point Memory
- Resume to Point
- Automatic Reverse Direction Sensing
- Skipped Line Detection
- Selection of feet/meters
- Built-in Clock
- Data/Time Tag
- Remote Functions on Flight Stick
- On-Ground Self-test

The new DEL NORTE Technology GPS Measuring Unit (GMU) provides a rugged, waterproof, and versatile GPS Receiver with multiple function capabilities and a range of options Set up is accomplished by using a menu driven Control and Display Unit (CDU). The Del Norte GMU can serve as either a Reference or Mobile GPS Unit. As a Reference Unit, the GMU, with its Establish Position capability, is able to derive site location to within one meter in a stand-alone mode over twenty-four hours and even better if left for forty-eight hours.

After setup the CDU may be disconnected to leave the single rugged, waterproof unit on site. By adding a 'second processor' option to the GMU, the Reference Station can also act as a differential monitor. As a mobile, the GMU may be interfaced to any of the user's data processing systems. For stand-alone operations the addition of the VGA board and optional second processor allow the GMU to drive a color display and incorporate third party software.

SPECIFICATIONS:

PERFORMANCE:
- Differential Dynamic: 1 - 3 meters, 1 meter CEP
- Update Rate : 0.1 seconds

SYSTEM ENVIRONMENT:
- Temperature: 0 - 55 degrees Celsius (32 - 130 degrees Fahrenheit)
- Vibration: Tested to MIL-STD-810-C

PHYSICAL/POWER CHARACTERISTICS:
- System Weight: 24 lbs (10.88 Kg)
- CDU Dimensions
  - W 4.2 in (10.6 cm)
  - H 7.7 in (19.5 cm)
- Super Trac Light Bar
  - W 15.0 in (38.1 cm)
  - H 2.0 in (5.1 cm)
  - D 5.5 in (14.0 cm)

142

- D 1.3 in (3.3 cm)
- GMU Dimensions
  - W 8 in (20.3 cm)
  - H 6.8 in (17.3 cm)
  - D 15 in (38.1 cm)

- Power Input : 11 - 32 VDC, 30 Watts

SYSTEM SUPPLIED WITH:

- GMU Mainframe
- Control/Display Unit
- Super Trac Light Bar
- Remote Step Switch
- GPS Antenna

- Differential Rx + Antenna
- Cables
- Shock Mounts
- Installation and Operation Manuals

OPTIONS:

- Differential Data Sources
  - Local Reference Tower
  - Portable Reference Station
  - FM Side-Band
  - Government MF Transmissions
  - Satellite Data Links
- Data Logger and Post-Processing/Plotter Software
- *Map Trac* Moving Map Display

SUPER TRAC LIGHT BAR:

- Pilot Programmable Displays
  - Digital HSI
  - Line/Pass Number
  - Distance Off-Track
  - Distance-to-go
  - Course Deviation
  - Area Sprayed
  - Custom Settings
  - Ground Speed

- Left/Right Guidance
  - Visible in Direct Sunlight
  - Dimmer Control for Low Light/Night Flying
  - Programmable Sensitivity
- Course Deviation Indicators
  - Programmable to nearest 0.1 of a degree

2) MODEL 2012 PORTABLE REFERENCE STATION

FEATURES/BENEFITS:

- Dedicated GPS Reference Station
- Lightweight & Portable
- Low-Cost

- 12-Channel GPS Receiver and Radio/Modem which can be in one box
- 'Self-Locating'

The Del Norte 2012 is the low-cost portable reference station solution. To compliment the 2012, a small, lightweight, and inexpensive UHF Mobile Data Link Transmitter and Receiver is available to feed Differential GPS Corrections to your mobile GPS receiver. Del Norte has trained engineers and technicians available for field deployment anywhere in the world to provide assistance with first-time installations or emergency needs

SPECIFICATIONS:

PHYSICAL & POWER CHARACTERISTICS:

- Weight 5 Kg
- Dimensions
  W 30 cm
  H 9 cm
  D 34 cm

- Operating Temperature
  0 - 50 Degrees Celsius
- Power
  11 - 14.5 vDC

SUPPLIED WITH:

- 12-Channel L1 Receiver
- UHF Transmitter and Modem
- Patch GPS Antenna w/Ground Plane
- Broad Band Omni Antenna

- Necessary Cables and Connectors
- Operator's Manual
- Comprehensive Product and Firmware Maintenance for One Year
- Training Available

SYSTEM OPTIONS:

- 215UL Mobile Data Link Receiver

RADIO SPECIFICATIONS:

- Frequency
  458.xxx MHz, 0.5 Watt (UK deregulated), options include other UHF, VHF, and HF frequencies on request
- Transfer Times

144

W/RTCM Format

Typical w/4 satellites, 0.4 seconds

Typical w/12 satellites, 1.0 seconds

- Baud Rates
300 to 9600

INITIAL DISTRIBUTION LIST

1. Defense Technical Information Center 2
    8725 John J. Kingman Rd, Ste. 0944
    Alexandria, Virginia 22304-6145

2. Dudley Knox Library 2
    Naval Postgraduate School
    411 Dyer Rd.
    Monterey, CA 93943

3. Chairman Physics Department 1
    Department of Physics
    Naval Postgraduate School
    Monterey, California 93943-5121

4. Dr. Phillip Pace, Code EC/PC 1
    Department of Electrical and Computer Engineering
    Naval Postgraduate School
    Monterey, California 93943-5121

5. Dr. Robert C. Harney, Code PH/HA 1
    Department of Physics
    Naval Postgraduate School
    Monterey, California 93943-5121

6. Commanding Officer Naval Research Laboratory 1
    Attn: Dr. John Montgomery
    Code 5700.00
    4555 Overlook Avenue, S.W.
    Washington, DC 20375-5339

7. Commanding Officer Naval Research Laboratory 1
    Attn: Dr. Frank Klemm
    Code 5710.00
    4555 Overlook Avenue, S.W.
    Washington, DC 20375-5339

8. Commanding Officer Naval Research Laboratory 1
    Attn: Mr. Roger Oxley
    Code 5720.00
    4555 Overlook Avenue, S.W.
    Washington, DC 20375-5339

9.   Commanding Officer Naval Research Laboratory 1
Attn: Mr. W. W. Everett
Code 5730.00
4555 Overlook Avenue, S.W.
Washington, DC 20375-5339

10.   Commanding Officer Naval Research Laboratory 1
Attn: Dr. Joe Lawrence
Code 5740.00
4555 Overlook Avenue, S.W.
Washington, DC 20375-5339

11.   Commanding Officer Naval Research Laboratory 1
Attn: Dr. G. E. Friedman
Code 5750.00
4555 Overlook Avenue, S.W.
Washington, DC 20375-5339

12.   Commanding Officer Naval Research Laboratory 1
Attn: Mr. Alfred Di Mattesa
Code 5760.00
4555 Overlook Avenue, S.W.
Washington, DC 20375-5339

13.   Commanding Officer Naval Research Laboratory 1
Attn: Mr. William M. Morris
Code 5761.00
4555 Overlook Avenue, S.W.
Washington, DC 20375-5339

14.   Commanding Officer Naval Research Laboratory 1
Attn: Mr. Jeffery A. Mills
Code 5763.00
4555 Overlook Avenue, S.W.
Washington, DC 20375-5339

15.   Commanding Officer Naval Research Laboratory 1
Attn: Dr. Allen N. Duckworth
Code 5707.00
4555 Overlook Avenue, S.W.
Washington, DC 20375-5339

16.   Commanding Officer Naval Research Laboratory 1
Attn: Mr. Andrew Hosmer
Code 5761.00
4555 Overlook Avenue, S.W.
Washington, DC 20375-5339